IMPROVED FISCHER-TROPSCH SYNTHESIS BY THERMAL MANAGEMENT OF THE CATALYST

by

SEYED AMIR JAFARI GHORESHI

Presented to the Faculty of the Graduate School of

The University of Texas at Arlington Submitted in Partial Fulfillment of the

Requirements for the Degree of

DOCTOR OF PHILOSOPHY

August 2021

Arlington, Texas, United States

Copyright © by Seyed Amir Jafari Ghoreshi 2021

All Rights Reserved

Acknowledgements

Words cannot express my gratitude to my mentor Dr. Frederick MacDonnell. He inspired me with his wealth of knowledge and endless motivation. Dr. MacDonnell, Thank you for your kind support. A special thanks to Dr. Brian Dennis for his guidance and encouragement. Without that, I would not have been able to accomplish what I have done. Many thanks to my committee members, Dr. Peter Kroll, and Dr. Rasika Dias, for their time and support during my Ph.D. journey at UTA.

I would like to thank all my lab mates and coworkers in CREST and Conrad Greer labs, especially Dr. Wilaiwan Chanmanee, who supported me during my research.

I would especially like to thank the love of my life, Dr. Fereshteh Maleki. You have always been supportive of me; I owe you everything in my life and career. I would like to mention my little son, Liam Aryo, who joined our lovely family in the middle of this academic journey. He is a sweet companion who was on my laps while I was doing research and writing manuscripts. And to my parents, Hamid, and Zahra and my brothers Ali and Mohammad. I would not be where I am today without their love and support. Its been six years we are far away

To all the others, though you have not been named, you are no less important.

July 15, 2021

Abstract

IMPROVED FISCHER-TROPSCH SYNTHESIS BY THERMAL MANAGEMENT OF THE CATALYST

Seyed Amir Jafari Ghoreshi, PhD

The University of Texas at Arlington, 2021

Supervising Professor; Dr. Frederick MacDonnell

The research in this dissertation consists of a novel catalyst design which is aimed at helping manage the temperature instabilities and heat-transfer within a catalyst particle and maintaining an isothermal temperature distribution throughout the catalyst bed, with the goal of improving control on the rate of reactions and tuning the chain propagation that leads to having high yields of desired products (liquid alkanes C5-C22) while suppressing undesirable competitive reactions (WGS, Boudouard) and consecutive byproduct formation (alpha-Olefin, Oxygenates, and tail gas C1-C4) during the Fischer-Tropsch synthesis (FTS). Comparing FTS performance of the thermally modified catalysts and core-shell (CS) composite structure catalyst with a conventional catalysts and egg-shell (ES) catalyst resulted in higher productivity with a maximized oil selectivity in thermally modified and core-shell catalysts with tither product distribution due to the better thermal management of the catalyst bed in such a highly exothermic reaction.

Table of Contents

LIST OF FIGURES

LIST OF TABLES

Chapter 1

IMPROVED FISCHER-TROPSCH SYNTHESIS BY THERMAL MANAGEMENT OF THE CATALYST

1.1. Introduction

It is estimated that over 143 billion cubic meters of natural gas, 3.5% of the total annual production and 19.8% of US natural gas consumption, is flared annually at oil-producing sites around the globe resulting in the addition of over 350 million tons of carbon dioxide to the atmosphere with no benefit to humankind.[1] Flaring such a large volume of natural resources that could be used to enhance economic growth is not a sustainable practice. This is primarily due to issues associated with capturing and, more importantly, transporting natural gas from the oil field to the population center. Pipelines are expensive to build and maintain, but it should be noted that if these stranded natural gas reserves could be transformed into liquid hydrocarbon fuels, then transport via trucks and railways for this now more valuable liquid transportation fuel could be realized and this resource used for a benefit. Similarly, much of the US natural gas reserves are found in locations from where it is not in areas with pipeline networks, and the 'stranded' natural gas is essentially unusable for anyone. The technology to convert natural gas to liquid fuel (GTL) already exists via a combination of known chemical processes, such as alkane steam reforming (ASR), autothermal reforming (ATR), partial oxidation (PO), and Fischer–Tropsch synthesis (FTS). The problem is that it is difficult to scale down these processes to a 'portable' 500-2000 bbl/day

operation in an economically feasible manner, as most such GTL operations are several billion-dollar investments.[2] To summurize, the gas flaring emits methane, carbon dioxide, and soot, but its capturing is “low hanging fruit” in delivering net zero emition.

1.2. Gast to Liquid Process and Fischer-Tropsch Synthesis Overview

The FT refers to German scientists and engineers Franz Fischer and Hans Tropsch, who catalytically developed the process of converting what so lately called syngas from gasified coal to liquid hydrocarbons at the Kaiser-Wilhelm-institute für Kohlenforschung, known nowadays as Max Planck Institue for Coal Research in a city named Mülheim an der Ruhr in the west region of Germany, in 1925.[3,4] The science was utilized rapidly to produce the proper diesel for Panzer tanks during WW II. The technology received intermittent attention for the next decades to produce sulfur-free diesel fuels in the Sasol facility in South Africa.[5]

The Fischer-Tropsch process is a well-known technology for producing synthetic hydrocarbons from a synthetic gas produced from any carbonaceous reserves such as coal, biomass, wastes, and exclusively natural gas resources. Methane is the primary raw hydrocarbon for the petrochemical industry if it could be economically converted to syngas. The largest natural gas reservoirs have existed mainly in Persian golf and Russia, and North America. This abundance of natural reservoirs tempts the companies to construct an economically viable and commercially scalable GTL plant.

The basic GTL process generally involves two significant chemical transformations: 1. the production of syngas with a specific H_2 to CO ratio from

natural gas and 2. the conversion of syngas to more value-added hydrocarbon products, exclusively synthetic fuels (C_7-C_{22} liquid hydrocarbons and C_{23+} waxes). The syngas production is mainly viable by natural gas reforming, and the later step could be done via Fischer-Tropsch (FT) technology. The fiq. 1. Shows the schematic diagram of the conversion of the natural gas to liquid hydrocarbons.

Figure 1. Catalytical conversion of the natural gas into liquid hydrocarbon products.

Guettel and Turek[6,7] listed the existing large-scale FTS plants across the globe. The Sasol facility commissioned in 1955 was the oldest plant with 2500 bpd capacity, and shell-Qatar with 140000 bpd, was an excellent example of sustainable conversion of natural gas to the liquid product. Finally, Kanellopoulos summarized the 33 small-scale GTL facilities that currently exist in the world and estimated that the production capacity of the synthetic oil could be equivalent to one-third of the middle easts oil reserves by developing these types of technologies.[2]

1.3. Fischer-Tropsch Catalysts

The Fischer-Tropsch Synthesis (FTS) is a heterogeneous catalytic reaction in which typical active metal catalysts used are Co, Fe, Ru, and Ni, which can dissociatively adsorb synthesis gas on catalyst sites.[8]. Among all of them, Co is most widely used in the low-temperature FT synthesis for high stability, high activity, more linear chain product selectivity, and low water-gas-shift tendency. Although the Nickle is highly active for hydrogenation of the carbon monoxide, it favors methane production under FT conditions compared to others[9]. Ruthenium is highly efficient in alkane production with lower temperatures but is not economically affordable. Finally, iron is viable metal as an FT catalyst widely used in high-temperature FT reaction conditions with more alcohols and olefins yield than cobalt with a high WGS reaction.

To maximize the dispersion of the active catalysts clusters, the textural promoters such as catalyst supports take into account the early 19th century. The cobalt-based FTS eventually became the "standard" catalyst in the first generation of industrial synthetic fuel production in the German Synthine site between 1925 and 1955. The catalyst was comprised of a nonreducible promoted Cobal and thorium oxide on kieselguhr support.[10–13]

1.4. Product and product distribution

The principal product distribution of the FTS consists of linear change paraffin and alpha-olefins.[14] The predominant products of a cobalt-catalyzed FTS with a temperature range between 200 to 290 and under enough gas pressure are a broad spectrum of the saturated straight chain hydrocarbons ranging from methane (C_1) to longer linear chain paraffin waxes with a carbon number higher than 30 (C_n where $n \geq 30$) is a mixture of hydrocarbons and water, with smaller amounts of alpha-olefins, branched alkanes, and oxygenated hydrocarbons such as alcohols and carboxylic acids such as formic, propionic, and acetic acid also produced.

The linear paraffin (alkane) can be stratified into different fractions, each with intrinsic value and associated issues. The very light hydrocarbons, C1 – C2, are a little different from natural gas and have little added value. The C3 – C4 fraction is reasonably valuable light condensates, as is the naphtha fraction (C5 – C11), both of which can be liquefied easily and transported as liquids. The most valuable fractions are the middle distillate, C12 – C22, which can be used as jet and/or diesel fuel. Hydrocarbons with higher carbon numbers begin to form solid waxes after C23, and those with C33+ are waxes that are difficult to melt.

The alkane product distribution in FTS is kinetically controlled as a surface polymerization mechanism modeled in the Anderson–Schulz–Flory (ASF) equation10,11, which reveals that the product distribution is a function of the chain propagation probability, a. Anderson considered the FTS as an ideal polymerization reaction that follows the distribution of mole fractions. Thus, the chances for either chain propagation or termination are basically constant regardless of the length of

the hydrocarbon chain but can be influenced by catalyst properties and reaction conditions.

The stoichiometry of the reactions involved in FTS can be expressed as follows:

$CO + 2H_2 \rightarrow (-CH_2-) + H_2O$	$\Delta_R H^\circ$ = -165 kJ/mol CO	FTS	(1.1)
$n\ CO + (2n+1)\ H_2 \rightarrow C_nH_{2n+2} + n\ H_2O$	< -165 kJ/mol CO	Alkanes	(1.2)
$n\ CO + 2n\ H_2 \rightarrow C_nH_{2n} + n\ H_2O$	< -165 kJ/mol CO	Alkenes	(1.3)
$n\ CO + 2n\ H_2 \rightarrow C_nH_{2n+2}O + (n-1)\ H_2O$	< -165 kJ/mol CO	Alcohols	(1.4)
$CO + H_2O \leftrightarrow CO_2 + H_2$	ΔH_R= - 41 kJ/mol	WGS	(1.5)
$2CO \leftrightarrow C + CO_2$	ΔH_R= - 271 kJ/mol	Boudouard	(1.6)

As shown, the primary reactions involve in the FTS process generate considerable heat energies. Moreover, by increasing the number of carbon in the hydrocarbon chain, the exothermicity of the reaction will be even higher. On the other hand, the FTS mechanism proceeds via stepwise addition of carbonaceous species (monomers), ending with a chain termination step as shown in the following scheme.

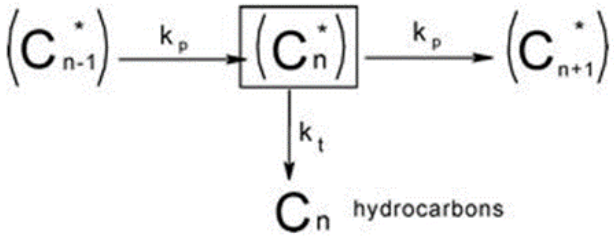

Figure 2. chain propagation - chain termination

Madon[15] has studied the growth of hydrocarbon chain in FTS was shown the maximum weight fraction of the produced hydrocarbon with n number of carbon present in the molecule is given by the equation 1.10. In equations k_P, and k_T stands for the rate of chain propagation and the rate of chain termination, respectively. The W_n is the weight percent of a product containing n carbon atoms, and α is the chain growth probability.

$$\alpha = k_P / (k_P + k_T) \quad (1.7)$$

$$W_n = n\,\alpha^{n-1}\,(1 - \alpha)^2 \quad (1.8)$$

$$P_n = \alpha^{n-1}(1-\alpha) \quad (1.9)$$

$$Wn,max = 4n\,(n-1)(n-1) / (n+1)(n+1) \quad (1.10)$$

It also was suggested by Madon[15] the rate of chain propagation probably decreases with increasing the carbon number, and it depends on the nature of the active sites and kinetics of the reaction. The a factor is known to be independent on the chain length and very sensitive to various parameters, including catalyst metal, reaction temperature, reaction pressure, hydrogen, carbon monoxide, water partial pressure, syngas composition, etc.

Figure 3. shows that, by plotting the weight percent of the product with n carbon versus the number of the carbon in the chain and solving the 1.8 equation for different α values, we could be able to have an estimation about the influence of the chain propagation on the production of the desired and undesired hydrocarbons. The results are summarized in Table 1.

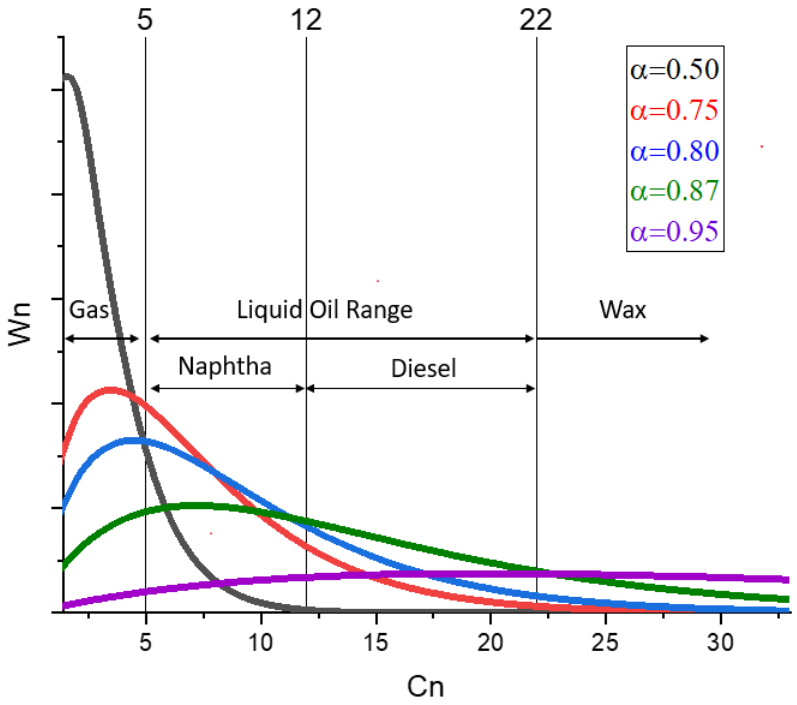

Figure 3. Effect of different α values on FT product distribution.

Table 1. By varying chain propagation leads to different product distributions.

α	Gas	Liquid oil	wax
0.50	71%	29%	0
0.75	29%	70%	1%
0.80	21%	75%	4%
0.87	10%	75%	15%
0.95	3%	58%	39%

As shown in table 1. and fig. 3. by increasing the chain propagation factor from 0.50 to 0.95, tail gas production will drastically decrease. However, the liquid range hydrocarbons production is limited to a particular value (75%). Therefore by turning the chain propagation for during the synthesis, we could be able to

determine each product range. Nevertheless, the α is depending on numerous parameters; a higher CO partial pressure results in increased surface coverage and, therefore, more significant chain growth probability; a higher H_2 partial pressure leads to chain termination and, therefore, a more negligible chain growth probability. Regardless of feedstock or catalyst, a high reaction temperature leads to faster hydrogenation which favors a significant methane CH_4 formation and less surface CH_2 and leads to a shorter average chain length. High temperature additionally results in elemental carbon deposition via the Boudouard reaction ($2CO \rightarrow CO_2 + C$) that deactivates the catalyst.

Assuming the reaction pressure and reagent partial pressures can be controlled via proper reactor design and operation, the temperature dependency of the reaction is often the most challenging parameter to control[16]. Thus, Failure to an efficient heat removal could cause a systematic problem throughout the process.

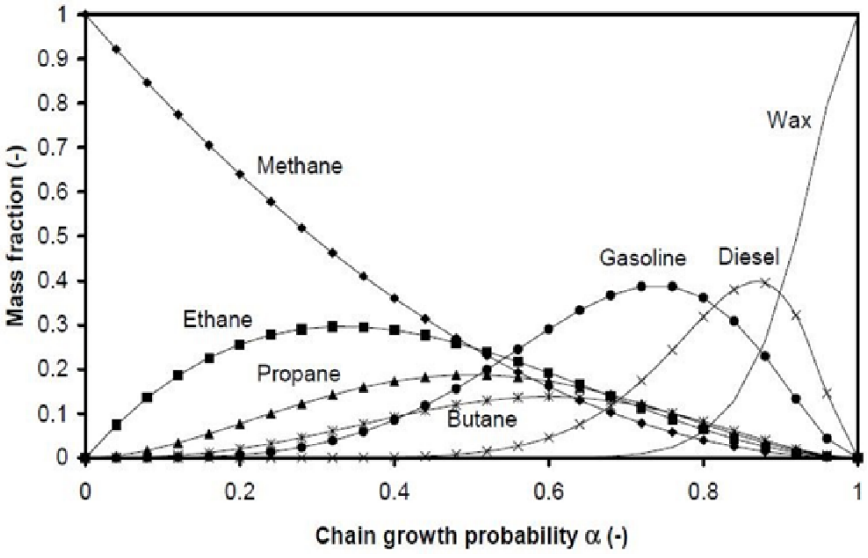

Figure 4. Products spectrum of FTS as a function of chain growth probability.

The Boudouard reaction is one crucial side reaction to be aware of and to avoid as carbon deposition can quickly full the catalyst and cause losses in time and expenses in new catalysts. Another adverse side reaction is FTS, where the principal product is CH_4 (or other light gaseous hydrocarbons C_1-C_4) as this is the starting material and is not wanted. Both the reformation of methane (via FTS) and the Boudouard reaction become problematic when the catalyst bed temperature is not managed correctly. Wide swings in catalyst bed temperatures and excessively high temperatures on the top portion of the catalyst bed can favor these side reactions and lead to attendant losses. Of course, the type and formulation of the catalyst is a critical factor in the performance of the FTS reactor. Catalyst performance depends on so many factors that elucidation of the optimum combination of properties is challenging. A review of the literature and our own experience shows that the following features are essential for supported metal catalysts in a packed tube reactor configuration. Assuming metal-oxide support is used (silica, alumina, or titania being the most common, a high surface area (100 – 200 m^2/g) and mesoporous structure (100 – 200 Å pores) give the best performance. These supports are impregnated with cobalt nitrate (at 10-30% cobalt by mass, 16% is typical), then calcined, and reduced in situ with hydrogen to give a highly dispersed cobalt metal on silica catalyst. The catalyst pellets should have a minimum 3 mm diameter in order to maintain an appropriate gas flow characteristic with reasonable pressure gradients. As the usable pellet surface area decreases with increasing size, pellet diameters in the 3-5 mm range is often optimal. Because of mass transfer limitations, a number of groups have shown that only the first 500

μm of catalyst support is vital for FTS of liquid hydrocarbons, as the core catalyst is mass starved and often too hot for high carbon number products.[17,18] Eggshell catalysts, in which only the first 500 μm of support is impregnated with active catalytic metals takes advantage of this to help reduce the unwanted reactions that generally occur further inside such a pellet.[18]

One factor frequently overlooked in FTS catalysts are the thermal properties of the catalyst. Silica, alumina, and titania supports have relatively poor thermal conductance and heat capacities. As the FTS reaction is very exothermic, local hot spots on an individual catalyst bead and radial temperature gradients within a packed catalyst bed can lead to a surprisingly large temperature differential (DT) in the reactor bed, often as high as 30 °C about the setpoint. As a is inversely proportional to temperature (i.e. more methane production at higher temperatures), Da is directly proportional to DT. If we aim to maximize production of the most valuable liquid hydrocarbon products an a of 0.85 is desired, as obtained from theory and this should be held as constant as possible across the entire reactor bed.

On the method to minimize DT in the reaction bed and therefore minimize a gradients, would be to use supports with good thermal conductance and high heat capacities. Towards this end, metallic foams and monoliths have been examined as catalyst supports.[19] While this modification reduces the magnitude of the DT, monoliths, and foams can exhibit relatively low vacant spaces (void volume) compared to high surface area solid supports, i.e. porous silica, alumina, and titania, which lowers the amount of catalyst available for the reaction per unit volume in the reactor.[20] Another solution is to use thermally conductive material such as

silicon carbide to mix with the catalyst.[21] Once loaded with cobalt, this catalyst showed improved FTS performance with higher C_{5+} selectivity. Lacroix et al.[22] compared the performance of foam FTS catalyst supports composed of alumina or of a silicon carbide composite after impregnation with cobalt. At CO conversion levels lower than 50%, the two catalysts display similar C_{5+} selectivity; however, when the CO conversion was increased to 70%, the C_{5+} selectivity of the silicon carbide foam supported catalyst was comparatively higher than alumina foam catalyst. Unfortunately, silicon carbide has comparatively lower surface areas than alumina or silica and costs considerably more.

Manipulating mesoporous catalyst carriers to exhibit desired characteristics such as maximizing surface area, tuning pore size, particle size and geometry, specific active sites, etc., is currently on the cusp between tailoring and design. It is shown that engineering in the required nanopore structure and properties can establish next-generation GTL processes. In addition to that, in the present investigation, we are trying to increase the overall thermal conductivity of the catalyst bed to maintain a semi-isothermal reaction condition within a catalyst particle and, therefore, throughout the bed.

Chapter 2

Synthetic preparation of large mesopore monolithic alumina for supported FT catalysis

2.1. Abstract

Powders with pore diameters and high specific surface areas invariably possess large pore volumes, and the resulting structure can be mechanically fragile. When necessary to fabricate these mesoporous aluminum oxides (MAs) into monolithic supports, such as spheres or pellets, the fabrication process can often cause to reduce the surface area or collapse and blind the pore structure, such that the desired textural properties are lost or result in mechanically fragile monoliths that crack and shatter under operational conditions. Pores are needed to minimize the challenging mass transfer kinetics of FTS but cannot be so large as to destabilize the solid support structural integrity when incorporated into a monolithic pellet or sphere. MAs prepared via the hydrolysis of aluminum isopropoxide with water or aqueous acid in various solvents, the presence or absence of several non-ionic polymer templating agents, and with or without autoclaving were explored and partially optimized to meet the support parameters for FTS outlined above. After calcination at 550 °C, the dominant crystalline phase was g-alumina, and nitrogen adsorption data revealed a wide range of textural properties. Hydrolysis of aluminum isopropoxide dissolved in toluene or IPA with water (6 H_2O/Al), in the presence of P123 templating polymer, and after autoclave treatment at 13 bar for xx h consistently yielded MAs with specific surface areas (S_A) in excess of 300 m^2/g, pore volumes (V_p) of 1.4 to 1.5 cm^3/g, and pore diameters (D_p) between 120 and 180 Å. Changing the hydrolyzing solution to 0.1 M nitric acid increased these

parameters to 340 m^2/g, 1.8 cm^3/g, and 190 Å. Replacement of the P123 with F127 (still using nitric acid) increased D_p to 210 Å but lessened the surface area to 233 m^2/g and V_p to 1.5 cm^3/g, respectively.

Further, optimization of the nitric acid, P123, autoclaved MA revealed that increasing the H_2O to Al from 5 to 7.5 consistently yielded MAs with D_p between 130 and 160 Å, V_p between 1and 1.4. Study of how the effect of different synthesizing parameters on the textural properties of the mesoporous aluminum oxide was investigated. Taking advantage of toluene as a solvent lead to the largest average pore diameter of 211 Å, while using tert-Butyl alcohol resulted in the smallest pore 50 Å. Furthermore, by combining some specific parameters, we can maximize the efficiency of using pore forming agents and consequently regulate textural parameters to the desired property and finally show how we can get the same properties with a non-templated synthesis method.

2.2. Introduction

The Fischer-Tropsch synthesis (FTS) of hydrocarbons and water from synthesis gas (typically hydrogen and carbon monoxide in a 2:1 molar ratio) could play a prominent role in the generation of carbon-neutral transportation fuels, i.e., naphtha, jet, and diesel fuels, assuming hydrogen becomes readily available from water-splitting technologies. For example, solar hydrogen could be used to reduce CO_2 to CO, mixed with additional hydrogen to make synthesis gas, and via FTS converted into liquid hydrocarbon transportation fuels, used traditionally. FTS is commonly performed using packed bed tubular reactors with a catalyst comprised of metallic iron or cobalt immobilized on silica, alumina, titania pellets, spheres, or related monoliths. For example, spherical balls with 3-5 mm diameters are reasonable choices as packing materials for a 1-3 cm diameter tube that can be up to 10 meters long, as the resulting void space allows for adequate flow at acceptable backpressures.

For maximum efficiency, the solid supports need to have a reasonable specific surface area (>100 m^2/g), and pore diameters in excess of 100 Å as the mass transport kinetics of the heavy hydrocarbon products are slow. Moreover, they must possess sufficient mechanical strength to prevent fracturing due to load or thermal fluctuations. For example, Zohdi[23] et al., in their investigation, studied the effect of mass transfer in fixed bed FT reactors which showed intraparticle mass diffusion will become a significant factor as it affects the Thiele module and, therefore, kinetic rates of the reactions in catalyst particle larger than 1.5 mm.

Khodakov et al.[24] examined pore size effects on FTS catalysis using cobalt on SBA-15, MCM-41, and commercial silica supports. They report that reaction rates and turnover frequency increased fivefold in the catalysts with 330 Å pores over those 20 Å pores. Moreover, the larger pore supports yielded more C_{5+} products. Additional interesting effects were attributed to the large pore diameters and volumes. In related studies, it was shown that the size of Co_3O_4 particles formed after deposition and calcination were proportional to the γ-alumina support pore diameter.[25,26] Saib[27] et al. showed in his study that the size of the cobalt crystallite size increased from 30 Å to 83 Å as the pore increased from 40 Å to 150 Å. Jung et al.[28] studied the effect of pore diameter on the performance of FTS over different silica supports and observed that by increasing pore diameter from 60 Å to 125 Å, CO conversion increased from 60% to 75.5 % meanwhile CO_2 selectivity reduced from 14% to 9% and also CH_4 selectivity reduced from 29.5 % to 19.8 % and C_{5+} selectivity increased from 55 % to 70 %. Ghampson[29] and coworkers demonstrated that the larger cobalt particles found in alumina support with larger pores (100 to 200 Å) were intrinsically more active catalysts. Their investigation on the effect of pore diameter on turnover of frequency (TOF) of the FT reaction revealed a linear relation up to a pore diameter of 130 Å.

The shaped (monolithic) catalyst supports in a macroscopic scale, maximizes the mass transfer rates of the reactant and product through the catalyst bed, and helps to provide accessibility of the reactant to the catalyst's activated surfaces minimizes the pressure drop along with the packed bed reactors. However, microscopically consisting of larger pore volume and pore diameter provides the

smoother mass diffusion for both reactants and products inside the catalyst particles. Depending on shaping technology, making catalyst spheres with adequate crushing strength and a uniform size could be more challenging if we deal with large pore monolith production. This challenge happens as micron-size particles bind together to form a paste. This process is occurring by adding acids, water, heating, and other chemical and physical requirements. During the shaping process of a highly textural alumina powder, it is expected that the initial properties will be subjected to some degree of changes, mainly decreasing. By peptizing the boehmite binder, it will bind with water, and other adjacent alumina particles that aggregate them all that whole dough becomes a smooth pseudo elastic mass before the extrusion. Although leading to having a high surface area support with high crushing strength, the pore size distribution is likely in the 40 to 80 Å range.[30] Therefore, as Euzen et al.[31] showed, with the addition of the acid, the pore volume is decreased due to the loss of larger pores. Pore diameter (P_d) and pore size distribution (PSD) get narrowed. Hence, it seems that peptizing is necessary to have a suitable mechanical property; however, it will be caused to losing some of the textural advantageous.[32]

We are interested in producing mesoporous alumina (MA) supports for FTS and set about determining the synthetic procedures needed to produce MAs optimized for FTS. Large pore Mam is also used in various catalytic applications, among them hydrodesulfurization (HDS) and hydroconversion and cracking of the large molecule residues require large pore supports. Saturation of the surface area,

especially in the central regions of the catalyst pellets and filled pore-mouth, is mentioned as the most common restriction which this obstruction has been decreased by using the enlarged pore size supports. Abasi-Halabi et al.[33] reported production of the unimodal large mesoporous pore alumina and its superiority compared with bimodal extrudates via the hydrothermal treatment of the alumina through autoclaving with ammonia vapor in 300 °C. It was discussed that a basic gas such as ammonia could enormously enhance the hydroxylation of alumina, therefore, enlarge the pores via Al-O-Al bond cleavage. However, the total pore volume of the catalyst remained constant (0.55-0.59 cm^3/g) volume of the pores in the 100 to 500 Å range decrease from 49 % to 18 % and the portion of the total volume for the pores with 500 to 1500 Å diameters boosted from 31 % to 73 %. Morel et al.[34] listed typical hydrotreating fixed bed catalyst properties, 1.2 to 6 mm diameter alumina spheres or extrudates with the surface area of 80 to 220 m^2/g and pore volume larger than 0.5 cm^3/g and pore diameter of 100 to 200 Å is a commonly used catalyst carrier.[35,36]

Commercially available monolithic mesoporous alumina (MAM) supports are provided in various phases, and surface characters as BASF provide alumina-based catalyst spheres with the surface area from 10 to 350 m^2/g with a pore volume of 0.5 cm^3/g. Sasol is commonly used as support in FT research, providing mesoporous alumina supports with surface area in 150 to 220 m^2/g ranges with a pore volume of 0.75 cm^3/g and average pore diameter of 60 to 70 Å. Saint-Gobain provides a high surface area (S_A) alumina support spheres ranging from 110 to 260 m^2/g with a pore volume of 0.55 to 1.05 cm^3/g and pore diameters ranging from 70

nm to 150 Å. They also supply high surface area silica spheres ranging from 160 to 250 m^2/g with a corresponding total pore volume of 0.6 to 1 cm^3/g and median pore diameter 110 to 120 Å.

Alumina is attractive because of its high thermal and chemical stability, amphoteric nature, and relatively low cost. Aluminum oxide is inherently mesoporous, but synthetic methods for producing high surface area and tuning pore diameter in specific ranges are challenging. The preparation of the relatively high surface area (200 m^2/g <) MA powder with a large average pore diameter (100-200 Å) is examined primarily based on sol-gel techniques and reported in different literatures[37–47]. MA mainly uses monolithic forms exclusively in plugged flow reactors to facilitate extra-pellet mass transfer and prevent pressure drop in a reactor. Therefore, the production of monolithic alumina bodies is developed through a variety of methods[48–53]. Granulation and oil-drop coagulation are the two most applied methods of choice for fabricating millimetric (0.5-10 mm) spherical bodies. Extrusion was the best technique for producing various shapes, while pelletizing is the technique for making the most tolerable tablets in heavy crushing forces applications.

In this study, we describe the preparation of MA powders found triple surface characters of MA powder drastically reduces through the process of fabricating to the monolith due to the using acidified solutions which destroying the larger pores, and MA powder loses the surface area multiple times calcinating and using additive as structural binders and strengtheners. Highly mechanical crushing strength is the additional requirement for having and stable monolith as in

adequate strength results in deformation and breakage and therefore increasing partial pressure of the reactor[4]. Therefore, finding a facile method of preparation monolithic MA particles in millimetric sizes with surface area higher than 200 m^2/g>, large pore volumes 0.7 cm^3/g> with high average pore diameter (9 Å to 16 Å) with narrow pore size distribution that possesses an adequate crushing strength is highly desired.

MA having these features will inherently possess macro pores and as of such can become structurally fragile as it reported in Subero et al.[54] studies that measured crushing strength of commercial alumina beads by Weibull's method, they concluded process parameters such as existing air bubbles, macropores, drying, calcining procedure and existing of multiple crystal phases of alumina and impurities are the root causes of losing mechanical strength. MA having these features will inherently possess large pore volumes and become structurally fragile, significantly as pore diameters exceed 300 Å.

Herein, we describe a parametric study of the effects of solvent, polymer templating agent, autoclaving, as well as the use of water, aqueous acetic acid, and nitric acid as gelation agents. Our primary target was a MA powder with a surface area over 300 m^2/g, pore diameters of 150 to 200 Å, and pore volumes between 1 and 1.5 cm^3/g. This type of support should retain its structural integrity while maximizing cobalt dispersion and cobalt island size while simultaneously minimizing the mass transfer limitations of the heavy hydrocarbons in the FTS process.

We are interested in producing monolithic 3-4 mm spheres of mesoporous alumina to support cobalt-based FT catalysts for use in a plug-flow reactor. We describe a parametric study of the effects of solvent, polymer templating agent, autoclaving, as well as the use of water, aqueous acetic acid, and nitric acid as gelation agents for the preparation of MA powders. Moreover, the processing of these powders into monolithic spheres is described, and the impact of this processing on the final textural properties of the solid support. Our target support would have a specific surface area, average pore volume, average pore diameter, and crush strength to match or beat some of the best-suited commercial mesoporous aluminas support for FTS. For example, if we limit these to supports with specific surface areas over 200 m^2/g, pore diameters in excess of 100 Å, and normalized (to 3 mm spheres) crush strengths of 25 N, only a handful of These include supports by Saint Gobain with was a MA with a surface area over 300 m2/g, pore diameters of 15 to 20 nm and pore volumes between 1 and 1.5 cm3/g. This type of support should retain structural integrity while maximizing cobalt dispersion and cobalt island size while simultaneously minimizing the mass transfer limitations of the heavy hydrocarbons in the FTS process.

2.3 Experimental

2.3.1 Materials and MA Synthesis

Aluminum isopropoxide, 98+% granular (AIP) was purchased from Alfa Aesar, Pluronic triblock copolymer (P-123) Sigma-Aldrich, Pluronic (F-127) Sigma-Aldrich, polyethylene glycol (PEG) with an average molecular weight of 900 Sigma-Aldrich, Glacial acetic acid 99.99+% (AA) Sigma-Aldrich, Nitric acid (NA) Fischer scientific, toluene (T) Macron, ethanol 200 proof from Decon, iso-propanol Fischer scientific, tert-Butanol +99.95% and 1-Octanol +99.95% Sigma-Aldrich.

Each synthesis consisted of some combination of dissolution of the reagents in various solvents, gelation by addition of water or aqueous acid, drying, autoclaving, and calcination. In cases where the sample was not autoclaved, the air-dried gel from the gelation step was crushed to a powder and directly calcined.

In order to describe the various steps, a detailed procedure for the preparation of one mesoporous aluminum oxide, identified as MA-T-P123-N-AC, is described in detail. In addition, the sample label describes many of the processing parameters. For example, MA indicates mesoporous aluminum oxide; the T indicates toluene was the solvent used in the gelation step; P123 indicates that the Pluronic triblock copolymer (P123) was used as the templating agent during the gelation step; N indicates that the gelation was initiated with 0.1 M nitric acid

solution, and AC indicates that the gel was treated in an autoclave prior to calcination.

2.3.2 Preparation of MA-T-P123-N-AC

A homogeneous solution of 50 g (0.20 mol) aluminum isopropoxide dissolved in 50 mL of toluene was prepared simply by mixing and stirring (The dissolution of AIP in alcohols often required some heating to obtain a homogeneous solution). Separately, a solution of 25 g P-123 dissolved in 50 mL IPA was obtained by gently stirring and heating the mixture at 60 °C for ~12 h. Additional IPA was added to make up for evaporated IPA during this time. The resulting clear solution was poured into the aluminum isopropoxide solution and stirred for 6 h at 60 °C. At this point, 27 mL 0.1 M HNO_3 was added with vigorous stirring, and within minutes a thick gel formed. The sample was left to stand at room temperature for 24 h during which the gel monolith shrank in size and is immersed in the solvent. The excess solvent was removed by decanting, and the resulting gel was crushed and left to air dry for 24 h. For autoclaving, the gel was placed in an Erlenmeyer flask and inserted into an 8 L Parr steel pressure vessel containing enough water (about 55 to 60 mL) to reach the desired pressure of 13 bar at 170 °C. The vessel was then closed and evacuated with a rough pump to remove most of the air present. Once the vessel was sealed, the autoclave heating program was as follows: 25 °C to 120 °C at 10 °C/min, stand for 3 hours at 120 °C, ramp at 1 °C/min to 150 °C, stand at 150 °C for 7 hours, ramp at 1 °C/min to 170 °C, stand for 12 h during which the maximum pressure observed was ~ 13 bar. The heating is turned off to cool, and the vessel allowed to return to room temperature over several hours, then

vented, and the product gel removed. The resulting gel was then air-dried and calcined in a temperature-programmed oven. The calcination program was as follows: room temperature to 150 °C at 10 °C/min, stand 30 min at 150 °C, ramp at 1 °C /min to 250 °C, stand at 250 °C for 1 h, ramp at 1 °C /min to 350 °C, stand at 350 °C for 1 h, ramp at 1 °C /min to 450 °C, stand at 450 °C for 1 h, ramp to 550 °C, stand at 550 °C for 5 h, slow cool to room temperature over 8 h.

Other MAOs were prepared in similar manners in which the gelation solvent, templating agent, peptizing agent, and autoclaving were varied or omitted.

2.3.3 Reparation of boehmite

the autoclave heating program was as follows: 25 °C to 120 °C at 10 °C/min, stand for 3 hours at 120 °C, ramp at 1 °C/min to 150 °C, stand at 150 °C for 7 hours, ramp at 1 °C/min to 170 °C, stand for 12 h during which

The boehmite powder was prepared with the similar method as described for the preparation of the MA-T-P123-N-AC, but a prolonged autoclaving method was conducted as follows: 25 °C to 120 °C at 10 °C/min, stand for 3 hours at 120 °C, ramp at 1 °C/min to 150 °C, stand at 150 °C for 7 hours, ramp at 1 °C/min to 170 °C, stand for 12 h, finally ramp at 1 °C/min to 220 °C, stand for 24 h during which the maximum pressure observed was ~ 13 bar. Then, the sample cools down to room temperature, and pressure decreased consecutively for 8 hours period. The obtained boehmite was then dried at 200 °C under air for 5 hours. Then the powder was grounded and sieved with mesh number 200 to obtain a dried boehmite powder with the particle size of 75 < microns and stored in a sealed container.

2.3.4. Preparation of spherical mesoporous alumina monoliths (MAMs)

Monolithic catalyst supports comprised of 3-4 mm spheres or cylinders are made from the MA powder described previously in combination with a binder (typically boehmite) and rheological additives as plasticizers, such as triethylene glycol (TEG). To have a desired crushing strength monolith, the addition of sole water will not be sufficient. Therefore, nitric, formic, and acetic acid are the preferable peptizing agents for making a stronger monolith. [55–57]

In a typical procedure for the production of spheres, 10 g boehmite ($Al(OH)_3$) and 40 g MA powder are thoroughly mixed and ground together before sieving through a 200-mesh sieve to ensure particle sizes < 75 micrometers. This powder is added ~40 mL of aqueous nitric acid (2% or 5%) or ammonium hydroxide (2% or 5%), and the mixture is stirred to make a gelatinous paste. The volume of acid or base is estimated from the pore volumes of the MA and boehmite powders and adjusted as needed to form a dough-like paste. The dough in some cases, is further refined by the addition of 4 mL (5 g) of TEG plasticizer. The resulting dough ball is kneaded for ~ 20 min, during which small additions of aqueous acid or base are added to keep the ball moist. When the resulting 'dough' has the rheology of Play-doh, the dough must be stiff but with a plastic property that has a constant flow threshold when it is ready for extrusion. The paste was extruded through a die template with 3.7 mm holes to form a spaghetti-like mass laid flat and cut at ~ 4 mm intervals. The still moist pellets are then loaded onto a boilie roller rack with an internal diameter of 3.7 mm. Reciprocating the top rack

of the boilie roller rack converts the pellets to spheres, which are then collected into a large beaker, covered with a watch glass, and allowed to dry over 48 h slowly. After this initial drying, the spheres are transferred to an oven and dried under a nitrogen atmosphere for 12 h at 85 C. The spheres are then calcined at 555 °C with a 10 °C/min ramp under 60 mL/min flow of the helium gas for 5 hours to yield the desired mesoporous alumina monolith spheres (MAM) having an average diameter of 3.1 ± 0.15 mm. In the present work, the boehmite's textural properties were S_A 318 m^2/g, V_p ~1.3 cm^3/g, D_p 120 Å. It is worth mentioning that using 100% boehmite as alumina source for monolith preparation leads to low textural characters.

2.3. MA Characterization

Thermogravimetry and differential thermal analysis (TG-DTA) was performed on the synthesized powder to determine the decomposition mass loss characteristics during calcination using a thermogravimetric analyzer (SDT Q600, TA Instrument), operating in the air flow of (100 mL/min) with a heating rate of 5 °C/min under air (20 cm^3/min) from 50 to 800 °C.

Textural properties of the MAs were determined from the nitrogen sorption isotherms obtained using a Tristar II volumetric analyzer (Micromeritics Co. Ltd). Samples were degassed at 160 °C under a nitrogen flow of 20 mL/min for 12 hours prior to the measurements. The specific surface area (S_A) was calculated by the Brunauner–Emmett–Teller (BET) method, using a P/P_0 range between 0.05 and 0.30.[58]. The total pore volume (V_p) and pore size distribution (PSD) were determined from the desorption isotherm at the relative pressure of 0.990 based on Barrett, Joyner, Halenda (BJH) model. The total pore volume (Vp) is derived from the BJH desorption cumulative volume of pores between 17.0 Å and 3000.0 Å diameter. The pore size, $D_{p,}$ is the pore diameter at the peak position of the PSD curve derived from the adsorption branch of the isotherm using the BJH method.

X-ray diffraction (XRD) data were obtained using a Bruker Advance-D8 powder diffractometer, using monochromatized Cu K_α radiation (λ = 1.54056 ˚A), and operated at 40 kV and 40 mA. The diffraction data were recorded between 2θ = 15° and 80° with an increment of 0.02° and step speed of 1 deg/sec. Crystallite phases were determined by comparing the diffraction patterns with those in the standard powder XRD patterns.

The average crushing strength of the monolithic catalyst spheres was measured based on ASTM (D4179) method by Shimadzu Precision Universal - tensile/crush tester. The compression test was carried out on a minimum of 10 single catalyst particles of each type by applying an axial force at a uniform rate of 1.0 N/sec until the catalyst particle crushes or collapses. Prior of each test, all catalyst samples were degassed under nitrogen at 120 °C for 2 hours and kept in a sealed vial.

2.4. Results and Discussion

2.4.1. General Features of the calcination product

The powder XRD patterns of the mesoporous alumina powder (sample NMA-I-N-AC-800-7.5) shown in Figure 5. It reveals that the seven most intense peaks would be indexed to the (1 1 1), (2 2 0), (3 1 1), (2 2 2), (4 0 0), (5 1 1), (4 4 0) reflections of ordered mesoporous γ-alumina with crystalline walls that prepared at 800°C.

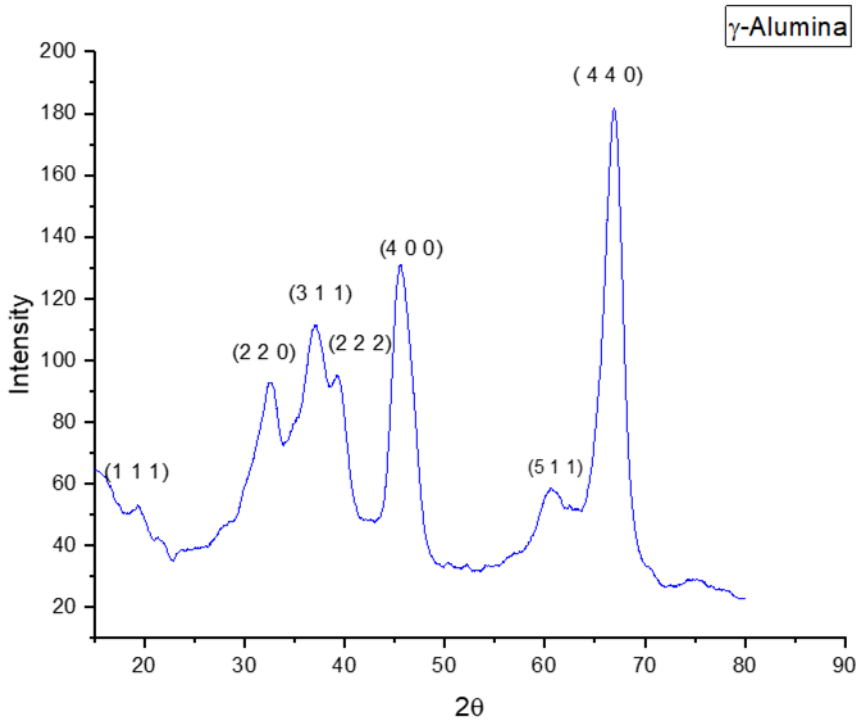

Figure 5. X-ray diffraction of the NMA-I-N-AC-800-7.5 alumina sample determining the γ-alumina phase.

The thermal decomposition of the synthesized boehmite γ-AlOOH was examined in figure 6. TG/DTG curves are showing two steps of the weight loss at

different temperatures, after initial weight loss due to the evaporation of the water, which is attributable to the loss of physical surface adsorbed water highest weight losses occurred at 410 °C, which is about 15% and based on TG curve analysis at 555 °C it shows the maximum weight loss 22%.

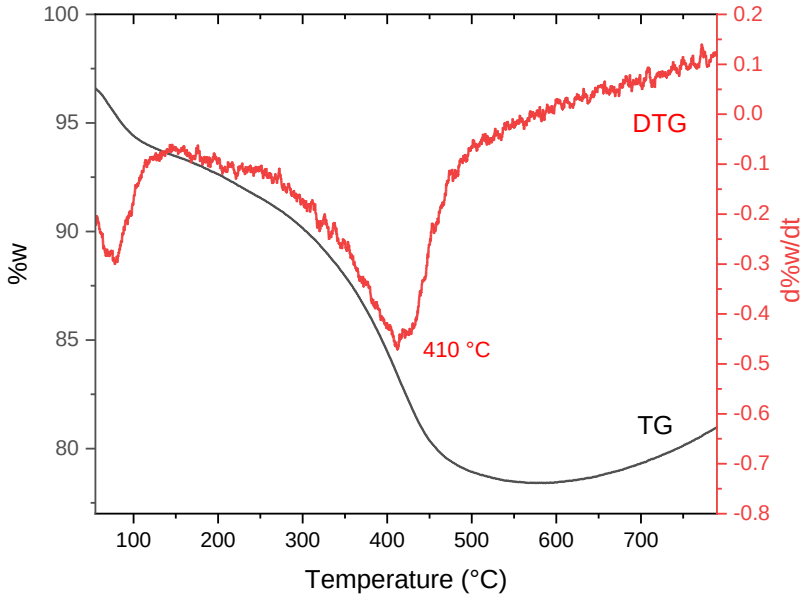

Figure 6. TG/DTG curves showing the percent weight loss rate of the synthesized boehmite.

Thermal decomposition of the synthesized boehmite γ-AlOOH (is this the gel prior to calcination??? Which sample specifically…do all gels give substantially similar TGA profiles??) was examined in the fig. xx. TG/DTG curves is showing two steps of the weight loss at different temperatures, after initial weight loss due to the evaporation of the water which is attributable to the loss of physical surface adsorbed water highest weight losses occurred at 410 °C which is about

15% and based on TG curve analysis at 555 °C it shows the maximum weight loss 22%.

2.4.2. Solvent and template effects on MAO

Hydrolysis and subsequent condensation polymerization of a non-aqueous solution of aluminum isopropoxide by addition of water or aqueous acids is a classic method for preparing a gel composed of an unorganized network of □-oxo and □-hydroxo aluminum (III) cross linked polymers. Prior to calcination, this gelatinous phase is frequently referred to as an alcogel, which given enough time to dry and age becomes γ-Al(O)OH or boehmite. AIP is freely soluble in toluene but often requires long times and heating to obtain a clear solution in alcoholic solvents. In order to examine how the dissolution solvent impacts the textural properties of the MA in the absence of a template, we prepared MAs from the using the following solvents to dissolve the AIP: ethanol (E), isopropanol (I), t-butyl alcohol (B), 1-octanol (O), or toluene (T).

All the MAs were first prepared as dried alcogels and the slow and stepwise calcination program, as described in the experimental, which is designed to first transition to boehmite (150 to 250 C) without losing the mesoporosity and ultimately transition to g alumina after finishing at 555 C. The nitrogen adsorption-desorption isotherms for calcined samples MA-E through MA-T are overlaid in Figure 3A. All exhibit type IV isotherms with the isotherms for MA-I, MA-O, and

MA-T falling into the H1 classification (cylindrical pores) whereas MA-E and MA-B show H3 type hysteresis (slit shape pores). Specific surface area (SA) was determined using the BET analysis of the isotherms and ranged from 180 and 470 m^2/g for the powders. BJH pore volume and diameters ranged from 0.51 to 0.90 cm^3/g. As seen in the PSD plots shown in Figure 3B, average D_p ranged from 48 to 100 Å. The textural properties for the MA powders are collected in Table 2.

Table 2. Structural parameters of MA samples using different solvents and calcined at 555 °C.

Sample	BET surface area	BJH total pore volume	BJH average pore diameter
	m^2/g	cm^3/g	$Å$
MA-E	428	0.51	48
MA-I	466	0.9	69
MA-B	482	0.47	50
MA-O	290	0.28	66
MA-T	182	0.6	100

MA-I, prepared with isopropanol, produces a MA with high surface area (466 m^2/g), relatively uniform mesopores with an average diameter of 69 A and the largest V_p at 0.9 cm^3/g of the group. MA-T has the smallest SA (190 m^2/g) but yields a substantially larger and broader pore size distribution, as seen in Figure 2B. D_p range from 50 to 150 Å, with a maxima at ~100 Å. Despite the loss in SA, MA-T has the second highest V_p at 0.6 cm^3/g. The other solvents gave MAs with intermediate SAs (200 to 400 m^2/cm) but with lower pore volume and diameters.

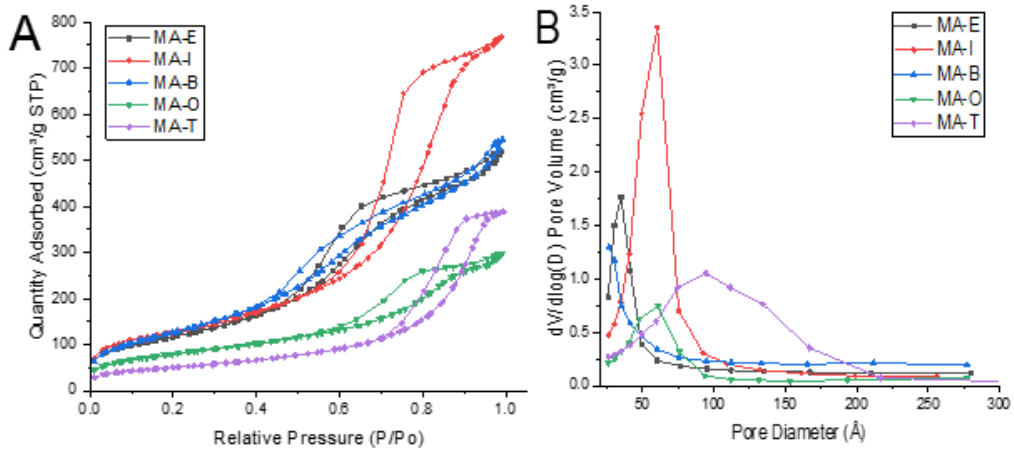

Figure 7. A) N2 adsorption-desorption isotherms of MAPs synthesized with different solvents. B) Pore size distribution (PSD) of the MAPs synthesized by various solvents.

2.4.3. P123- Templating effect

Addition of the templating polymer, P123, to each of these preparations increases the pore volume and average D_p, regardless of the solvent. Significantly, many of the MAs now have average D_p >100 Å and TPV near 1 cm^3/g or more. The PSD plots, shown in Figure 4B, show the increase in D_p and a broadening of the pore sizes. Surface areas were more consistent, coming between 300 and 400 m^2/g for all samples. The template had the biggest impact on the textural properties of MA-T-P123 over MA-T. The SA increased to 321 from 182 m2/g, pore volume doubled to 1.23 cm3/g, and D_p ranged from 60 to 220 A peaking at 141 Å. This preparation was repeated using the polymer F127 as the templating agent yielding MA-T-F127 which possessed similar SA, pore volume and a slight decrease in the average pore diameter (110 A) relative to MA-T-P123. When the water is replaced with 0.1M nitric acid as the gelation agent, the speed of gelation increases and the resulting product MA-T. The textural properties of the template-assist synthesized

MAs are listed in table 3. and figure 8.A. shows the different isotherms derived from each sample. The effect of using P123 on pore size distribution of the MAs are shown in figure 8.B.

Table 3. Textural parameters of templated MA samples using different solvents synthesised with P123 as pore forming agent and calcined at 555 °C.

Sample	BET surface area	BJH total pore volume	BJH average pore diameter
	m^2/g	cm^3/g	$Å$
MA-E-P123	372	0.56	61
MA-I-P123	302	1.11	113
MA-B-P123	370	0.93	91
MA-O-P123	316	0.86	102
MA-T-P123	321	1.23	141

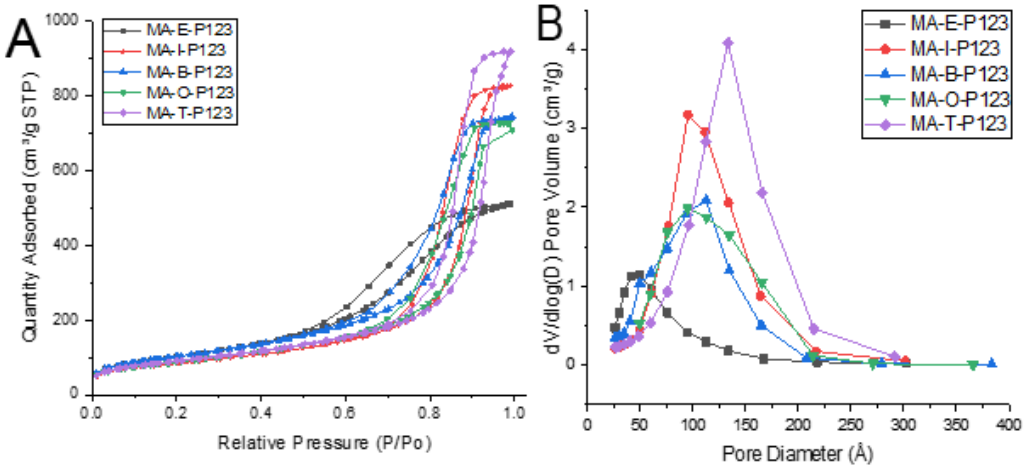

Figure 8. A) N_2 adsorption-desorption isotherms of the templated MAPs synthesized with different solvents and. B) Pore size distribution (PSD) of the templated MAPs synthesized by various solvents.

2.4.3. Autoclaving

There is complimentary linkage between boehmite synthesis condition and tuning the alumina porosity.[31] Creation of the large mesopores are mostly due to of formation of voids between randomly stacked crystallites.[59] Marvin, Johnson and Mooi[60] during their investigation about origin of pores in alumina catalysts found that there is a correlation between the size of boehmite crystallite along the [021] axis and pore diameter of the calcinated alumina. developing of such highly crystalline mineral requires a prolonged aging process. However, aging of boehmite and pseud-boehmite was studied by Ono et al.[61] ana Papee et al.[62] it is been reported that autoclaving is delicate to handle to production of highly crystalline boehmite whereas reduces H_2O to Al molar ratio from 1.6 to 1.12 consecutively surface area decreases from 308 to 189 m2/g and crystallites medium size increases from 60 to 100 Å.

Next, we investigated the effect of hydrothermal autoclaving of the alcogel as a method to improve the textural properties of the MA product. The intermediate temperatures and high partial pressure of H_2O experienced during autoclaving are thought to accelerate the transition to boehmite and is reported to increase the gel pore volume and diameters.[63] Bauer showed that aluminum trihydrate (gibbsite) proceeds smoothly to gelatinous microcrystalline of boehmite upon autoclaving at pressure of less than 200 psi and the temperatures < 200 °C.[63] Our data revealed a substantial improvement in the MA pore volume and pore diameter with minimal impact on SA. The alcogels generated for MA-E-P123 through MA-T-P123 were

subjected to 48 hours autoclaving during which the partial pressure of water varied from 85 to 190 psi as the vessel was slowly heated (1 °C /min) from 130 to 170 °C. The resulting MA samples are labelled MA-E-P123-AC through MA-T-P123-AC. As seen in Figure 5A and B and the data in Table 1, the surface areas of the autoclaved MAs fall between 282 and 340 m2/g, representing a small decrease from the non-autoclaved samples, but a tighter distribution of SAs. Most notable is the substantial increase in pore volume and diameters for all samples, excepting MA-B-P123-AC and MA-O-P123-AC. The MAs prepared from isopropanol and toluene have the most promising textural properties with pore volumes of 1.52 and 1.44 cm3/g and peak pore diameters of 220 and 180 A, respectively. The PSD plots reveal a narrower PSD for MA-T-P123-AC and a very large PSD for MA-I-P123-AC, ranging from 50 to 400 Å. The effect of autoclaving on textural properties of the various MAs are listed in table 4.

Table 4. Textural parameters of autoclaved MA samples with various solvents synthesised with P123 as pore forming agent and calcined at 555 °C.

Sample ID	BET surface area	BJH total pore volume	BJH average pore diameter
	m^2/g	cm^3/g	*Å*
MA-E-P123-AC	282	0.79	108
MA-I-P123-AC	337	1.52	128
MA-B-P123-AC	312	0.77	93
MA-O-P123-AC	298	0.93	117
MA-T-P123-AC	300	1.44	180

We observe substantial increases in the average of the V_p's, and D_p's for the MAs made with all five solvents for each progression: non-templated to polymer

templated synthesis (Avg V_p increase from 0.5 to 0.9 cm3/g; Avg D_p increases from 66 to 100 Å) and then polymer templated synthesis to autoclave treatment of the templated alcogels (Avg Vp increase from 0.9 to 1.1 cm^3/g; Avg D_p increases from 100 to 145 Å), demonstrating definite improvements in mesoporosity. Figure 9.A. shows the related isotherms for autoclaved sampes. Figure 9.B. shows the effect of autoclaving on improving the pore size distribution of the samples.

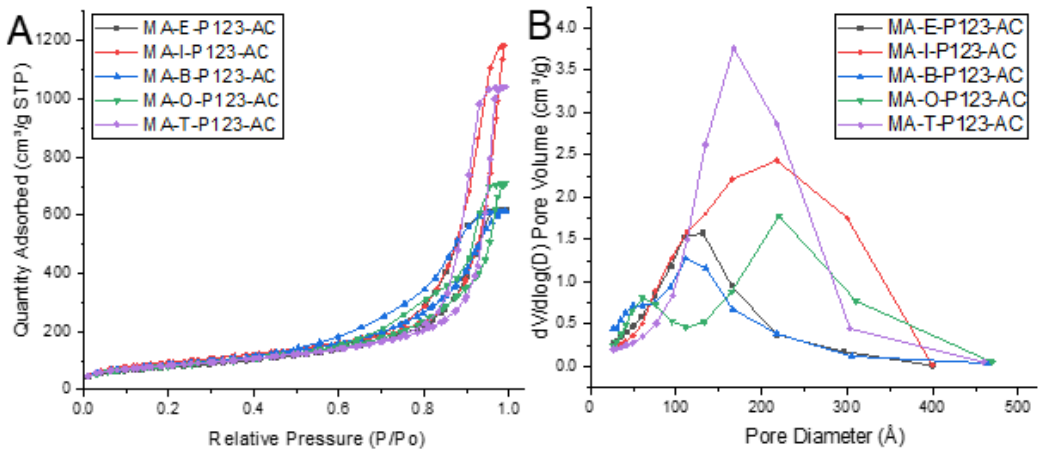

Figure 9. A) N_2 adsorption-desorption isotherms of the Autoclaved-templated MAPs synthesized with different solvents and. B) Pore size distribution (PSD) of the related MAPs.

At this point, it is clear that isopropanol and toluene are the two best solvents for the MA synthesis in terms of mesoporosity. We decided to attempt to further optimize the MA-T system by examining different templating polymers and enhancing the gelation rate by substitution acidic aqueous solutions for water in the polymerization/gelation step. These results are collected in Table 5. Simply changing the gelling agent from water to 0.1 M acetic acid or 0.1 M nitric acid considerably accelerated the rate of gelation, as is expected by shifting the pH downwards.

On different templates in presence of the toluene was studied. As shown in figure x, despite applying PEG enlarged the surface area close to 453 m2/g, after autoclaving it reduced to 356 m2/g followed by increase in pore volume and pore diameter. Using F123 and P123 resulted with the same surface area (300 m2/g) but larger average pore diameter close to 180 Å in P123 case.

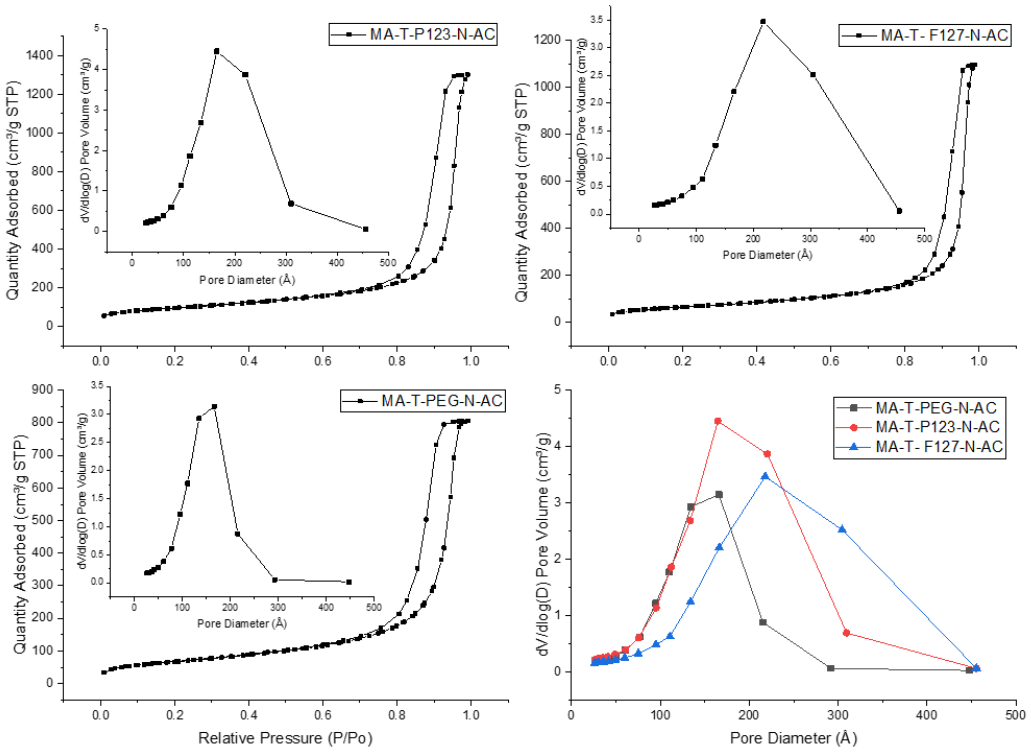

Figure 10. N_2 isotherms and PSD plots of MAs prepared by different pore forming agents using toluene as solvent and peptized by nitric acid solution, all samples were autoclaved prior to calcinaation at 555 °C.

Table 5. Nitrogen adsobtion of MA samples using toluene as solvent and vaying pore forming agents and peptizing.

Sample ID	BET surface area	BJH total pore volume	BJH average pore diameter
	m^2/g	cm^3/g	$\AA$
MA-T-PEG	453	0.91	89
MA-T-PEG-AC	356	1	112
MA-T-PEG-N-AC	242	1.11	158
MA-T-P123	321	1.23	141
MA-T-P123-AC	300	1.44	180
MA-T-P123-N-AC	340	1.82	190
MA-T-F127	330	1.12	110
MA-T- F127-AC	300	1.56	157
MA-T- F127-N-AC	233	1.53	211

The isopropoxide provides three equivalents of base and the process faster than when hydrolysis is conducted with aqueous acid (0.1 M HNO3 and 0.1 M HOAc) -oxides, hydroxides, and the sol-gel synthesis of MA is Somebody reported that mesoporous alumina with large pore volumes and good overall surface area is obtained via hydrolysis of Al alkoxides in alcoholic solvents. We first examined the synthesis of MA using the hydrolysis of aluminum (III) isopropoxide in four different alcohols of increasing lipophilicity with and without a nonionic polymer template using the sol-gel method. The molar ratio of water to aluminum was fixed at 6:1 and the gel isolated from the excess disperser (alcohol or toluene), dried and calcined by slow heating (1C/min) from room temperature to 555 °C and then maintained at 555 C for 5 h. A typical isotherm for these MA's is shown in Figure 7. and could be classified as a type IV isotherm with different hysteresis loop, excepting that there is almost no microporosity observed. From the figure above

regardless of pore forming agent type, regardless of nonionic template type, evacuation of the xerogel leads to a significant increase in formation of the wider pores in (the pore range between 100- 270 Å). (in case of samples with P123 the range is 120-460 Å)

We found an increase in pore size followed by decreasing in surface area in autoclaved samples in the order of EtOH>T>IPA>1OA>TBA. Among them, MA-E-P123-AC reached to 108 Å, 0.79 cc/L with 282 m^2/g surface area, represent 77% increase in average pore diameter and 30% increase in pore volume but 24% decrease in surface area. Meanwhile, in MA-I-P123-AC case a marginal increase in all indices observed. In all cases a cylindrical shaped pore demonstrated from their isotherm however, IPA showed a broader and both TBA and 1OA demonstrated a bi-modal PSD which is shown in the figure 7.

In another approach utilizing toluene as solvent speeded up the process without necessity of heating. The results are shown in the table 4. indicates that in MA-T-P123-AC using toluene instead of alcohols shifted average pore diameter by 52 Å to the larger pores in compare to the MA-I-P123-AC which was the largest pore diameter using alcohols.

Effects of nitric acid as a peptizing agent on nitrogen adsorption isotherms and the PSD of MA are shown in figure 10. As can be seen in these figures, regardless of pore forming polymer the IV type isotherm with H1 loop was

confirmed cylindrical shape pores. Hydrolyzing the aluminum precursors with 0.1 M nitric acid increased the average pore diameter in all cases but has different effect on surface area. In P123 surface are, pore volume and pore diameter increased, while in PEG and F127 surface area and deceased and in F127 it maximized the average pore diameter to 211 Å.

Synthesis of the MA in absent of pore forming agent is studied and effect of various combination of different peptizing agents in IPA and Toluene solvent with different water to aluminum molar ratios is provided. The textural parameters derived from nitrogen isotherms are summarized in table 6. Results confirm that, hydrolyzing the sample with 0.1 M acetic acid increases the pore diameter by almost two folds from 85 Å to 157 Å in compare with hydrolyzing with water. Almost same increase happens in case of with and without autoclaving. Using IPA exhibited a high surface area of 325 m^2/g in compare with 251 m^2/g of toluene while average pore diameter and total pore volume in both cases had close values. Peptizing with 0.1 M acetic acid can increase the pore diameter by 16 % and 10% total pore volume in compare with nitric acid with the marginally close surface area 330 m^2/g if IPA be the solvent the differences were respectively 13 % and 14 % with 22% shrinkage of surface area in toluene case. It is also shown that by increasing molar ratio of water over aluminum from 2 to 5 then 7.5 and finally 12 the surface area continuously increases from 295 to 325 then 333 and 406. However, 5:1 molar ratio gives the maximum pore diameter of 157 Å.

2.4.4. Peptizing

Numerous studies have demonstrated the feasibility of the influence on hydrolysis and condensation rates via implementation of the synthesis parameters such as varying pH, H_2O/Al ratios, aging condition, and calcining temperature … in previous section we examined the aging condition with autoclaving of the obtained gel for boehmite production. In the following section we examined the acceleration of the hydrolysis/condensation rate by peptizing of the Al precursor with acidic solutions. Series of mesoporous aluminum oxide samples were synthesized in the same method that is mentioned in the toluene solvent subsection (2.2) except hydrolyzed with 0.1 molars nitric acid rather than DI water which resulted to create a significant increase in pore volume before larger pore diameter. In this work, the hydrolysis with an acidic solution is called peptizing. Peptizing with the acidic solution leads to a very fast hydrolysis that consists of relatively smaller crystallites with a certain reticulated structure and network.[64]

2.4.5. Non-templated synthesis

We tried a synthesis method in the absence of typical pore forming agents. Herein, 100 grams of AIP was dissolved in 90 grams IPA or toluene (if IPA its necessary to heated at 85 °C but not in toluene case) then samples were peptized with different amount of (H_2O/Al molar ratios H_2O/Al:2 equal to 18 grams, H_2O/Al:5 equal to 45 grams, H_2O/Al:7.5 equal to 67grams, H_2O/Al:12 equal to 108 grams) get hydrolyzed with DI water or 0.1 molars nitric acid or 0.1 M acetic acid solution dropwise added till a thick gel formed. The alcogel kept at room temperature for 24 hours then excess alcohol/toluene decanted then it kept in the hood to let rest of the alcohol vaporize (so call it a wet gel) then wet gel transferred in a proper container and autoclaved at 85-190 psi pressure and 120-170 °C for 48 hours. Then xerogel cooled down and depressurized slowly for the next (3^{rd}) day in autoclaving chamber (autoclave pressure maintains with addition of water in autoclave chamber). Finally, samples calcined with a ramp of 1 °C/min up to 555°C for 5 hours to create a pure mesoporous gamma-alumina.

Furnace program is as follows: Room temperature to 150°C with ramp of 10°C/min and keep it for 30 minutes. Then, heat up to 250°C with a 1°C/min then keep it 1 hour then with the same method sample step by step calcined 350°C and °450°C and final temperature is 555°C and keep it for 5 hours. Then let it cool down to 400°C in 3 hours and in the end to room temperature in 5 hours.

Table 6. Textural characters ofnon-templated MA samples varying the synthesis parameters.

Sample ID	BET surface area m^2/g	BJH total pore volume cm^3/g	BJH average pore diameter Å	H_2O/Al
MA-I-2A-AC-555	295	0.69	75	2
MA-I-5A-AC-555	325	1.6	157	5
MA-I-7.5A-AC-555	333	1.57	153	7.5
MA-I-12A-AC-555	406	1.41	120	12
MA-I-7.5N-AC-555	327	1.42	132	7.5
MA-I-7.5N-AC-800	218	1.14	163	7.5
MA-I-5A-AC-420	437	1.5	111	5
MA-I-5W-AC-555	372	1.42	85	5
MA-I-5A-555	369	0.92	91	5
MA-T-5N-AC-555	260	1.37	133	5
MA-T-5A-AC-555	251	1.57	150	5

The importance of the H_2O/Al molar ratio and how optimized hydrolysis can significantly boost the quality of the pores is shown in Figure 11. Despite the average of the BJH pore volume and pore diameter of the sample with $H_2O/Al = 5$ (green graph) is a little bit larger than the sample with $H_2O/Al = 7.5$ (blue), the sample with $H_2O/Al = 7.5$ has higher incremental pore volume in the pores wither than 160 Å. Figure 11 indicates that pores larger than 160 have a higher surface area in graph comparing to others.

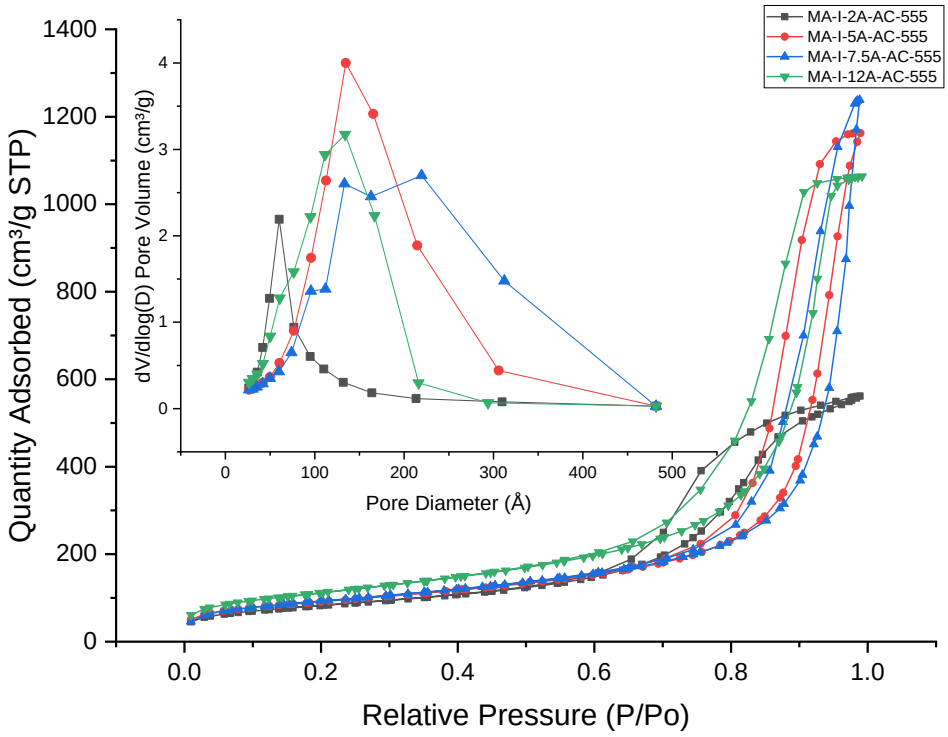

Figure 11. N_2 adsorption-desorption Isotherms and BJH Desorption Incremental BJH Desorption dV/dlog(D) Pore Volume vs. Pore Distribution comparing different H2O:Al molar ratios- all samples hydrolyzed with 0.1 molars acetic acid and then autoclave treated and finally calcined at 555°C.

A series of samples were prepared to vary H_2O/Al molar ratios by the non-templated method described previously IPA was used as the corresponding solvent, peptized with 1 M acetic acid solution. All boehmite made by autoclaving of the dried gel, and finally, all samples were calcined gradually heating from room temperature to 555 °C at 1 °C/min and soaked at 555 °C for 5 hours, finally allowed the sample to cool to room temperature over 4 hours in the furnace. The textural properties of the obtained samples with H_2O/Al molar ratios varying from 2,5,7.5, 12 were then investigated using N_2 adsorption method. It is well known that at H_2O/Al <10, solely boehmite (γ-AlOOH) will be produced. The boehmite is crystalline with an fcc sublattice that could form a high surface area with suitable textural properties γ-Al_2O_3 (tetragonal) type by controlled calcination between 400

°C to 800 °C.[31] By increasing H_2O/Al molar ratios, the other classes of aluminum compounds will create such as bayerite α-$Al(OH)_3$ or gibbsite γ-$Al(OH)_3$.[31,65]

The importance of the H_2O/Al molar ratio and how optimized hydrolysis can significantly boost the quality of the pores is shown in figure 11. From a textural point of view, It is evident that by increasing H_2O/Al molar rations from 2 to 5 the resulted surface area improves from 295 to 325 m^2/g, both total pore volume and average pore diameter enlarged from 0.69 to 1.60 cm^3/g and 75 to 157 Å, respectively. Despite the average of the BJH pore volume and pore diameter of the sample with H_2O/Al = 5 (green graph) is a little bit larger than the sample with H_2O/Al = 7.5 (blue), the sample with H_2O/Al = 7.5 has higher incremental pore volume in the pores wider than 160 Å. Figure xx indicates that pores larger than 160 Å have a higher surface area in the blue graph comparing to others. An increase in surface area from 333 to 406 m^2/g happened with a steep loss of both pore volume and pore diameter associated with increasing H2O/Al ratios from 7.5 to 12, which it probably caused by forming the bayerite along with boehmite in excess of the water.

We decided to investigate two other parameters on non-templated samples by picking the MA-I-7.5A-AC-555 formulation as a candidate with an optimum textural property. In the first step, we prepared the same sample formulation but used 0.1 M nitric acid rather than acetic acid to investigate the effect of different acids on the resulting alumina's textural properties and labeled it as MA-I-7.5N-AC-555. Using nitric acid, we face a marginal decrease in all tripled textural indexes listed as follows: 327 m^2/g, 1.42 cm^3/g, and 132 Å. The second parameter

that we studied was the calcination temperature of the boehmite in which we divided the MA-I-7.5 N-AC boehmite into two portions and calcined them with 555 °C and 800 °C and labeled the former as MA-I-7.5N-AC-800. by comparing two samples, a steeped decrease in surface area 218 m^2/g and a marginal decrease in pore volume (1.14 cm^3/g) of the sample calcined at higher temperature reported along with a 23 % increase in average pore diameter from 132 to 163 Å was shown as expected. In a separate attempt, we prepared a sample with the same formulation as MA-I-5A-AC-555, but we calcined it at the lower temperature of 420 °C and labeled it as MA-I-5A-AC-420. Herein, we observed an increase in surface area from 325 to 437 m2/g in a sample calcined at 400 °C and a marginal decrease in pore volume from 1.60 cm^3/g down to 1.50 cm^3/g and loose of pore diameter from 157 to 111 Å.

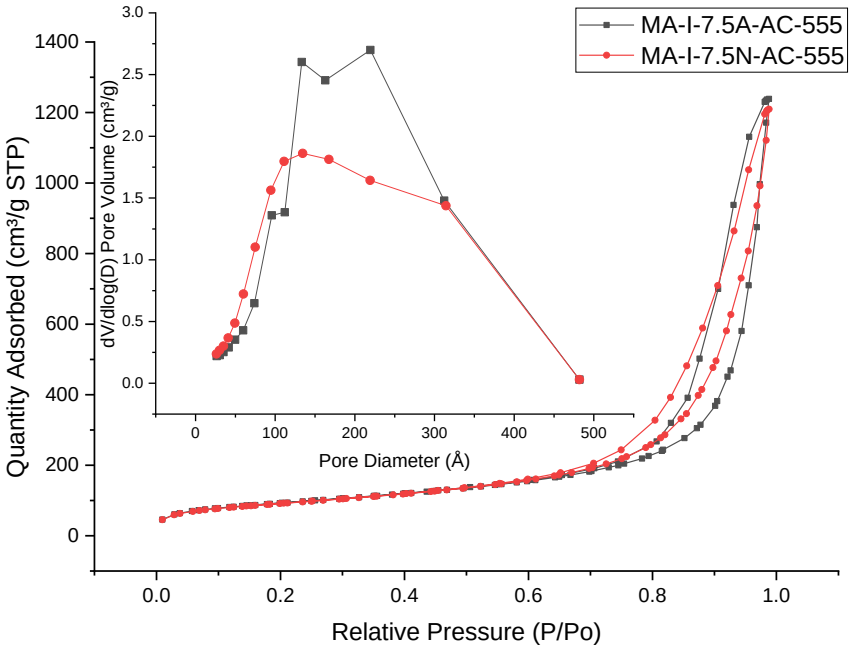

Figure 12. effect of different peptizing agents on textural properties of the non-templated MA samples with 7.5 water to aluminum molar ratio.

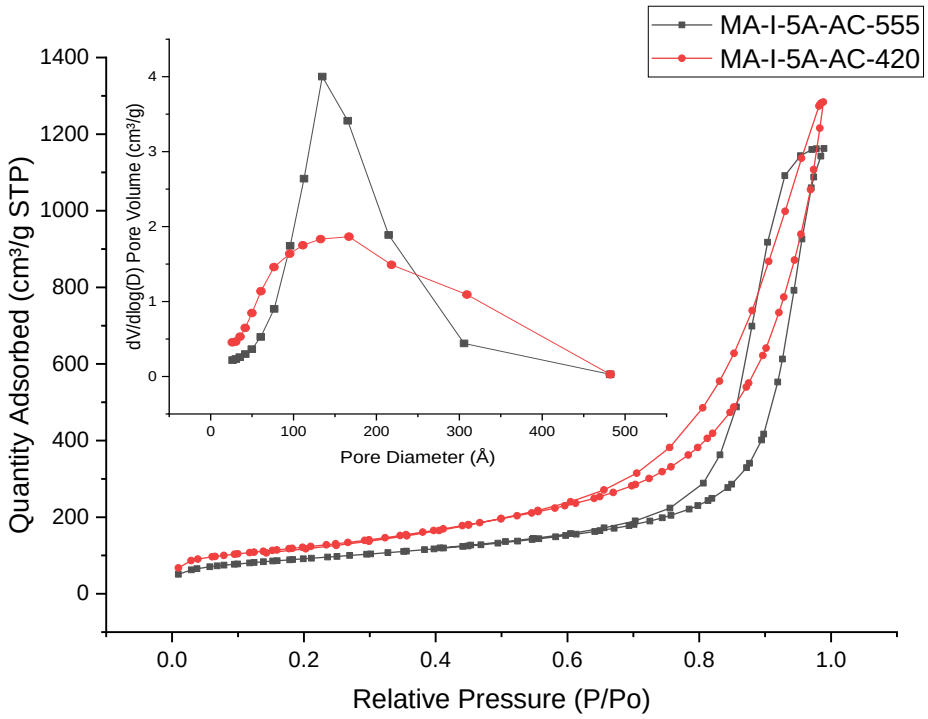

Figure 13. effect of different calcining temperatures on textural properties of the non-templated MA samples with 5 water to aluminum molar ratio.

The effect of solvent was the other subject to investigate such a sample with the formulation of the MA-I-5A-AC-555 was prepared, and toluene was used as the solvent rather than isopropanol and labeled as MA-T-5A-AC-555, the specific surface area of the sample drastically decreased from 325 to 251m^2/g while both pore volume and pore diameter have changed by narrow margins from 1.57 to 1.60 cm^3/g and from 157 to 150 Å, respectively. The effect of different peptizing agents was investigated concerning the toluene as a solvent, so the formulation of the sample MA-T-5A-AC-555 was followed with switching from acetic acid to nitric acid with the same concentration and the sample was labeled as MA-T-5N-AC-555. The textural properties followed the same trend as we expected from comparing MA-I-7.5A-AC-555 and MA-I-7.5N-AC-555. By switching acetic acid with nitric acid in a toluene medium, we measured a marginal increase in surface area from 251 to 260 m^2/g; however, 14.5% shrinkage in the total pore volume of the sample from 1.57 to 1.137 cm^3/g and 11.5% negative shift in average pore diameter from 150 to 133 Å was reported.

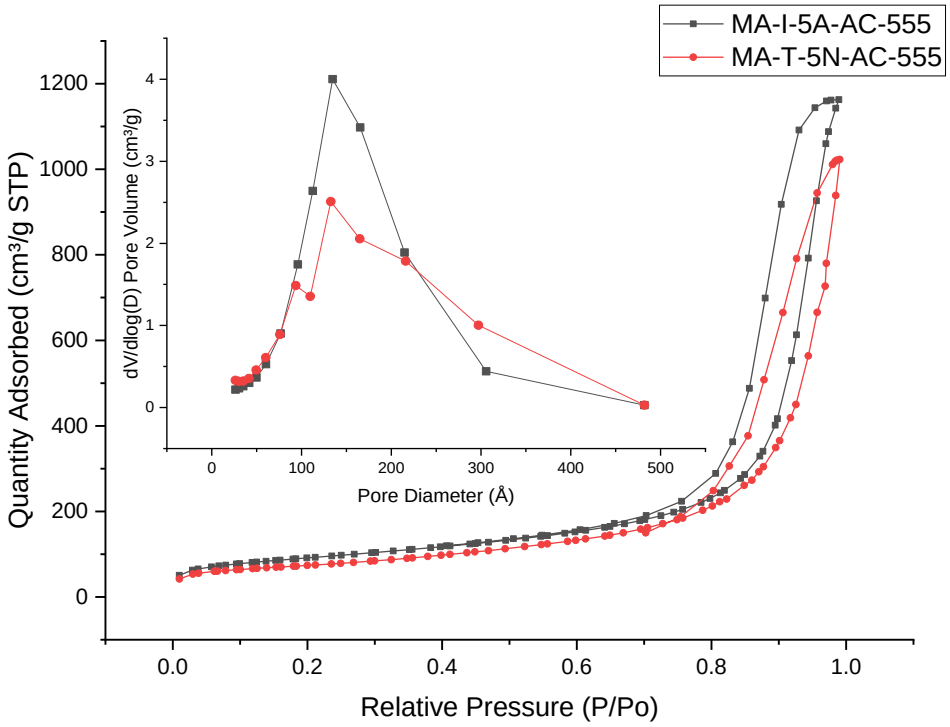

Figure 14. effect of different solvents on textural properties of the non-templated MA samples with 5 water to aluminum molar ratio.

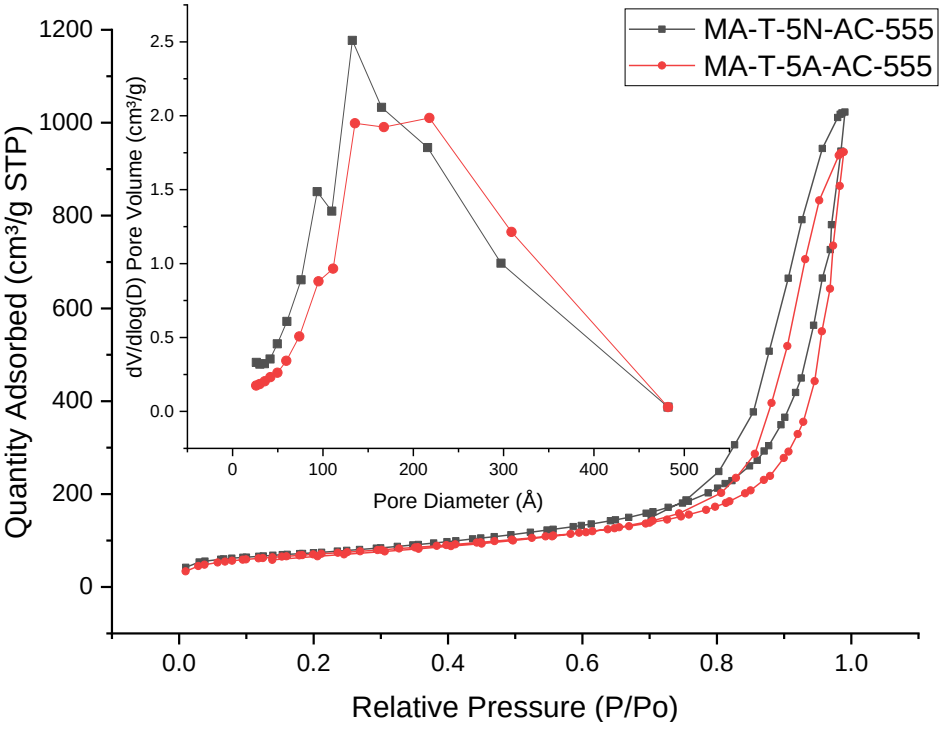

Figure 15. effect of different peptizing agents on textural properties of the non-templated MA samples with 5 water to aluminum molar ratio.

The effect of autoclaving through gel treatment was studied with a non-templated synthesis method as we prepared a sample with the exact formulation of the MA-I-5A-555, but we did not treat the boehmite with autoclaving. The resulting texture showed autoclaving helps the boehmite arrange a better crystallite network as the calcining of both samples at 555 °C almost doubles down pore volume from 0.92 to 1.60 cm^3/g and pore diameter from 91 to 157 Å with the marginal decrease in surface area from 369 to 325 m^2/g.

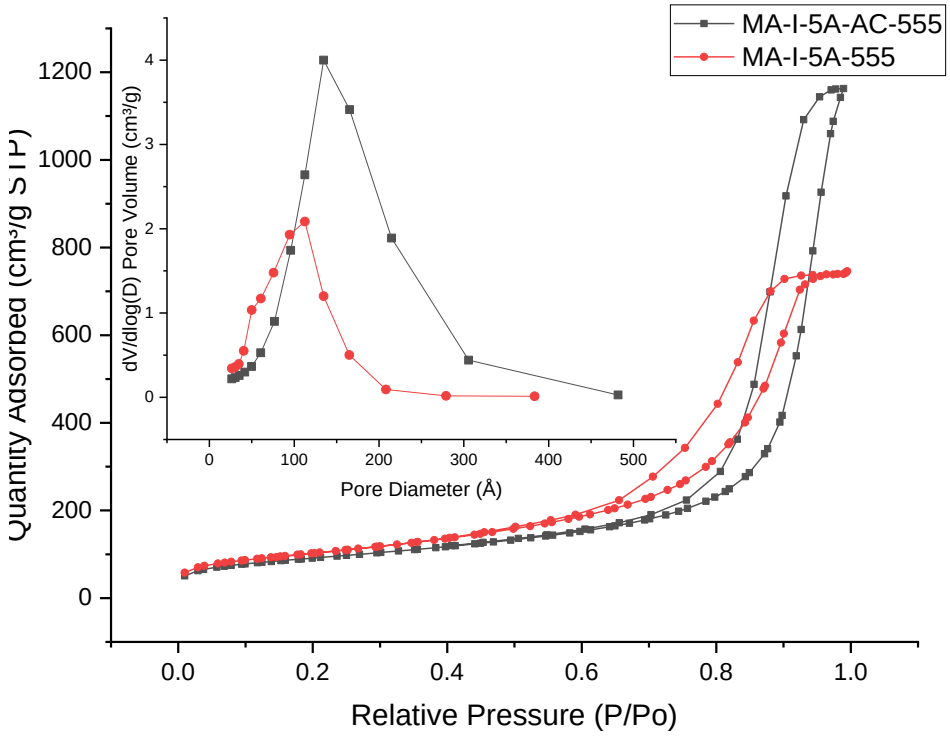

Figure 16. effect of autoclaving on textural properties of the non-templated MA samples with 5 water to aluminum molar ratio.

Finally, the effect of peptizing with acetic acid was investigated with the preparation of a sample with the same synthesis formulation AS MA-I-5W-AC-

555but using pure water rather than acidified and labeled as MA-I-5A-AC-555. By comparing two samples, an increase in surface area from 325 to 372 m^2/g was measured by N_2 adsorption, however volume of the pores gets more minor from 160 cm^3/g in a peptized sample to 1.42 cm^3/g in the hydrolyzed sample, and respectively, this trend was accelerated by drastically decreasing of the pore diameter from 157 to 85Å.

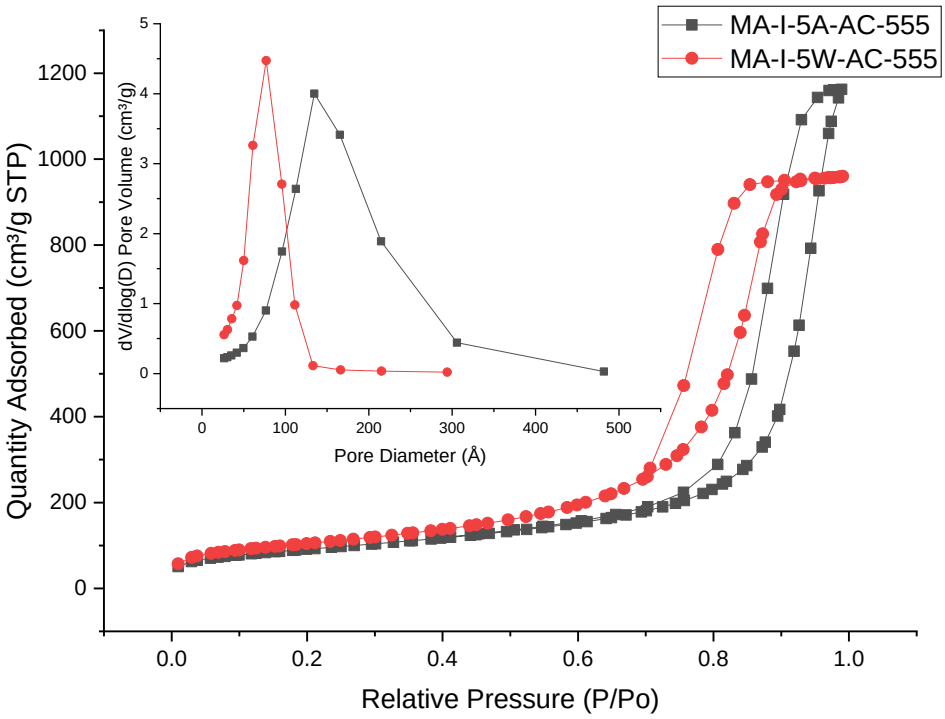

Figure 17. comparing the effect of peptized with non-peptized synthesis on textural properties of the non-templated MA samples with 5 water to aluminum molar ratio.

2.4.6. Monolith

We examined four different MA powders as the mesoporous phase that was mixed 4:1 with boehmite to construct monolithic spheres. The resulting monoliths and their textural properties are indicated in Table 18. Each MA had SSA in excess of 200 m^2/g and average pore diameters between 130 and 180 Å. In addition, spheres made from 100% boehmite were prepared. For alumina source, as preparation method was described previously. The reason is that the prepared support will have suitable surface characteristics if stabilized calcined alumina particles were stick together with helping a peptized boehmite gel. The obtained MAPs were chosen from the high surface area ranging between 218 m^2/g to 300 m^2/g and large pore volume (1.37 cm^3/g to 1.56 cm^3/g) and high pore diameter ranging between 133 Å to 180 Å.

Table 7. Textural properties and crushing strength test of MAM1 prepared by pure boehmite.

Method	Reagents	MAM1 Boehmite			
		BET Surface area m^2/g	BJH Pore volume cm^3/g	BJH Pore diameter $Å$	Crushing Strength N/mm
	Powder	318	1.3	116	NA
A	2% nitric	194	0.2	46	13
B	2% nitric + 5% TEG	202	0.3	56	11

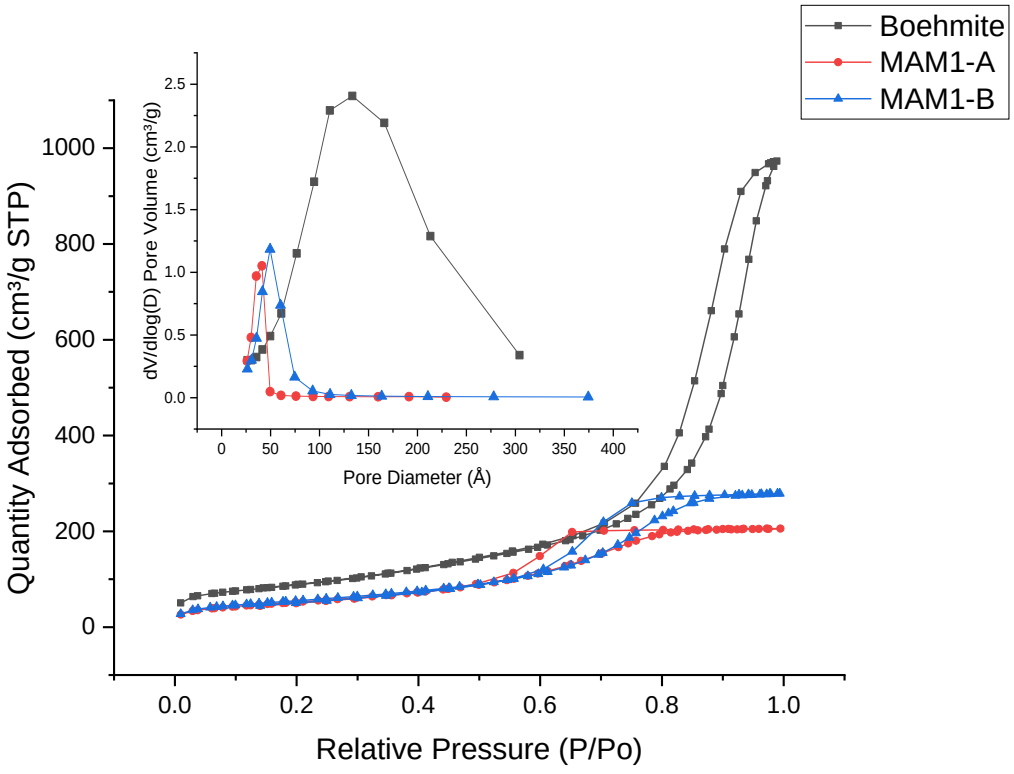

Figure 18. Isotherms and PSD of the boehmite and MAM1 samples were prepared by different methods.

The spherical supports were characterized by nitrogen adsorption-desorption for specific surface area, pore-volume, and pore diameter and tested for mechanical crushing strength. Table 9. shows that using four types of mesoporous alumina powders (MAP) varying in textural characters leads to mesoporous alumina monolith (MAM) with different textural properties and crushing strengths. In addition, each powder sample was treated with various concentrations of nitric acid or ammonium hydroxide to compare the effect of acid or base appetizers on the final monolith. Furthermore, using different concentrations of the peptizing agents ends up in significant changes in outcomes.

Table 8. Textural properties and crushing strength test of MAM2 prepared by different methods from MA-T-P123-AC.

Method	Reagents	MAM2		MA-T-P123-AC	
		BET	BJH	BJH	Crushing Strength
		Surface area	Pore volume	Pore diameter	N/mm
		m^2/g	cm^3/g	Å	
	Powder	300	1.44	180	NA
A	2% nitric	243	0.71	85	3.7
B	2% nitric + 5% TEG	230	0.72	120	7
C	5% nitric	202	0.45	88	14
D	2% NH4OH	206	0.75	129	9.3
E	2%NH4OH + 5% TEG	210	0.93`	136	4.3
F	5% NH4OH	200	0.75	108	13.3

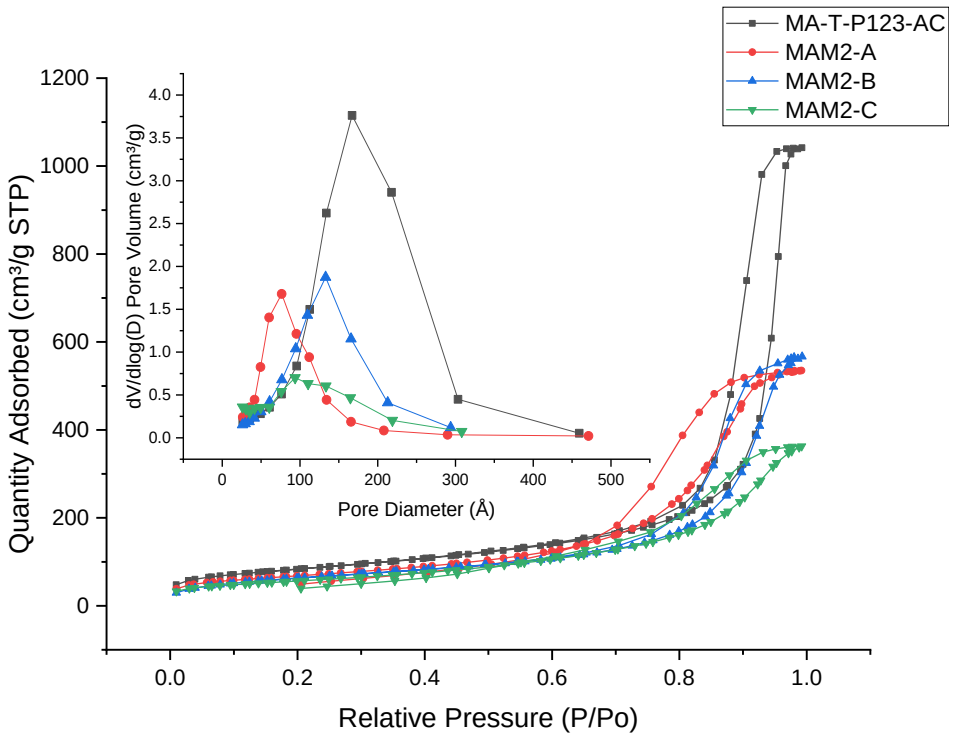

Figure 19. effect of methods A, B, C on textural and physical properties of the MAM2 samples.

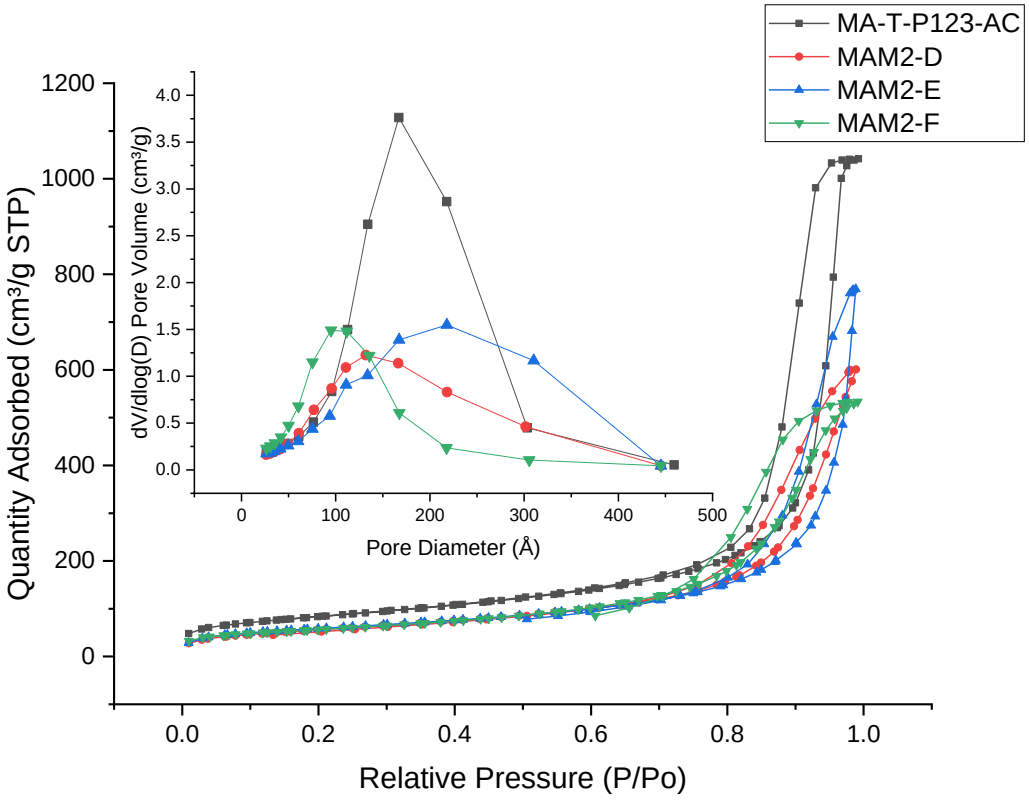

Figure 20. effect of methods D, E, F on textural and physical properties of the MAM2 samples.

Table 9. Textural properties and crushing strength test of MAM3 prepared by different methods from MA-T-F127-AC.

Method	Reagents	MAM3 MA-T-F127-AC			
		BET Surface area m^2/g	BJH Pore volume cm^3/g	BJH Pore diameter $Å$	Crushing Strength N/mm
	Powder	300	1.56	157	NA
A	2% nitric	255	0.67	91	11.6
B	2% nitric + 5% TEG	227	0.74	122	7
C	5% nitric	167	0.62	87	15
D	2% NH4OH	232	0.62	103	9.7
E	2%NH4OH + 5% TEG	252	0.85	116	6
F	5% NH4OH	203	0.47	80	13.6

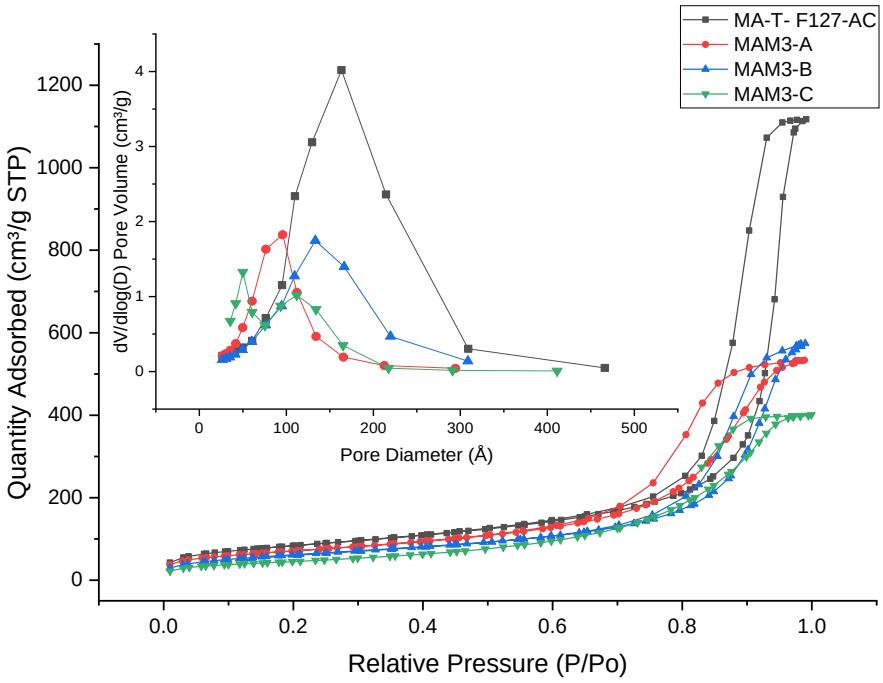

Figure 21. effect of methods A, B, C on textural and physical properties of the MAM3 samples.

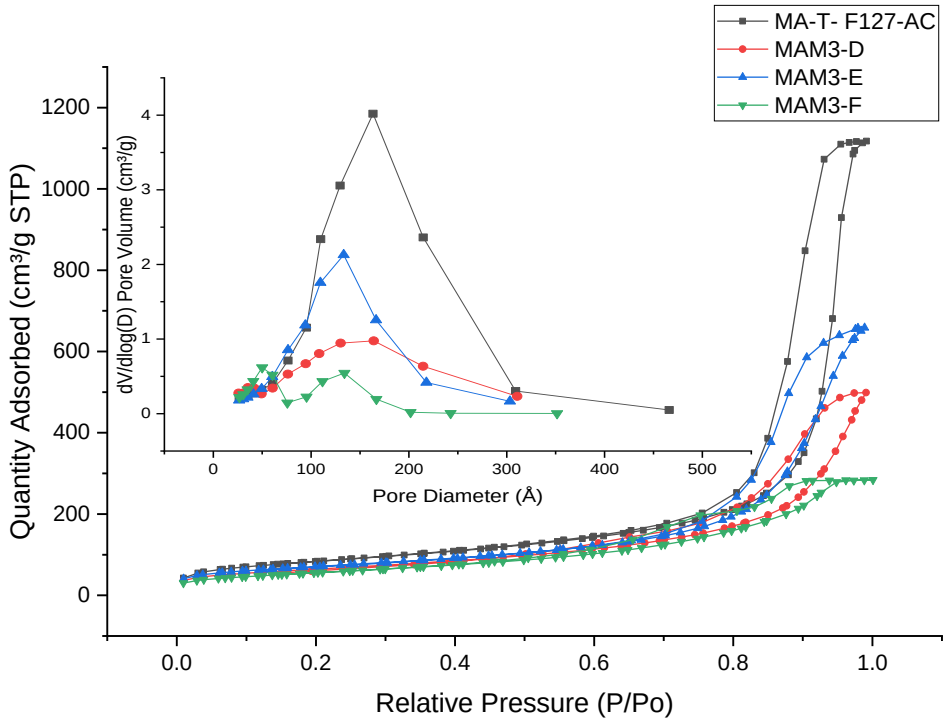

Figure 22. effect of methods D, E, F on textural and physical properties of the MAM3 samples.

Table 10. Textural properties and crushing strength test of MAM4 prepared by different methods from MA-T-5N-AC.

Method	Reagents	MAM4 MA-T-5N-AC			
		BET	BJH	BJH	Crushing Strength
		Surface area	Pore volume	Pore diameter	N
		m^2/g	cm^3/g	Å	
	Powder	260	1.37	133	NA
A	2% nitric	214	0.4	56	13
B	2% nitric + 5% TEG	225	0.48	79	9
C	5% nitric	197	0.33	82	17
D	2% NH4OH	227	0.65	104	9.6
E	2%NH4OH + 5% TEG	237	0.83	131	9.6
F	5% NH4OH	163	0.46	85	13.6

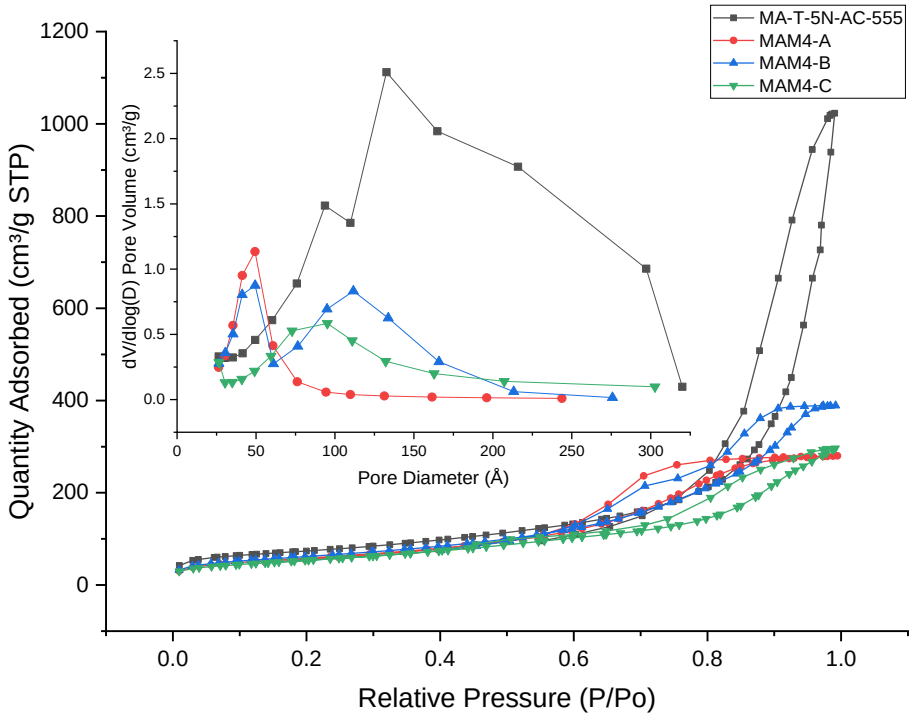

Figure 23. effect of methods A, B, C on textural and physical properties of the MAM4 samples.

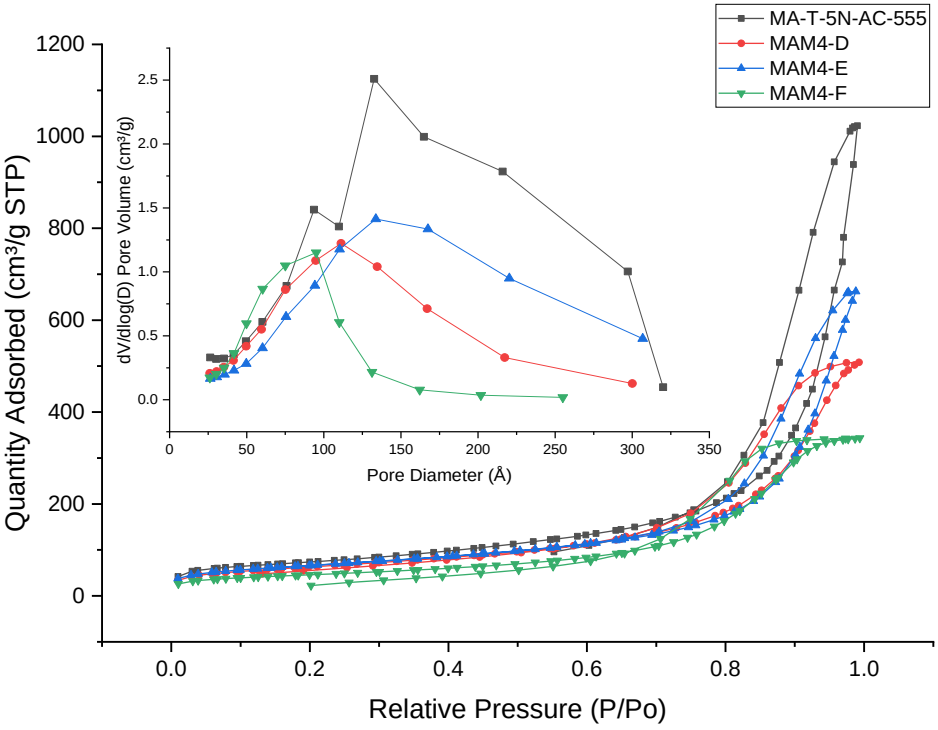

Figure 24. effect of methods D, E, F on textural and physical properties of the MAM4 samples.

Table 11. Textural properties and crushing strength test of MAM4 prepared by different methods from MA-I-7.5N-AC-800.

Method	Reagents	MAM5 MA-I-7.5N-AC-800			
		BET	BJH	BJH	Crushing Strength
		Surface area	Pore volume	Pore diameter	N
		m^2/g	cm^3/g	Å	
	Powder	218	1.41	163	NA
A	2% nitric	180	0.42	78	12.3
B	2% nitric + 5% TEG	23	0.77	122	6.7
C	5% nitric	141	0.36	89	21.3
D	2% NH4OH	205	0.73	123	10.3
E	2%NH4OH + 5% TEG	202	0.87	142	9.6
F	5% NH4OH	117	0.52	98	14.3

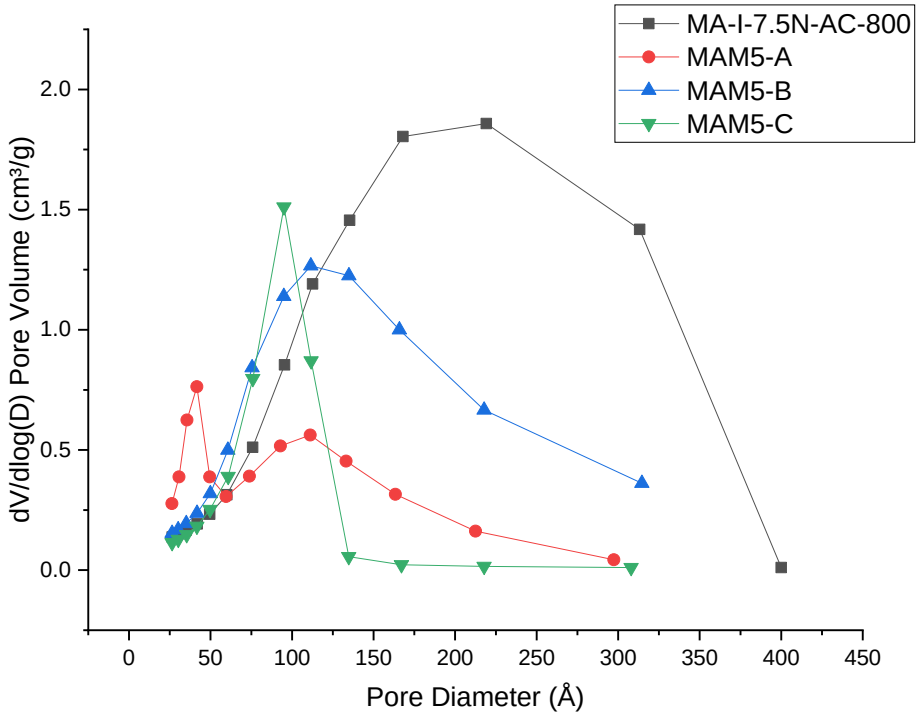

Figure 25. effect of methods A, B, C on textural and physical properties of the MAM5 samples.

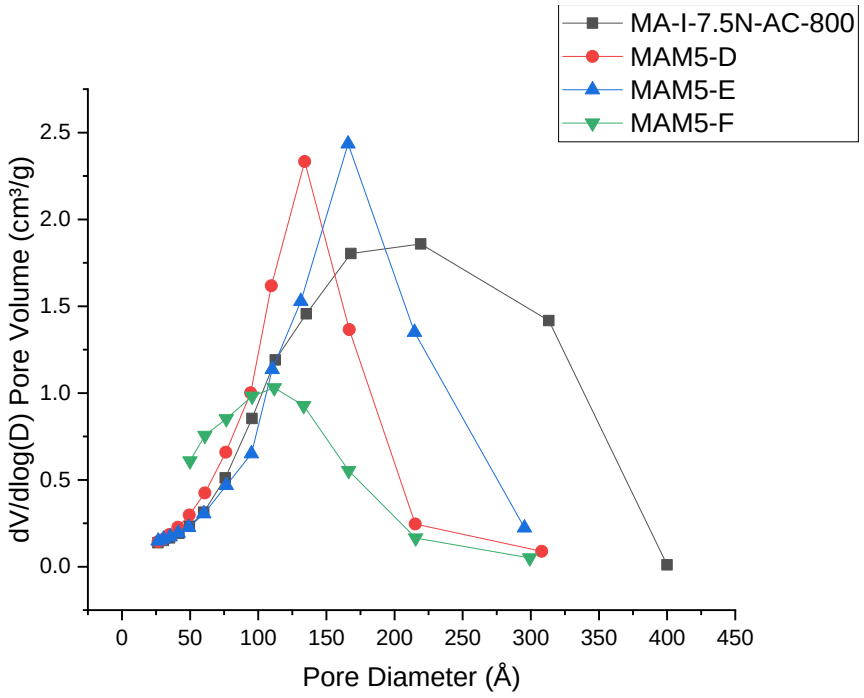

Figure 26. effect of methods D, E, F on textural and physical properties of the MAM5 samples.

In all cases, surface characters reduce due to adding acidic or basic solution through the paste process and secondary calcination. The specific surface area and pore volume decreased by increasing the concentration of acidic and basic peptizing agents from 2% to 5% in all cases and crushing strength increase 28 to 72%. However, using a plasticizer and lower concentration of peptizing agents is helping to prevent such a decrease in surface area, total pore volume, and average pore diameter. Furthermore, adding 5% TEG to our paste before final kneading keeps our fabricated monolith in the desired properties as crushing strength was measured as 18 to 29 N per single pellet. The textural properties reformed, surface area either increased or did not changed was 200 m^2/g > in all samples, total pore volume increased it was in 0.48 to 0.93 cm^3/g depending on initial MAP used for a sample satisfies our desired goal. By comparing the average pore diameter, it is evident that using a plasticizer helped to form larger pores with wider pore diameters. In all cases in which it yielded 116 Å to 142 Å depending on the initial pore diameter of the MAP except one case which it increased from 56 Å to 79 Å caused by using a smaller initial pore diameter MAP (133 Å). Using a higher concentration of the peptizing agents (5%) leads to having very tough spheres but losing the majority of the textural values, and using nitric acid makes the monolith 5 to 30% harder than using the same concentration of the ammonium hydroxide. Comparing with commercially available catalyst supports we were able to make as the top graded products in the market, our lab made catalyst support had higher textural properties and adequate crushing strength compared to all commercial alumina supports, and

very close to some silica spheres supplied by Saint-Gobain, please see the following table.

Table 12. Commercially available MAMs with their textural and physical properties.

			Textural and mechanical characters of commercial catalyst support spheres				
Supplier	**Product Code**	**Material**	BET	BJH	BJH	Crushing Strength	Diameter
			Surface area (m2/g)	Pore volume (cm3/g)	Pore diameter (Å)	N/mm	mm
Sasol	Spheres	Alumina	170	0.45	80	45	1
Sasol	Spheres	Alumina	220	0.75	50	28	1.8
Sasol	Spheres	Alumina	220	0.75	50	26	2.5
Saint-Gobain	Accu Spheres	Alumina	204	0.79	106	13	2.1
Saint-Gobain	UniSpheres	Alumina	248	0.89	94	9.7	1.6
Saint-Gobain	UniSpheres	Alumina	237	0.79	87	12	1.6
Saint-Gobain	Accu Spheres	Alumina	279	0.82	93	10	1.6
Saint-Gobain	Accu Spheres	Alumina	214	0.95	120	8.3	2.2
Saint-Gobain	SA 62135	Alumina	215	0.67	80	6 to 14	1 to 5
Saint-Gobain	SA 6*217	Alumina-Silica	115	0.55	80	6 to 14	1 to 5
Saint-Gobain	SA 6*227	Alumina-Silica	225	0.7	80	6 to 14	1 to 5
Saint-Gobain	SA 62240	Alumina	220	0.64	90	6 to 14	1 to 5

Table 9. shows that the best method of formulation for lowest impact on textural properties of the monolith can be chosen from B, D, and E methods. Among them, method D shows satisfactory results in both textural and mechanical terms. Regardless of the initial surface characters by using 2% ammonium hydroxide on all prepared samples, a sufficient crushing strength was measure as minimum as 9.3 N/mm, and maximum as 10.3 N/mm, and all products possess surface area higher than 205 m^2/g and pore volume between 0.62 to 0.75 cm^3/g along with high pore diameter between 103 to 129 Å, on each sample depending on the texture of the starting alumina. Depending on the textural properties of the MAP used in monolith preparation, by increasing the concentration of acidic or basic plasticizer from 2% to 5 %, the textural properties could decline by a different order of magnitude in all cases 35 to 50 % increase in crushing strength were measured. Therefore, using 2% peptizer is superior to higher concentrations. Among acidity or basicity of the peptizing agent, ammonia shows a better effect on the pore diameter of the MAM as in all Methods using the 2% base (D and E) the pore diameter was higher than 103 Å. By adding 5 % TEG as plasticizing to 2% ammonia formulation in all cases, the pore diameter enlarged between 7 to 27 Å concerning the MAP used in the formulation. Mixing TEG and base also helped to boost both surface area and total pore volume of the MAM. It seems that with the E method, the surface area increases if the implemented MAP has a value of 260 $m^2/g>$ and pore volume, regardless of the MAP always increases between 19% to 37%. Using 2% acid and %5 TEG (method B) generally increases the surface area

of the MAM in comparison with method A; however, it acts as a pore widener, same as in E formulation as an average of 43% increase in pore diameter was measured. From a mechanical stability perspective, although coupling peptizing agent and leads to lower crushing strength, all produced MAMs have passed the limit of 6 N/mm and are suitable to use as catalyst carriers.

By comparing our lab made supports with their commercially available peers from table 7. and 9. it is evident that all listed monoliths have passed our primary requirements of having a 200 m^2/g > surface area with a large pore volume of 0.62 cm^3/g > and a narrow and enlarged pore diameter of higher than 100 Å which is mechanically stable with the minimum of 6 N/mm (equivalent to 18 N for a 3mm diameter size single sphere)

Therefore, the following samples passed our quadruple requirements and in two or three indexes are better than the best commercially available support:

MAM2-B, MAM2-D, MAM2-F, MAM3-B, MAM3-D, MAM3-E, MAM4-D, MAM4-E, MAM5-D, and MAM-E.

It is worth mentioning that all MAMs made from 100% mesoporous γ-alumina and no inorganic impurities such as Si, MA, Na, Ca, … is not used as structural promoters. In addition, none of the MAMs shown any crack or collapse during the further treatments like impregnation, calcination, and reductions steps in the FTS catalysis.

Chapter 3

High Thermally Conductive Fischer-Trosch Catalyst Design and Preparation

3.1. Introduction: Catalyst and supports requirements

Operating an exothermic reaction exclusively FT reaction via a tubular reactor packed with a conventional catalyst is known to be an uphill task. Poor heat transfer and non-uniform mass transfer regime through the catalyst bed is the paramount issue in the process that limits profitability. To maximize the efficiency of FTS process, the catalyst needs to meet some requirements such as the size of the catalyst particles, the shape of the catalyst, morphology and textural properties of the catalyst, mechanical stability, high attrition resistance, high lifetime, activity, etc.

FTS catalyst comprises two main components, an active component, a precious metal such as cobalt, nickel, iron, and ruthenium, that triggers the reaction that could be promoted with a minor amount of a secondary metal such as ruthenium, rhenium, platinum, etc.

A mesoporous material that is typically made of refractory oxide could act as catalyst support. It usually is a passive component that could not interact with the reactant by itself but could maximize the active metal dispersion by providing a large surface area and regulating the interparticle mass transfer by having a specific morphology character. Among them, alumina, silica, and titania are the most well-established materials used as catalyst support in heterogeneous catalysis. In past decades, the effect of various properties of the catalyst support has been investigated in the heterogeneous catalysis field exclusively in FTS. Since the reaction occurs at the surfaces, it is an indispensable requirement for catalyst support to maximize active metal dispersion through a large surface area, typically

with surface areas larger than 150 $m^2 g^{-1}$, which could substantially reduce operating costs while maintaining higher productivity.[66,67]

Having a substantially large pore volume is essential for catalyst support to uphold a smooth mass diffusion in FTS25–29 for small size reactants, which could provide an uncovered active site to them and for high molecular weight product species that consists of a large number of product species of pore volume larger than 0.5 mL g^{-1}. In addition, support with large pore volume is capable of burdening more active metal through the impregnation. Meanwhile, the size of the active metal nanoparticles determines the pore diameter parameter as it was studied with Zhan et al.[68] Furthermore, products selectivity and reaction rate depends on the pores' geometry, as mentioned in numerous studies.[24,29,68,69]

The size and shape of the catalyst were investigated by Iglesia et al.[70,71] 1-3 mm catalyst preferably in spherical shape is recommended to minimize the pressure gradient across the bed. In addition, large catalyst particles will provide higher mechanical stability and smother mass transfer. On the other hand, Miloš et al.[72] suggested using either 0.2 – 0.5 mm fully impregnated or larger size spheres with an egg-shell distribution of cobalt with a thickness of lower than 0.13 mm for lower methane selectivity. Moreover, they must possess sufficient mechanical strength to prevent fracturing due to load or thermal fluctuations. For example, in their investigation, Zohdi et al.36 studied the effect of mass transfer in fixed bed FT reactors, which showed intraparticle mass diffusion would become a prominent factor as it affects the Thiele module and, therefore, kinetic rates of the reactions in catalyst particle larger than 1.5 mm. Khodakov et al.[24] examined pore size effects

on FTS catalysis using cobalt on SBA-15, MCM-41, and commercial silica supports. They report that reaction rates and turnover frequency increased fivefold in the catalysts with 330 Å pores over those 20 Å pores.

Moreover, the larger pore supports yielded more C_{5+} products. Additional interesting effects were attributed to the large pore diameters and volumes. In related studies, it was shown that the size of Co_3O_4 particles formed after deposition and calcination were proportional to the γ-alumina support pore diameter.[25,26] Saib[27] et al. showed in his study that the size of the cobalt crystallite size increased from 30 Å to 83 Å as the pore increased from 40 Å to 150 Å. Jung et al.[28] studied the effect of pore diameter on the performance of FTS over different silica supports and observed that by increasing pore diameter from 60 Å to 125 Å, CO conversion increased from 60% to 75.5 % meanwhile CO_2 selectivity reduced from 14% to 9% and also CH_4 selectivity reduced from 29.5 % to 19.8 % and C_{5+} selectivity increased from 55 % to 70 %. Ghampson[29] and coworkers demonstrated that the larger cobalt particles found in alumina support with larger pores (100 to 200 Å) were intrinsically more active catalysts. Their investigation on the effect of pore diameter on TOF revealed a linear relation up to a pore diameter of 130 Å. Morel et al.[34] listed typical hydrotreating fixed bed catalyst properties, 1.2 to 6 mm diameter alumina spheres or extrudates with the surface area of 80 to 220 m^2/g and pore volume larger than 0.5 cm^3/g and pore diameter of 100 to 200 Å is a commonly used catalyst carrier.

From a heat transfer perspective, regardless of the size of the reactor tube, radial heat removal becomes more effective at higher velocities with larger catalyst

particles, as is shown in a study by Sie et al.[73]. Both partial pressure drop in the reactor vessel along with catalyst performance are the determining factors to an increase of particle size and velocity.[74] Therefore, there is a complimentary linkage between all required factors for an optimum operation of a profitable FTS process. In other words, all these requirements needed to be followed, and each one of them has a vital role in the process outcome. Among all of them, heat transfer seems to be the most challenging factor. Poor thermal conductivity of the traditional materials applied as catalyst carriers was the subject of some studies in recent years. Monolithic and honeycomb catalysts are known for their advanced plugged flow advantages. Visconti et al.[75] investigate metallic monolith catalyst bodies with high thermal conductivity for FTS in 1-inch diameter tubular reactors. It was shown that wash-coated metallic monolith could remove large amounts of heat from reaction sites with minimized mass diffusion restriction and low-pressure drop. However, as a simulated solid-phase temperature profile was shown, there was a non-uniform temperature distribution in the bed. Despite the high CO conversion (70%), low volumetric productivity (caused by large reactor tube made it not effective as it was supposed to be. On the other hand, one of the challenges in using significant monolithic catalysts for FT is that we need to apply the porous catalyst on the frame by wash coating techniques that make the monolith very fragile, and the concentration of the acid needed for the process will decline the textural properties of the porous material. Furthermore, fabrication of the commercial scale metallic monolith with wash coating techniques is a tedious and costly process. Lacroicx et al.[22] were suggested using silica carbide foam as FT catalyst; due to the low surface

area of the SiC, it was coated with Al_2O_3 by the same wash coating technique as Visconti et al.[75] tried, Although the Catalyst demonstrated an excellent thermal conductivity and the lowering CH_4 and CO_2 selectivity, it had a low surface area (20 – 25 m^2/g) and also the syngas was diluted with Ar gas with a 1:1 molar ratio that could help to manage the thermal related challenges. According to their study, loading 30% Co on SiC will result to produce a high amount of waxes as the chain growth probability (α) as high as 0.91 while using conventional alumina could lead to 0.85 as α value which is showing the higher liquid product with 7% more CO conversion but lower and higher methanation. Coating SiC fame with Al_2O_3, though, could show an efficient C_{5+} productivity performance among those three catalysts by 75 % CO conversion and 79 % C_{5+} productivity. Fratalocchi et al.[76] were investigated the thermal behavior of the Pt promoted Co catalyst supported on Al_2O_3 which was packed into the metallic foam, tmpreture runaways and fluctuations was exceptionally reduced but the catalyst was making a high amount of methane between 11% to 33.3 % along with that CO2 selectivity was as high as 7.1% at 240 C when they tried to increase the CO conversion as high as 67.5%. The large size of the catalyst, along with using a low surface area alumina (59 m^2/g) and small pore volume (0.20 cm3/g), could be mentioned as the other reasons for having low volumetric productivity. The same crew investigated a small egg-shell catalyst by loading Co on γ-Alumina with better textural properties than the previous study in a compact FT reactor that could maintain 10 % CH4 selectivity. However, CO conversation was as low as 45.5% by increasing the temperature to 240 C the could increase the conversion as high as 55% methane selectivity and marginally lower

C5+ selectivity in their best run; however, they had to use 24 vol.% inner gas to have better control on the thermal behavior of their catalysis.[77]

Poor and slow heat removal of the conventional packed bed reactors makes them the most crucial rig to use in the FTS process. Temperature oscillations, the large temperature gradient in the catalyst bed, non-homogeneous temperature distribution within a catalyst particle, local hot spots, and cold spots are known as the main issues regarding the temperature-related challenges in applying fixed bed reactors. The mentioned instabilities introduce several drawbacks: low liquid product (C_{5+}) selectivity, increasing unfavored product selectivities such as CH4, CO2, C2H6, C3H8, and other low-value gaseous hydrocarbons. Moreover, soot formation by the Boudouard reaction could partially deactivate the catalyst by covering the particle's outer surfaces and clogging the reactor tube, resulting in a high-pressure drop through the reactor.

The partially deactivated catalyst particles lead to lower carbon conversion which, necessitating the re-generation of the whole catalyst bed.

In addition, permanent catalyst damages such as sintering, agglomeration, and physical damages such as breakage and blocking the surface of the catalyst particles are the other possible consequences of the inefficient heat exchange.

3.2. Catalysts and catalyst support preparation

The selectivity of the FTS is strongly influenced by a combination of thermal, diffusional, and reactional limitations within the catalyst.[70] The mass diffusion is improved by deposition of the active catalyst on a thin layer of the catalyst, such as an egg-shell catalyst. The reaction condition within the catalyst pellet is enhanced by controlling the pressure of the reaction, optimizing the H_2 to CO ratio, maximizing the Cobalt dispersion, promoting the reducibility of Cobalt nanoparticles, etc. Heat dissipation of the catalyst pellet could increase by using thermally conductive catalyst support. In this chapter, we are trying to explain the preparation of various catalyst support and different approaches to modifying their FT performance.

The prepared support candidates classified into six different categories:

1- Conventional mesoporous silica-supported egg-shell catalyst (CMS-ES)

2- Mesoporous alumina monolith egg-shell catalyst (MAM-ES)

3- Fully impregnated mesoporous alumina monolith catalyst (MAM-FI)

4- mesoporous alumina monolith core-shell catalyst (MAM-CS)

5- Thermally modified mesoporous alumina monolith egg-shell catalyst (X-MAM-ES) with five different types of a thermal modifier, which could sub-divided based on modifier as:

- Aluminum modified egg-shell catalyst (Al-MAM-ES)
- Copper modified egg-shell catalyst (Cu-MAM-ES)

- Rainey Cobalt modified egg-shell catalyst (RC-MAM-ES)
- Graphite modified egg-shell catalyst (Gr-MAM-ES)
- Silica carbide modified egg-shell catalyst (SC-MAM-ES)

6- Aluminum modified core-shell catalyst (Al-MAM-CS)

Herein, we first educate about methods of fabricating the above catalyst supports, and then the required techniques for preparation of fully impregnated and egg-shell impregnation of both conventional and fabricated supports will

3.2.1 Conventional catalyst support

Herein, all the experiments done with a conventional silica carrier were performed via mesoporous silica spheres with a 4 mm diameter and BET surface area of 220 m^2/g, pore volume of 0.85 cm^3/g, an average pore diameter of 120 Å, and mean crushing strength of 56 N purchased from SAINT-GOBAIN.

3.2.2. Preparation of monolithic sphere and pellet MAO catalyst supports

Monolithic catalyst supports comprised of 3-4 mm spheres can be made from the MAO powder described previously in combination with a binder (typically boehmite) and plasticizers, such as triethylene glycol (TEG) or methyl cellulose (MC). In a typical procedure for the production of spheres, the boehmite and MAO powders are freshly ground and sieved using a 200-mesh sieve to ensure particle sizes < 75 micrometers. A paste is prepared by mixing 10 g boehmite and 40 g MAO powder for 5 min before peptizing by addition of ~40 mL of 0.1 M nitric acid and mixing to form a gelatinous paste. The volume of nitric acid is estimated from

the pore volumes of the MAO and boehmite powders and adjusted as needed to form a dough-like paste. The dough is further refined by the addition of 4 mL (5 g) of TEG plasticizer, which is mixed and kneaded into a dough-ball for ~ 20 min, during which small additions of nitric acid (0.1 M) are used as needed to keep the appropriate moisture content. When the resulting 'paste' has the rheology of Play-doh, it is ready for extrusion. The paste was extruded through a die template with 3.7 mm holes to form a spaghetti-like mass of cylinders laid flat and cut at ~ 4 mm intervals. The still moist pellets are then loaded onto a boilie roller rack with an internal diameter of 3.7 mm. Reciprocating the top rack of the boilie roller rack converts the pellets to spheres, which are then allowed to slowly dry over 48 h by placing them in a plastic jar with the lid left loose. After this initial drying, the spheres are transferred to an oven and dried under a nitrogen atmosphere for 12 h at 85 °C. The spheres are then calcined at 555 °C under 60 mL/min flow of the helium gas for 5 hours to yield the desired mesoporous aluminum monolith (MAM) supports, having an average diameter of 3 mm. The spherical supports were characterized by nitrogen adsorption for surface area, pore-volume, and pore diameter and tested for mechanical crushing strength.

3.3. Impregnation of the catalyst support with metal salts.

The study explored the alumina or silica-supported catalyst with different forms of cobalt loading. A traditional loading method (fully impregnated) catalysts are typically demonstrated by a uniformly distributed active metal on the support surface, which is prepared by the incipient wetness impregnation (IWI) method.

The IWI is the most commonly used technique for the preparation of supported Co catalysts in FTS studies in which support pores are thoroughly filled with an aqueous precursor of Co salt.

In this work, the FTS catalysts were comprised of principally alumina or silica supports upon which a mixture of cobalt and ruthenium metals were impregnated, calcined, and reduced/activated. The reduced catalyst generally was composite of support and metals in which metal comprises 20% by mass cobalt and 1.5% ruthenium by mass.

A typical impregnation procedure using commercially available 3 mm monolithic spherical silica pellets, available from Saint Gobain, is described below. The commercial support was cleaned by calcination in the air from 25 °C to 400 °C with a 1°C/min ramp and kept at 400 °C for 5 hours. Immediately prior to impregnation, the support pellets were pre-treated to 120 °C under flowing nitrogen to remove any adsorbed moisture. We typically measure a 7 to 12 % mass loss at this step, showing absorbed water is a significant factor.

The support was then impregnated using the incipient wetness impregnation (IWI) method, in which the support is wet with a volume of dissolved metal salt in an aqueous solution equal to the total pore volume of the support (as calculated based on the measured pore volume/g). Ten grams of silica pellets are wet with 8.5 mL of an aqueous solution containing 10.1 g $Co(NO_3)_2 \cdot 6\ H_2O$ of 97.7 % pure (2.0 g cobalt). These pellets were then dried at 85 °C for 12 hours in air. Upon

cooling to room temperature, the pellets were wet with 8.5 mL of an aqueous solution containing 0.39 g of $RuCl_3 \cdot 3H_2O$ of 99.0 % pure (0.15 g Ru) and again dried at 85 °C for 12 hours. The salt impregnated catalyst pellets were then calcined in a temperature-programmed oven starting at 85 °C and ramping at 1 °C/min to 350 °C at which it was held for 6 hours, and then left to cool to room temperature. This pre-catalyst is generally reduced in-situ immediately prior to an FTS run using a hydrogen atmosphere to generate the active metal-supported catalyst. Temperature programmed reduction (TPR) studies of small samples (about 200 milligrams) of the pre-catalysts were performed in order to develop an appropriate reduction/activation procedure.

3.3.1 Fully impregnated mesoporous alumina catalyst support

Typical FT catalysts were prepared by thorough impregnation of the support particles via an active metal precursor. One of the main challenges in preparation of these class of catalysts will be the uniform dispersion of the active component on the particle surface area, which requires a decent impregnation technique and relies on various parameters such as textural characters of the support surface area, pore-volume, and diameter of the pores, the used solvent, pretreatment of the support prior to the impregnation, PZC of the support, etc.[55,78,79]

A typical CMS-FI catalyst was prepared with impregnation procedure using commercially available 3-4 mm monolithic silica spheres CMS, available from Saint Gobain, is described in the previous section.

The mesoporous alumina monolith (MAM) spheres with 3 mm diameter prepared with the same method and labeled as MAM-FI.

3.3.2 Egg-shell impregnated mesoporous catalyst supports; MAM-ES, and CMS-ES

Egg-shell catalysts are defined by only having a portion of the outermost solid support impregnated with the active metal catalysts. For FTS, an impregnation thickness of ~500 microns is desired as this is about the maximal diffusion lengths for the long-chain hydrocarbon products. The egg-shell design means that the bulk of the core of the catalyst support is inactive. As the core tends to be the hottest region in a fully impregnated catalyst sphere, the egg-shell design eliminates this 'hotspot' which is presumed to be primarily generating light gaseous hydrocarbons, like methane. [80]

The preparation of egg-shell catalysts requires practice and patience and because of the inhomogeneity of the metal salt distribution is harder to quantify. The procedure involves preparing thick, semi-viscous 'melts' of the metal salts, either neat or as ethanolic solutions, and dispersing the melts on a preheated large petri dish (70 °C) and rapidly adding and rolling the solid support spheres around in the melt to absorb the liquid. The total metal loading is done over several such absorption steps. The thickness of the impregnated layer is followed by halving 2-3 spheres and observing the depth of the impregnation into the sphere. When the process is complete, the egg-shell catalyst has the same metal loading of 20% cobalt and 1.5 % ruthenium per gram of catalyst, but in this case, the metal is not distributed homogeneously throughout the support. Thus, regions with no active metals present and regions in which the cobalt and ruthenium local concentrations are higher than in the uniformly impregnated solid supports.

Therefore, egg-shell impregnation performed via on prepared MAM with surface area 230 m^2/g, pore volume of 0.72 cm^3/g, and BJH average pore diameter of 120 Å and sample labeled as MAM-ES; also, the same method was applied to prepare an egg-shell type catalyst with conventional mesoporous silica supports that its textural properties were measured by N_2 adsorption as surface area 220 m^2/g, pore volume of 0.8 cm^3/g, and BJH average pore diameter of 120 Å and the obtained sample labeled as CMS-ES.

3.4. Thermally modified mesoporous alumina catalyst supports

The traditional substances were used as catalyst support are recognized as inferior thermal conductive materials. Alumina, silica, and titania are among the most common materials used as support in heterogeneous catalysis reactions for their chemical and thermal stability along with having required textural properties such as high surface and decent pore volume. However, it was clear that the poor thermal conductivity of such materials will be problematic exclusively when we are dealing with an exothermic reaction.

In accordance with the current project, in the first approach, we tried to prepare a series of novel catalyst supports which they have a composite structure and properties aiming to have more thermal conductivity compared to conventional catalyst support. Therefore, the present investigation's thermally promoted catalyst support composition comprises a series of novel catalyst carriers that were designated to have some thermally conductive additives in their structure. This importance was done by uniformly dispersing micron-size powders of the thermally

conductive materials with our mesoporous alumina and binder during support fabrication previously explained in section 3.2.2. During the fabrication process, a known amount of highly conductive materials such as aluminum, copper, graphite, Rainey cobalt, and silica carbide in powder form were added to our mesoporous aluminum oxide and boehmite binder and well mixed in a container for a decent amount of time to have a homogenized powder mixture. Then, a peptizing agent and plasticizer were added to the blended powder, and after enough kneading, a dough-like paste formed and will be ready for further extrusion and shaping process. The support beads are obtained by heat treatment of the disintegrated extrudates and spheronized beads. From now on, we call that thermally conductive powder a "thermal promoter." We assume that if it is mixed homogenous, we are supposed to have a thermal promoter particle next to a reaction site. Therefore, generated heat resulted in exothermal reaction in that active site would be transferred and dissipated to the adjacent lower temperature reaction sites that probably are not hot in the meantime. With that thermally promoted composite structure help, we assumably have more overall temperature homogeneity. Therefore, we would be able to avoid the creation of hot spots and even cold spots during such a highly exothermic reaction.

3.4.1. Thermally modified mesoporous alumina support using aluminum powder

Composite catalyst support containing 16 % wt. Aluminum/Alumina is prepared as follows:

1.6 g Aluminum powder sample with a size of smaller than 70 micrometers was added to a mixture of 2.0 g boehmite and 6.9 g mesoporous gamma-alumina and well mixed for 10 minutes to have a homogenous dispersion of the powders. Then, 5mL of 0.1 molar solution of the nitric acid were gradually added to the mixture while it was kneading for 20 minutes, and then 2 mL of TEG solution was added to the paste. The obtained paste was introduced into the extruder with a cylindrical die of diameter length between 3.7 mm and extruded gently to cylindrical rods get extruded. Prior to the extrusion, soft paste rods get cut to smaller pieces with 3.7 to 4 mm length. Finally, pellets were introduced in a boilie roller rack, so a spherical shape smooth paste formed. With the same procedure described in section 2.4.6. all-spherical pastes dried and pre-heated and finally calcined at 550 °C for 5 hours with a 1 °C/min ramp. The spherical paste has a 3.7 mm diameter, and after calcination, a uniform 3 mm diameter catalyst support gets formed. The catalyst support was labeled as Al-MAM-E.

It is noted that based on thermal gravimetric analysis results, it was shown in figure 6. A boehmite binder loses 25 % wt. of its mass when it is calcined at 410 °C and higher temperatures resulting from phase change to gamma-alumina. This

weight loss needs to be considered in all future calculations related to the final support composition.

3.4.2. Thermally modified mesoporous alumina support using copper powder

A 16 % wt. the copper powder was mixed with the MAM paste prepared with the same method as described in the previous section, the resulted paste was extruded and spheronized to prepared a uni-sized thermally modified composite catalyst support. Finally, the obtained support was impregnated as the egg-shell form with 20% Co and 1.5% Ru and labeled as Cu-MAM-ES.

3.4.3. Thermally modified mesoporous alumina support using graphite powder

With the same method as described in section 3.4.1. a 22 % wt. Graphite powder was mixed with the MAM paste. The thermally promoted composite catalyst support was fabricated with the same size and geometry. Obtained support was impregnated as the egg-shell form with 20% Co and 1.5% Ru and labeled as Gr-MAM-ES.

3.4.4. Thermally modified mesoporous alumina support using Rainey cobalt

With a similar method as described in section 3.4.1. a 17 % wt. Rainey Cobalt powder was mixed with the MAM paste to prepare the thermally modified composite catalyst support. Supports further extruded and shaped to form 3 mm diameter beads. Finally, the obtained beads were impregnated with the egg-shell

coating method with 20% Co and 1.5% Ru and labeled as and labeled as RC-MAM-ES.

3.4.5. Thermally modified mesoporous alumina support using SiC

With the same method as described in section 3.4.1. a 17% wt. Silica carbide powder was mixed with the MAP and peptized with nitric acid to prepare a MAM paste. Next, the SiC modified catalyst support composite was fabricated, dried, and calcined to create uniform 3 mm diameter beads. Finally, the obtained support was impregnated as the egg-shell form with 20% Co and 1.5% Ru and labeled as SC-MAM-ES.

3.5. Core-Shell designed catalyst supports

Introduction

The FTS using egg-shell Catalyst resulted in producing more C5+ products by taking advantage of having better mass transfer reported in many studies.[18,71,81–83] Based on our result and regardless of catalyst support as it examined via conventional silica and fabricated alumina catalyst carriers, the product of the egg-shell catalysis FTS will be dominant waxes. This is caused by the lower partial pressure of the products and specifically produced water in the pores that favor the later chain termination of the synthesis. In one preferred embodiment, the core-shell composite catalyst support comprises by replacing the unused inert ceramic core of the egg-shell type catalyst with a high thermally conductive material such as copper and considering the core as a thermal reservoir and preventing hot spot incidence.[84–88]

3.5.1 Core-Shell mesoporous alumina support; MAM-CS

In an embodiment precession, copper spheres with a diameter of 2 mm coated with the MA paste that was made with the same method described in section 3.2.2. with a coating thickness of 650 to 750 micrometers. The obtained core-shell samples dried at room temperature in a loose-tight container for two days, then pre-heated in a dried oven for a day. Then the dried core-shell pellets were transferred to a tube furnace and calcined at 550 C for 5 hours with 1 °C/min ramp under 100 SCCM helium flow.

It is worth mentioning that helium is the best choice for thermal management of the composite material during the sintering or calcining due to the high thermal properties, and it is superior to other gases such as nitrogen and air. Therefore, impregnated MAM-CS were prepared according to the method described in section 3.3.2. Herein, the volume of the cobalt precursor is derived based on the total mass of MAM coated on the copper core by subtracting the total mass of the catalyst from the total mass of the copper core.

3.5.2. Thermally modified core-shell mesoporous Aluminum - alumina supports

In an embodiment, 2 mm diameter supper conductive copper spheres were coated with an Al-MAM paste which the preparation method as previously described in section 3.4.1. to form a thermally modified shell with a conductive copper core composite support. Next, the soft spheres dried and calcined with the same method as previously described in section 3.5.1. Then, obtained support was impregnated with cobalt and ruthenium and labeled as Al-MAM-CS.

4. Fischer-Trosch reactor unit: Introducing the rig

4.1. Introduction

Production of synthetic fuels via catalysis requires certain reaction conditions. These thermodynamical parameters such as temperature and pressure of the reaction could indicate the preferred type of reactor which could be chosen between slurry bubble column, fluidized bed, and tubular plug-flow reactor. As mention by Davis[89], fixed bed tubular reactor is the most widely used design due to the numerous advantages such as high catalyst loading capacity, high volumetric productivity, high carbon conversion, low methane, and carbon monoxide production, ease of operation and maintenance, reliability, cheaper catalyst, and no need for product separation and refining. However, Scaling up is limited by the non-efficient thermal conductivity of the catalyst particles, high-pressure drop gradient over the reactor column.

As mentioned in the first chapter (1.3. Fischer-Tropsch Catalysts), most disadvantages could be minimized by choosing a proper catalyst size or optimized by conducting a proper operational condition. Among them, heat transfer limits remained as the major drawback.

Conducting an FT run is exclusively challenging when operating in a tubular reactor, as there will be temperature oscillation, temperature runaway, and the creation of hot spots in the catalyst bed, which could cause safety issues and permanent catalyst deactivation, and reduces the productivity of the process. To avoid the creation of hotspots and thermal runaways in all similar studies in academia and industrial research labs, researchers are using different techniques

such as using a very narrow reactor tube or introducing an inert gas, mostly nitrogen, as an internal syngas coolant or diluting the active catalyst with any kinds of catalytically inert materials such as quartz chips, or silica carbide pellets or unloaded catalyst supports. In some reactor designs, researchers are taking advantage of cooling jackets wrapped around the reactor tubes or in industrial reactors introducing the high-pressure steam passing through the reactor tubes to help. However, these solutions could result in a decline in volumetric production and, therefore, lower profitability, hence increasing capital expenditure (CAPEX) of the process.

Based on the purpose of the present investigation, we increase the thermal property of the catalyst to have proper thermal management. However, a proper design of the reactor and heat removal capacity must be considered before any investigation. Therefore, the applied rig described as follows:

The Fischer-Tropsch synthesis was carried out in a single tubular ¾", 316 stainless steel reactor with 17 mm inner diameter and 1 mm thickness in which 10 grams of catalyst was loaded that corresponds with the nominal catalyst bed volume of 15.7 cm^3 (the occupied volume by thermocouple rod is removed from the calculation) which occupied with a 7.6 cm of active bed length. In a manner to have the catalyst bed fixed in its position inside of the reactor, the bed was held by aluminum wool at both ends. It is worth noting to mention that regardless of catalyst type in all catalyst loading cases, we deliberately prevent using diluent. The reactor was kept hot during the process with a heat gun blowing the hot air through the reactor shroud. Simulink and Arduino controlled the temperature and airflow. As

shown in figure 3. the feeding gas (H_2 and CO) was introduced from the top of the reactor to the active bed. The catalyst was in-situ reduced in the presence of the 100 SCCM of the 99.999% hydrogen gas flow adjusted by a Sierra mass flow controller (MFC) equivalent to the gas hour space velocity (GHSV) of 380 h^{-1} at 400 for 24 hours in atmospheric pressure conditions. To have a reliable activation after the reduction was completed, the catalyst was cooled down to 150 ℃ while the hydrogen gas is still flowing with the same space velocity. Then, the system was pressurized by hydrogen up to 300 PSI using an Equilibar back pressure regulator (BPR). Then, the reactor temperature increased with the 0.5 °C/min ramp to keep the desired reaction temperature setpoint, and simultaneously activated catalyst was pre-treated with the same gas hourly space velocity of syngas with a 2:1 molar ratio of H_2/CO for the next 24 hours. The amount of introduced syngas was calculated based on the molar mass ratio in which for total mass flow of 100 SCCM of syngas, 69.5 SCCM H_2, and 30.5 SCCM of CO were mixed at the outlet of the MFCs in a mixing vessel prior to passing through the reactor tube. For measuring the temperature, 12 J-type thermocouples were involved in each run for continuously monitoring the thermal behavior of the reaction and parts, and seven thermocouples were measuring the temperature in the core of the reactor. Here, each thermocouple (TC) gets arranged in order to have a 1.9 cm (¾ inches) distance from the next TC. Three other thermocouples were measuring the wall temperature at the outer surface of the reactor tube in their fixed positions. These 3 TCs are arranged to be in the same radial axis as one of the inner TCs. One TC measures the temperature of the hot trap, and the other TC is using it to control the heating element of the

heat gun. The multi-thermocouple were inserted through a tee that connected the feeding line of the reactor and sealed to have a fixed position inside of the reactor. The very end part of the reactor was connected to a 240 mL Parr bomb and was used as a hot trap and the temperature was kept constant to be set at 150 °C in all runs. All liquid and gaseous products are assumed to leave the surface of the catalyst bed and to flow through the hot trap. The exhaust of the hot trap was connected to the BPR unit with a stainless steel tube which is kept at 120 °C with heating tape to avoid any rapid condensation of the products through the pressurized line before venting out to the condenser. The BPR unit continuously maintains the pressure of the reactor with the stable amount of 300 PSI which is controlling via static pressure of the N_2 gas. Therefore, all volatile molecules could pass through the connecting vessels and tubes and moving forward to the line by helping a continuous flow of unreacted gas and leaving the BPR unit. The gaseous products were then condensed at 0 °C by a glass condenser which kept cool by circulating the coolant (glycerol) fluid via a chiller. Liquified products that contain C_{5+} hydrocarbon products and water with alcohols will be collected in a dripping at the bottom of the condenser. The liquified light oil and aqueous products could be collected routinely from this unit. Other gaseous products were exhausted out from the top part of the condenser where it was mixing with a constant amount of N_2 that is used as an internal standard for tail gas composition analysis via gas SRI 8610C chromatogram (GC). The gas mixture then passes through a gas drier unit, which is a sealed column packed with a desiccant pellet to get demoisturized before it passes through the outlet mass flow meter for measuring the tail gas flow. In the

end, the composition of the tail gas is examined continuously via a GC equipped with a Restek (Shin) column, FID, and TCD units. Typically, unreacted H_2 and CO followed by light hydrocarbons such as CH_4, C_2H_6, and CO_2 will be detectable by the GC, and the result could be quantified by comparing the peak areas with an internal standard S(N_2). A routine daily inspection needs to be held by the operator to avoid any leakage through the lines and connections. Figure. 27. Show the schematic diagram of the FT rig.

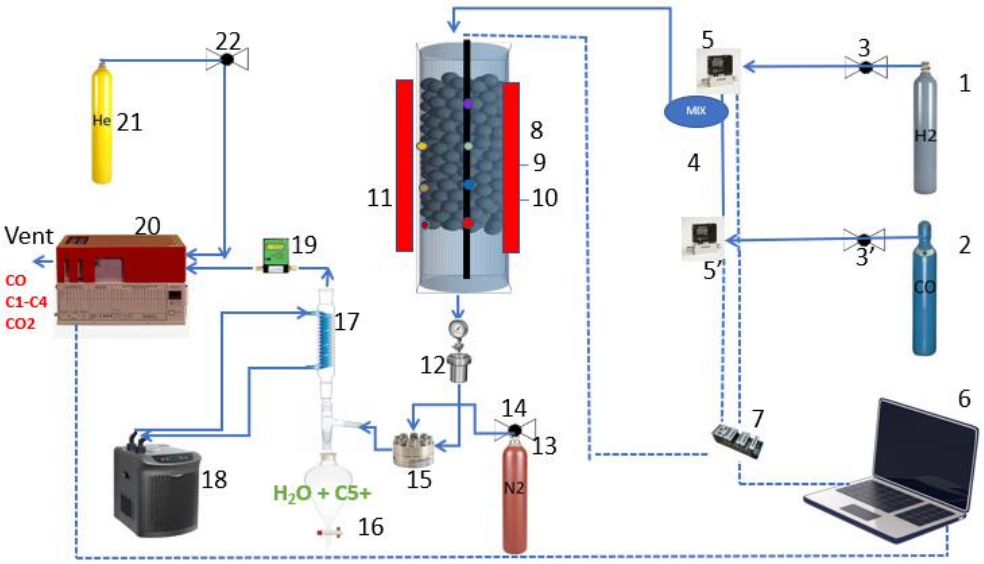

Figure 27. Figure 28. The schematic diagram of the FT rig (1) Hydrogen cylinder; (2) carbon monoxide cylinder ; (3,3') pressure regulator;(4) Mixing chamber; (5,5') mass flow controller; (6) Computer;(7) NI data collector modules; (8) Reactor wall;(9) Multipoint- thermocouple;(10) Catalyst bed ;(11) wall thermocouple ;(12) hot-trap and Pressure gauge;(13) Nitrogen cylinder;(14) pressure regulator;(15) Back pressure regulator;(16) Product collector;(17) Condenser;(18) Chiller;(19) Wet gas flowmeter;(20) Gas Chromatograph;(21) Carrier gas ;(22) pressure regulator

4.2. The Heater Unit

One of the essential requirements of the running of FT reaction is that the reactor walls constantly need to be kept at a certain temperature to maintain a proper temperature to the catalyst and keep it activated. In the current design, hot air was continuously blowing through a stainless steel shroud with a 4.5 cm diameter that was surrounding the reactor tube. The hot air was maintained by a heating gun that the temperature and airflow were under control with the Simulink program. During the reaction, the shroud was wrapped with an insulator to maintain better thermal stability. The hot air was blowing through the shroud from an entry with 1.5 cm diameter and after circulation through the cylinder, it was blowing out through an outlet. Previous researcher implemented CVSAM for obtaining effective thermal conductivity and its sensitivity. This calculated sensitivity can be advantageous in determining reliability of the system for example ball grid array package , moreover neural network can be used to predict temperature of heat generating body. Finite volume code has been developed for capturing heat transfer

Figure 28. Actual FT reactor demonstrating the 1.9 cm reactor tube surrandeed by a 4.5 cm diameter stainless steel shroud with an entry and outlet maintaining hot air flow to kepp the wall of the reactor in a desired temprarue.

phenomena in heat generating bodies. Furthermore sensitivity is derived using CVSAM, which is helpful for predicting reliability of system as ball grid array package. in addition, neural network can be used to predict temperature of heat generating body. Complex Variable Semi Analytical method (CVSAM) is advantageous in capturing sensitivity regardless of determining step size, which has been implemented in inverse analysis. These sensitivity values are helpful in measuring reliability of the system including ball grid array package. moreover, machine learning is used to predict temperature of heat generating body. Numerical inverse analysis is used to predict properties of heat generating material by measuring temperature at outer boundary. Accuracy and efficiency of the method is enhanced by using accurate sensitivity information by use of Semi-Analytical Complex Variable Method (CVSAM). Sensitivity information is beneficial in determining reliability of the system like ball grid array package. In addition, machine learning can be used to predict temperature of heat generating bodies.[90–94]

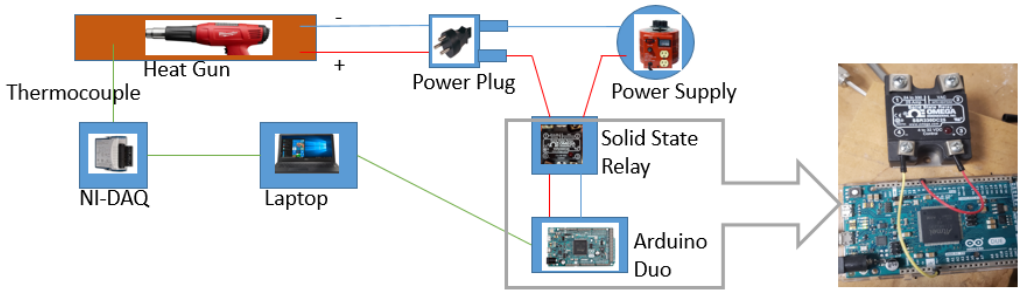

Figure 29. Flow diagram of the heating system connected to the controlling system.

4.3. Control hardware and Software set-up

To monitor the operation, hardware such as thermocouples, a data acquisition system, and a microcontroller has been installed. Temperature data from a thermocouple is transmitted to a computer via the data acquisition system (NI DAQ 9211). Using thermocouple blocks, this data is then interpreted and read in MATLAB Simulink. This data is then compared to the set temperature in Simulink software, and the error is fed into the PID loop to control the gain. The gain is used to control the heater via the Arduino microcontroller. A PWM signal is generated by the microcontroller to control the power of the heater during the process setup.

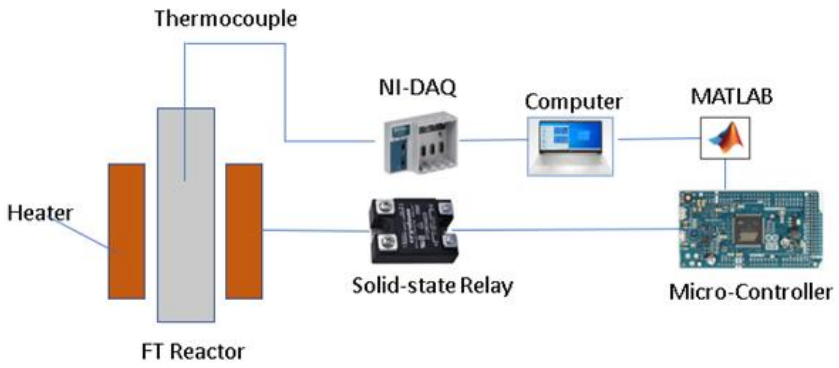

Figure 30. Control Hardware/software Setup

4.4. PID controllers

A PID controller minimizes the error value between the desired set-point value and the actual system output value (the feedback signal). It is done by calculating the output signal as follows:

u(t) = kpe(t) +ki Z e(t)dt +kd de dt

where u(t) is the output, e(t) is the error signal measured between the desired setpoint and the system output, kp is the proportional gain, ki is the integral gain, and kd is the derivative gain. Those three gains combined with the tracking error signal determine the proper output value for the system on the next time step. In a manner to solve this time continuous function in a discretized time system, one needed to discretize the function u(t). For the differential function from u(t),

Thermocouples and an auto-tune PID controller are used in this experiment. Temperature oscillation has been observed via this PID controller at + 110/-30 C around the fixed temperature of 245 C. Since exothermic reactions occur in such a short time, an auto-tuning controller is insufficient to keep the temperature stable around the critical temperature of 245 °C.

4.5. Augmented control loop

A novel augmented control loop has been developed to solve the problem of auto-tune PID controllers. Here On/Off switch was used prior system reaches to the activation temperature. When the temperature reaches 235 °C, the heater is switched off by changing the set temperature for the PID controller to 235 °C. It

sets error to zero or negative and consequently sends no signal to the heater (Heater OFF). Due to the thermal inertia of the system, temperature increases up to 245C then heat is added due to the exothermic reaction of the process. As the heater is switched OFF, the system's temperature increases up to a specific temperature (~255 °C to 258 °C) and then starts decreasing. At this moment, the control loop senses a decrease in temperature and sets the reference temperature as 255 °C. Error signals for PID become positive, and it switches ON the heater. Heat added by the heater is proportional to the error signal, which provides adequate heat not to increase temperature beyond control. Again, around temperature 245 °C, exothermic reaction adds heat to the system and starts increasing temperature, and the control process repeats to maintain the temperature at +/- 4 °C.

4.6. Simulink diagram

A MATLAB program Simulink was used to create a modified control loop for the FT reactor system. Figure 3 depicts an overview of the Simulink diagram, which includes temperature input from the system and output to the Arduino as PWM signals. There are two start blocks. The first start block starts the temperature reading, while the second start block starts the derivative subsystem. The interpreted MATLAB function shown in this figure contains MATLAB code for communicating with a DAQ system and reading temperature data. Overall, three separate subsystems are used, which are detailed in the following sections.

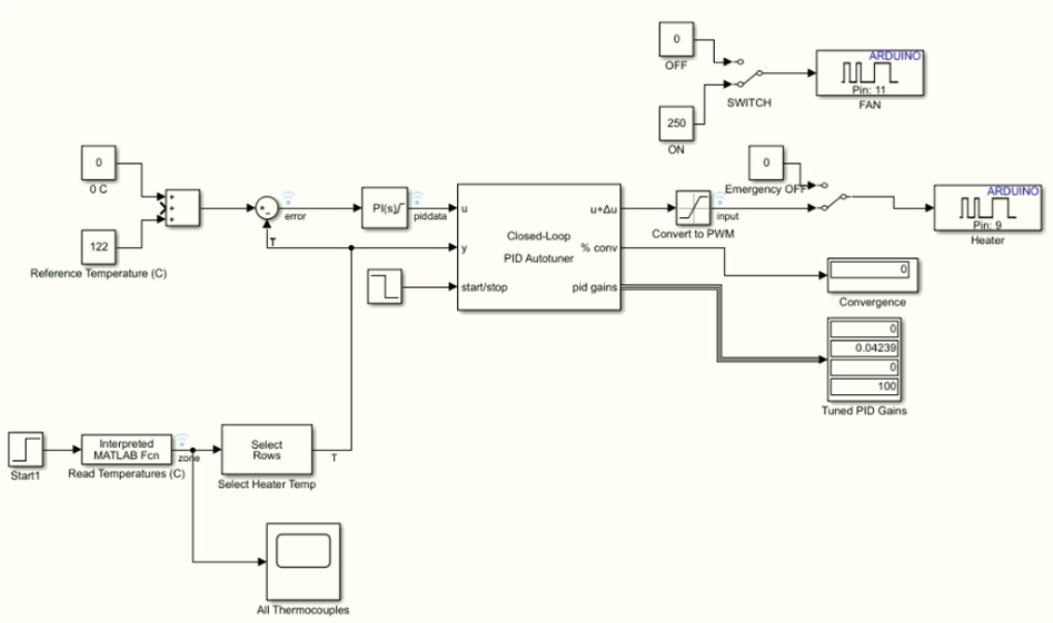

Figure 31. The general Simulink diagram.

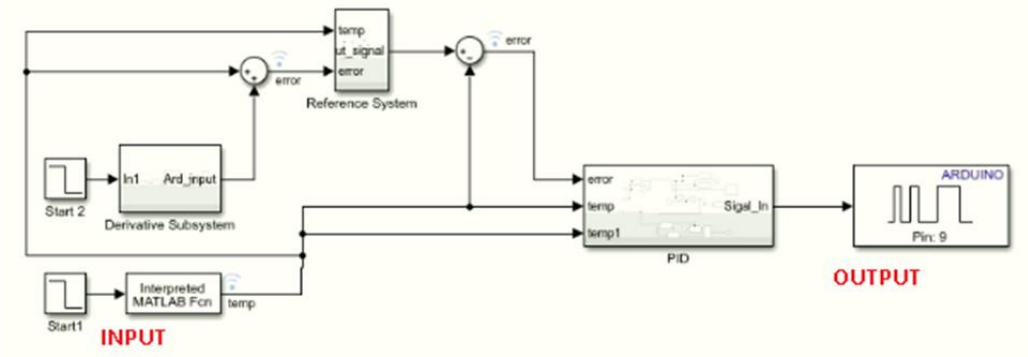

Figure 32. Modified Control Loop Overview- Simulink Diagram.

4.7. Derivative Subsystem

The derivative subsystem is started by the second start block. This subsystem's interpreted MATLAB function compares temperature to a previous time step and outputs the difference (dT). Further if else blocks evaluate this difference and set a new reference temperature difference, for example, if dT is positive, it provides a reference temperature of -10 degrees Celsius, whereas dT is negative, it provides a temperature of +10 degrees Celsius.

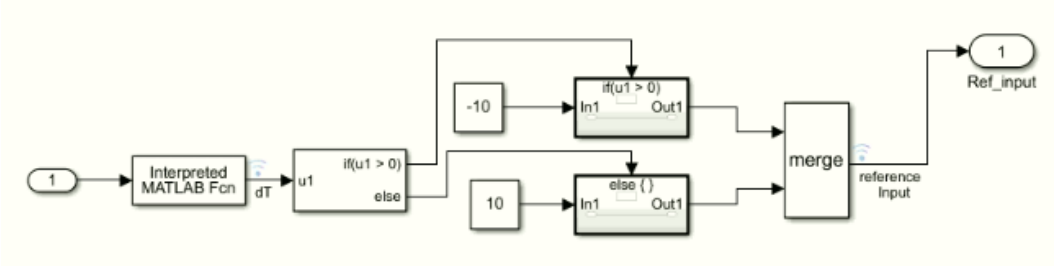

Figure 33. Derivative Subsystem - Simulink Digram.

4.7.1. Reference Subsystem

The reference subsystem receives two inputs: the first is a temperature reading from the system, and the second is the difference between the reference temperature difference from the derivative subsystem and the temperature reading from the system. The first if block compares the system temperature and sets the reference temperature for the PID control loop. i.e., if the temperature is greater than 528K, it sets the temperature to 528; if the temperature is less than 508K, it sets the temperature to 508. It sets the temperature of the second input signal while it is between 508 and 528. It has been determined in this loop that the system is not overshooting at any point in time due to the time lag of temperature measurement.

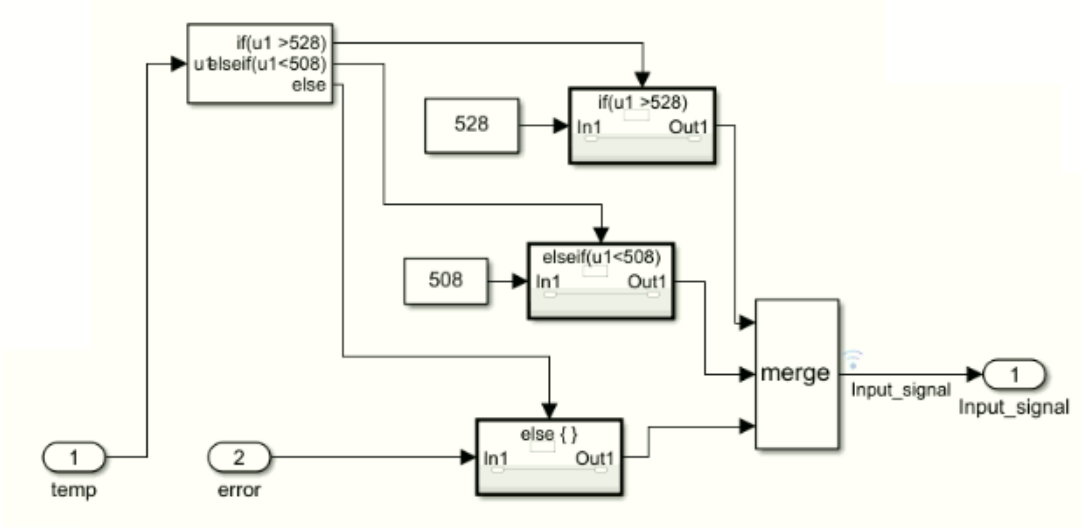

Figure 34. Reference Subsystem- Simulink Diagram.

4.7.2. PID Subsystem

As shown in Figure 6, the PID subsystem employs standard MATLAB functions. There are three input signals to this subsystem. The first is an error for the PID function loop, and the other two are system temperatures. Here, the PID function sends signals that are compared to 255 to generate PWM signals for the Arduino microcontroller, which controls the heater based on this signal. Another safety loop is added here to prevent the system from overshooting. This extra safety loop compares the system temperature to 547 K and sends 0 to the Arduino, causing the heater to be turned off and the system to be protected.

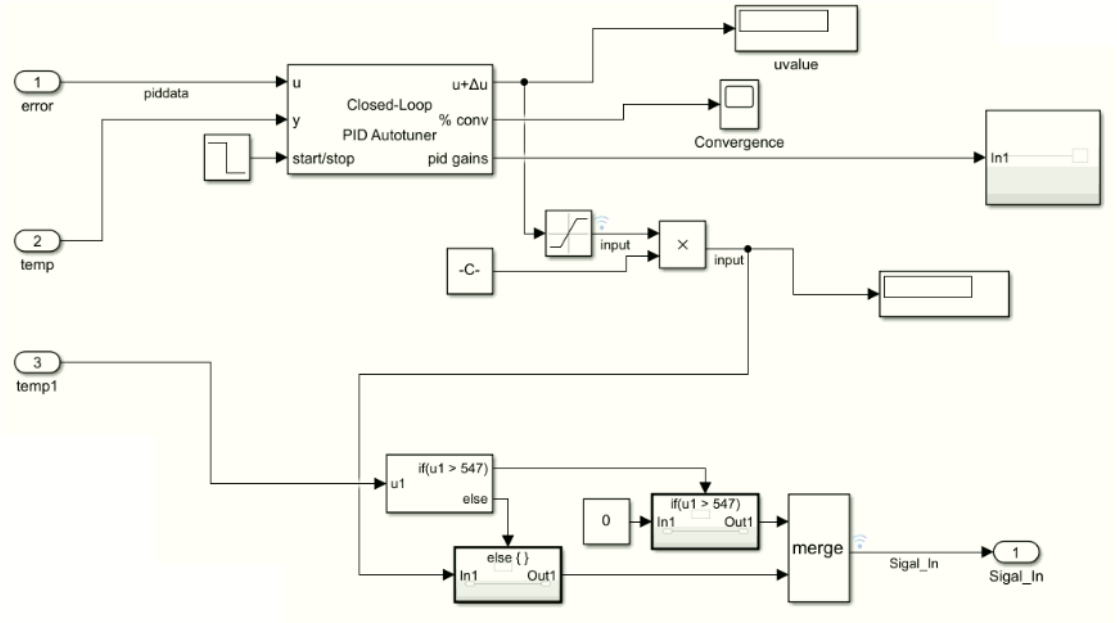

Figure 35. PID Subsystem - Simulink Diagram.

Chapter 5

Fischer-Tropsch Synthesis

5.1. Introduction

In this chapter, we conclude the FTS performance for all catalysts candidates. All prepared catalysts were active in FT reaction conditions. The FT catalysts candidates classified into seven different categories:

1- Conventional mesoporous silica-supported egg-shell catalyst (CMS-ES)
2- Conventional mesoporous silica-supported fully impregnated catalyst (CMS-FI)
3- Mesoporous alumina monolith egg-shell catalyst (MAM-ES)
4- Mesoporous alumina monolith fully impregnated catalyst (MAM-FI)
5- Mesoporous alumina monolith core-shell catalyst (MAM-CS)
6- Thermally modified mesoporous alumina monolith egg-shell catalyst (X-MAM-ES) with five different types of a thermal modifier (X) could sub-divided based on modifier as:
    - Aluminum modified egg-shell catalyst (Al-MAM-ES)
    - Copper modified egg-shell catalyst (Cu-MAM-ES)
    - Rainey Cobalt modified egg-shell catalyst (RC-MAM-ES)
    - Graphite modified egg-shell catalyst (Gr-MAM-ES)
    - Silica carbide modified egg-shell catalyst (SC-MAM-ES)
7- Aluminum modified core-shell catalyst (Al-MAM-CS)

Synthesis of the mesoporous alumina powder (MAP) and fabrication of monolith (MAM) are explained in detail in chapter 2. Preparation of thermally modified X-MAM-ES, core-shell MAM-CS, and Al-MAM-CS supports are discussed in chapter 3. The Impregnation techniques to customized deposition of the Cobalt and Ruthenium on support for the preparation of The egg-shell and fully impregnated catalyst are discussed in section 3.3.2.

In this study, the catalyst was weighed and loaded into the reactor to repeat the same bed volume of 15.7 cm^3 with a 7.6 cm packed length for all examined catalysts. The total mass of the applied catalyst varied due to the mass of added thermal promoters. The total mass of Cobalt and Ruthenium was calculated based on the mass of mesoporous silica or alumina (CMS or MAM) used in the support composition. Each FT run was typically continued for at least one month before termination. Before carrying out the FTS, The catalyst IS reduced in-situ under hydrogen flow of 380 h^{-1} a 400 °C during a time period of 18 hours. The performance of the FT catalysts was examined at the constant pressure of 300 PSI under 380 h^{-1} and 760 h^{-1} GHSV of syngas and two different temperatures at 245 °C and 255 °C for egg-shell impregnated catalysts (CMS-ES, MAM-ES, X-MAM-ES, MAM-CS, Al-MAM-CS). As expected, conducting the FTS reaction under higher syngas flow or higher temperatures (760 h^{-1} GHSV and 255 °C) was not practically feasible for fully impregnated catalysts (CMS-FI, and MAM-FI); the FT runs were investigated under mild reaction conditions (380 h^{-1}, and 245 °C) regarding temperature runaway issues. The molar ratio of the H_2 to CO in the

syngas is maintained at 2:1 in the absence of any other coolant gas that regularly is mixed with it, such as N_2, He, Ar.

The catalysts have the overal CO conversion in range between 50% to 75%, methane selectivity in the range between 5% to 22%, C_{5+} selectivity of 70% to 87%, and productivity of the C_{5+} 1.3 to 25.9 mg per unit volume of the reactor per hour.

The Outcome/Products of the FTS are classified into tail gas, liquid oil, wax, and aqueous phase. The tail gas content was continuously monitored by GC with a sampling loop in every two hours. In addition, the flow of the gaseous was continuously recorded during the operation by a digital flow meter (FMA 4000 Omega). The product liquid oil was separately collected in the cold and hot traps. The condensed oil in the cold trap was collected and labeled as the light oil (LO) as a routine basis. The hot trap contains heavy oil (HO) and wax (if any was generated). By depressurizing of the hot trap in the end of each running circle the HO and wax get separated as HO passed the tubing and collected in the collector while the wax remains in the hot trap liner. The aqueous phase, which contains the produced water and alcohols also was collected with the LO in the cold trap.

Figure 36. The Fischer-Tropsch Reactor with multi-point thermometers on top and a hot trap sample collecter at the bottom.

5.2. Thermal conductivity measurment

Measuring thrmal conductivity of the catalyst bed was the important tool to help underastanding of the catalyst performance. For instigating the temperature, five J-type thermocouples Z1 to Z5 were inserted in the centre of the catalyst bed for continuously monitoring the thermal behavior of the reaction. Each thermocouple (TC) get arranged in order to have a 1.9 cm (¾ inches) distance from the next TC. Three thermocouple zones W2, W3, and W4 are placed respectively on the outer side of the reactor wall opposite of the Z2, Z3, and Z5 for radial heat transfer measurement. The heat transfer measuring's were examined through a stainless-steel single tubular fixed-bed reactor with 20.3 cm length, an internal diameter of ID = 17.3 mm and 1 mm wall thickness with a feeding syngas from the top of the reactor. In this research we decided to calculate the temperature differences within the catalyst bed by subtracting two adjacent TCs along the central thermocouples and calculating the axial tempreture gradient by dividing by the distances (1.9 cm). Therefore, Axial tempreture gradient under syngas flow between Z3 and Z2 in the following graph is calculated as $\Delta T_{Axial} = (T_{Z3}-T_{Z2})$ /1.9 = (248-246)/1.9 = 1.05 °C/cm. The radial temperature gradient calculated with subtracting of a termocouple zone and corresponding thermocouple attached to the wall of the reactor divided by the 7 mm the radial distance. For example for the following graph $\Delta T_{Radial} = (T_{Z3}-T_{w3})$ /7 = (248-222)/7 = 3.7 °C/mm is the calculated radial temperature gradient. By the same calculation for all adjacent and cross thermocouples we will be able to take an overal perspective from tempreture distribution through the bed.

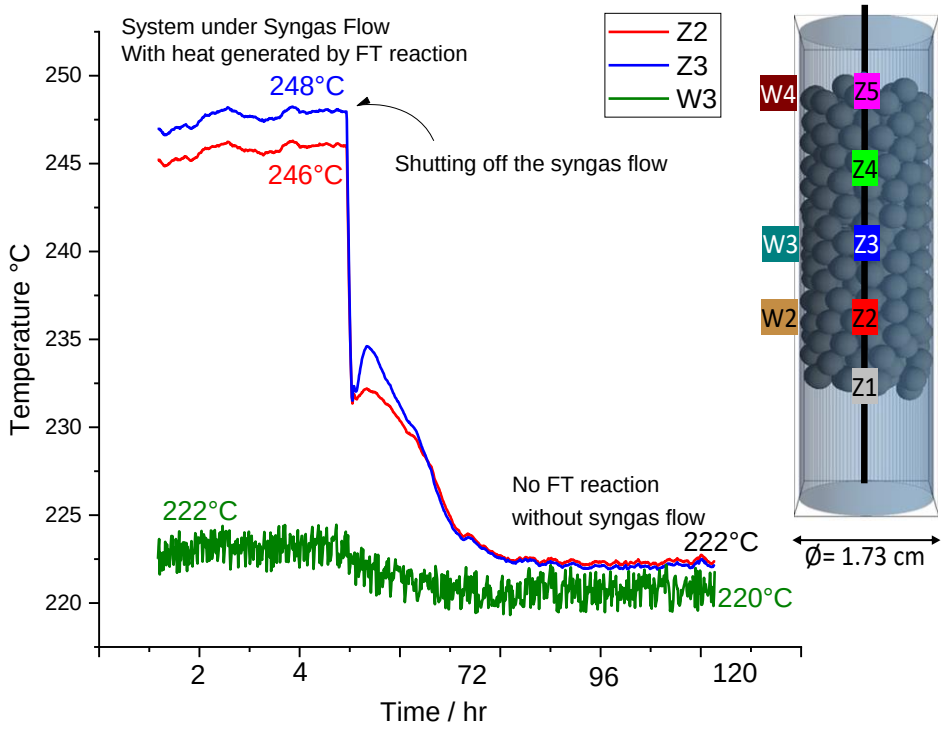

Figure 37. Thermal beahavior of the catalyst bed showing temperature profile for two adjacent central thermocouples Z2 AND Z3 and one wall thermocouple W3 corresponding to the Z3.

As shown in the Figure 37. the tempreture profile of two central points of the catalyst bed was studied under FTS reaction condition while the catalyst bed was under syngas flow and generats heat caused bt exothermisity of the FT reaction, and temperature of those zones in absence of the syngas flow without FT reaction. This graph is showing that estimating the thermal conductivity through stagnant nitrogen test could not provide the right measure as the thermal conductivity of the catalyst needs to be calculate based on tempreture of the bed through the FT reaction under the same reaction conditions.

5.3. The Catalyst Characterization

The primary parameters of the catalysts were evaluated prior to loading in the Fischer-Tropsch reactor tube. The catalysts were characterized using a Nitrogen adsorption-desorption method via a fully automated, three-station, BET surface area, and BJH porosity analyzer, Temperature Programmed Reduction (TPR), Crushing strength test.

The following chapter briefly summarizes the results of these preliminary tests applied in the present research.

5.4. Catalyst Evaluation

The catalysts were reduced in-situ under hydrogen flowing at 400 °C for 18 to 24 hours at a GHSV of 385 h^{-1} and atmospheric pressure. The system's temperature allowed to reduce to 150 °C where the syngas with a 2:1 molar ratio of hydrogen to carbon monoxide was introduced at a 300 PSIG. The temperature ramped slowly to 245 °C while the syngas was flowing with a GHSV of 380 h^{-1}. The systems were initially allowed to maintain a steady state over the first day of activation. Therefore, produced liquids during the first 24 hours of the synthesis were collected separately and not to be counted in the FTS productivity calculations. Furthermore, The performance of the catalysts was scrutinized under 765 h^{-1} and 255 °C.

5.5. Temperature programmed reduction (TPR)

The temperature-programmed reduction (TPR) experiment was carried out with a customized setup using TA Instruments, the Q600 DSC-TGA.(Fig. 42.) Percent mass-loss rate vs. temperature resulted from TPR, using 0.2 g of a calcined catalyst with a 20 SCCM flow rate of a mixture of 3% H_2 and 97% N_2 gas. Temperature was raped at a rate of 2 °C/min from 50 °C up to 600 °C.

The catalysts showed to reduce at temperatures lower than 400 °C, which represents the Co_3O_4 reduction by the negative peaks shifting to the lower values form was shown in TPR plots well proved that in the presence of the Ru as promoter Co reducibility has been drastically influenced.

The sample was taken from impregnated parts of the support in both egg-shell and core-shell catalysts. Figures 38. and 39. show the Ruthenium's reduction promoted Cobalt deposited on MAM surface at 330 °C after an initial mass loss in the temperatures lower than 100 °C due to the evaporation of the adsorbed moisture.

In thermally improved catalyst series, the sample contains the conductive powder. For example, in the Cu-MAM-ES catalyst, the TPR was separately performed on both support and impregnated outer shell.

The figure 40. and 41. shows the reduction of the copper powder at 321°C in the presence of the hydrogen gas, in figure 41. reducibility of the impregnated (shell) section of the Cu-MAM-ES examined by TPR method and it was showing that at 338°C the catalyst will be reduced.

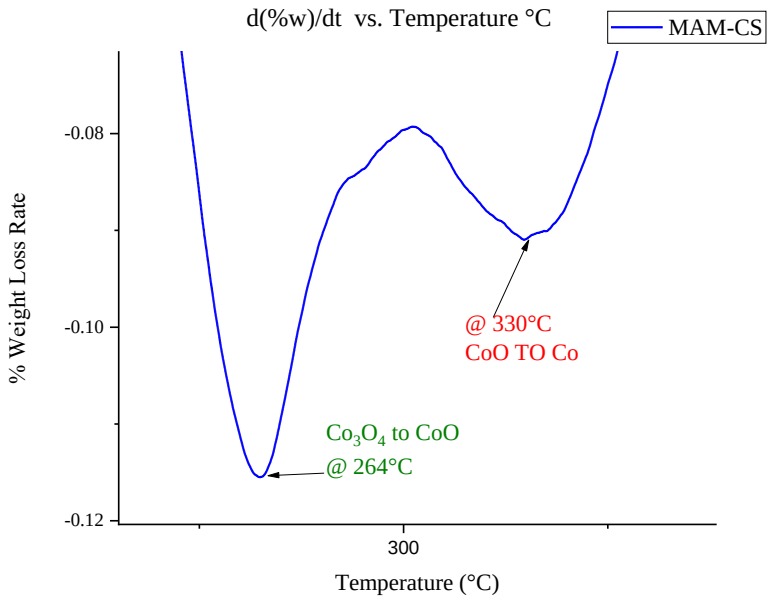

Figure 38. Temperature programmed reduction (TPR) of the 20% Co/1.5% Ru/MAM-CS support (shell sample)

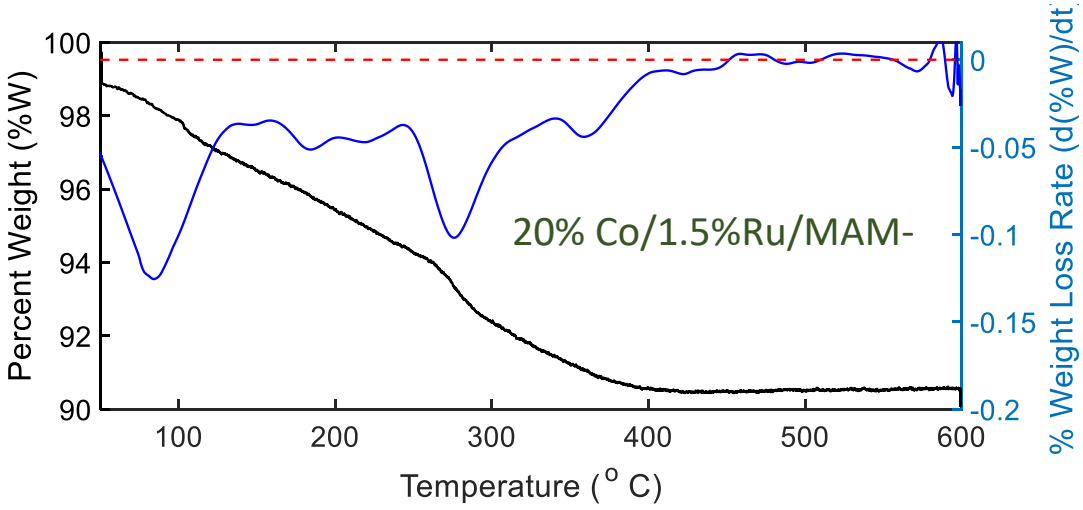

Figure 39. Temperature reduction program (TRP) of the 20% Co/1.5% Ru/MAM-ES support.

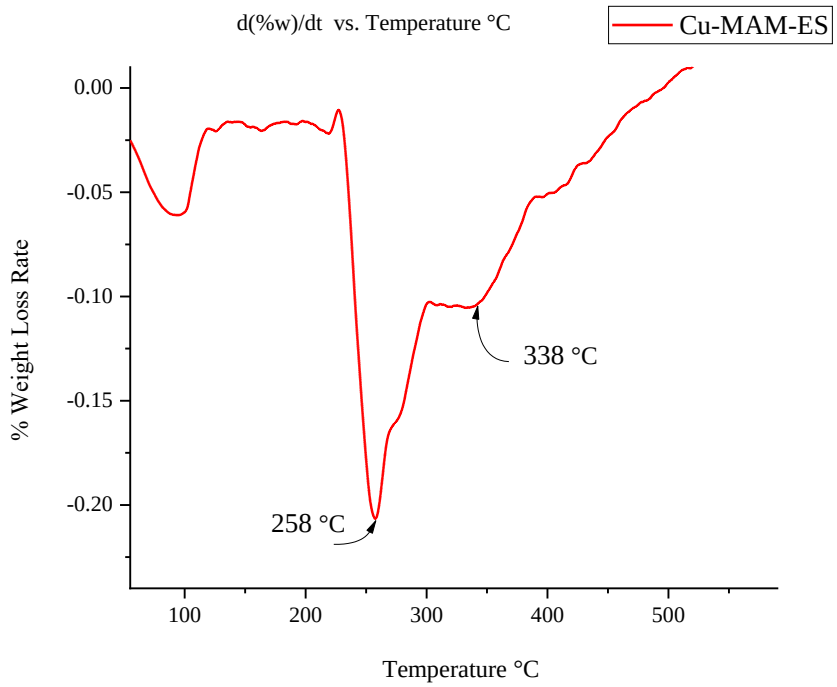

Figure 40. Temperature programmed reduction (TPR) of the 20%Co/1.5%Ru/Cu-MAM-ES support.

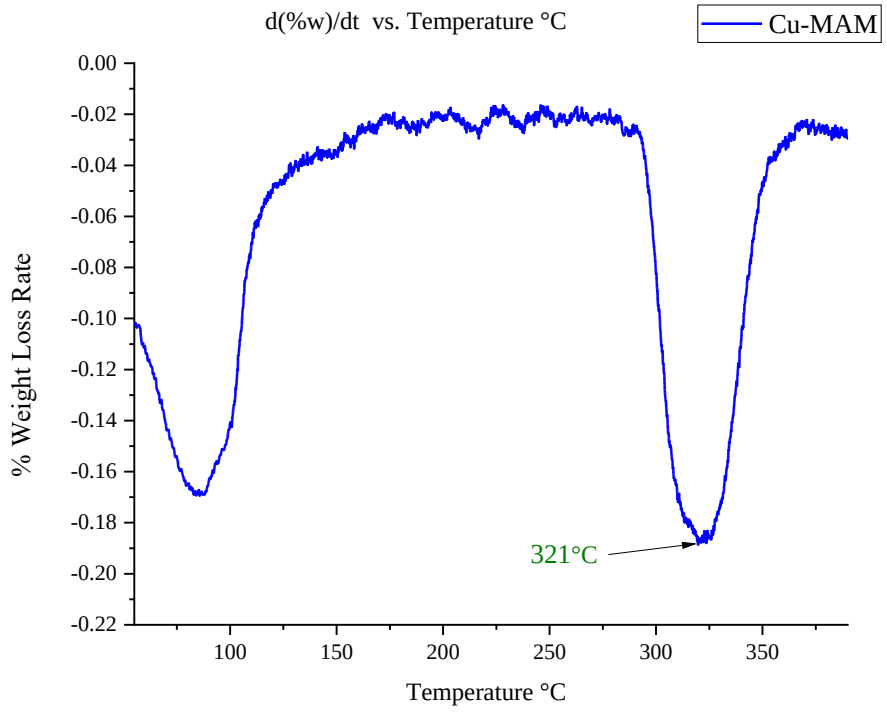

Figure 41. Temperature programmed reduction (TPR) of the Cu-MAM support.

Figure 42. TPR experiments caried out via TA Instruments, the Q600 DSC-TGA with dual beam sampler and reference,

#	Surface Area	Pore volume	Pore volume	Comment
	m2/g	cm3/g	Å	
1	230	0.72	120	MAM
2	225	0.75	120	calcined at 400 C
3	202	0.65	124	Impregnated and calcined
4	182	0.47	130	After 50 days Reaction

5.6. Nitrogen adsorption-desorption

Textural properties of the bare, impregnated, and used catalyst supports were measured by the nitrogen adsorption-desorption isotherms obtained using a Tristar II surface area and porosity analyzer (Micromeritics Co. Ltd) shown in figure 43. Samples were degassed at 160 °C under a nitrogen flow of 20 mL/min for 12 hours prior to the measurements. The specific surface area (S_A) was calculated by the Brunauner–Emmett–Teller (BET) method, using a P/P_0 range between 0.05 and 0.30. The total pore volume (V_p), average pore diameter (D_p), and pore size distribution (PSD) were determined from the desorption isotherm at the relative partial pressure P/P_0 of 0.990 based on the Barrett, Joyner, Halenda (BJH) model. The total pore volume (V_p) is derived from the BJH desorption cumulative volume of pores between 17.0 Å and 3000.0 Å diameter. The pore size, $D_{p,}$ is the pore diameter at the peak position of the PSD curve derived from the adsorption branch of the isotherm using the BJH method.

#	Surface Area	Pore volume	Pore volume	Comment
	m2/g	cm3/g	Å	
1	230	0.72	120	MAM
2	225	0.75	120	calcined at 400 C
3	202	0.65	124	Impregnated and calcined
4	182	0.47	130	After 50 days Reaction

Table 13. Textural properties of the MAM-ES support, before and after 50 days of FTS.

Figure 43. Tristar II surface area and porosity analyzer (Micromeritics Co. Ltd) with sample degassing unit and vaccum pump.

5.7. Crushing strength test

Mechanical stability of the prepared catalyst particles is one of the critical parameters for determining the reliability of the process. A catalyst with a decent crushing strength could prevent failure in the fixed bed reactor due to the maldistribution of syngas and fluid products flow and significant pressure drop through the catalyst bed. However, this matter could hamper the non-efficient catalysis and series of consequences which results in the pilot plant shutting down.

The average crushing strength of the monolithic catalyst spheres was measured based on ASTM (D4179) method using a crushing strength tester. Figure 41. shows the Shimadzu Precision Universal - tensile/crush tester (TCE-N300).

Before each test, all catalyst samples were degassed under nitrogen at 120 °C for 2 hours and kept in a sealed vial. The compression tests are conducted on a minimum of 10 single catalyst particles of each type by applying an axial force at a uniform rate of 1.0 N/sec until the catalyst particle crushes or collapses.

Figure 44. The lay out of the Shimadzu Precision Universal - tensile/crush tester (TCE-N300).

Chapter 6

Results and discussions

6.1. Introduction

The primary result presented in the current chapter is summarized concerning the observed behavior of the FT process over the studied condition and varied by different thermally modified catalysts.

The present study aimed to figure out a novel catalyst support to help manage the temperature differences in a single catalyst particle and, consequently, through the reactor's active bed by increasing the local heat dissipation capacity of the catalyst particles. To keep all the catalytic parameters constant such as textural properties, shape, and size of the catalyst particles, the mass of Co and Ru, and impregnation method, we prepared all catalysts samples with the same materials and techniques.

6.2. FTS by the fully impregnated catalysts; CMS-FI and MAM-FI

In this investigation, we first tried to carry out the FTS without using any diluent by a typical fully impregnated catalyst on two different catalyst support materials with closely identical textural properties. The FTS using a fully impregnated support on both conventional silica (CMS-FI) and alumina (MAM-FI) spheres were done at 245 °C, 300 PSI, under 380 h^{-1}GHSV of syngas with 2:1 molar ratio of H_2:CO. The physical properties of both catalysts are listed in the following table.

The temperature profile of the FT reaction related to the central thermocouple (Z3) is shown in fig. 45. The temperature instability and non-uniform temperature distribution in the catalyst bed caused by the poor thermal conductivity of the porous support decreases the profitability of the FTS for typical fully impregnated catalysts. These thermal difficulties made the process impossible to investigate in higher temperatures or higher syngas flows. The result leads to 1.3 and 1.7 mg C_{5+} product per unit volume (mL) of the reactor per hour for CMS-FI and MAM-FI, respectively. The CO conversion was 55% for silica and 57% for alumina-supported cases, and temperature gradients ranged from 17-17-7 °C/cm for axial and 17.618.2 °C/mm for radial indexes.

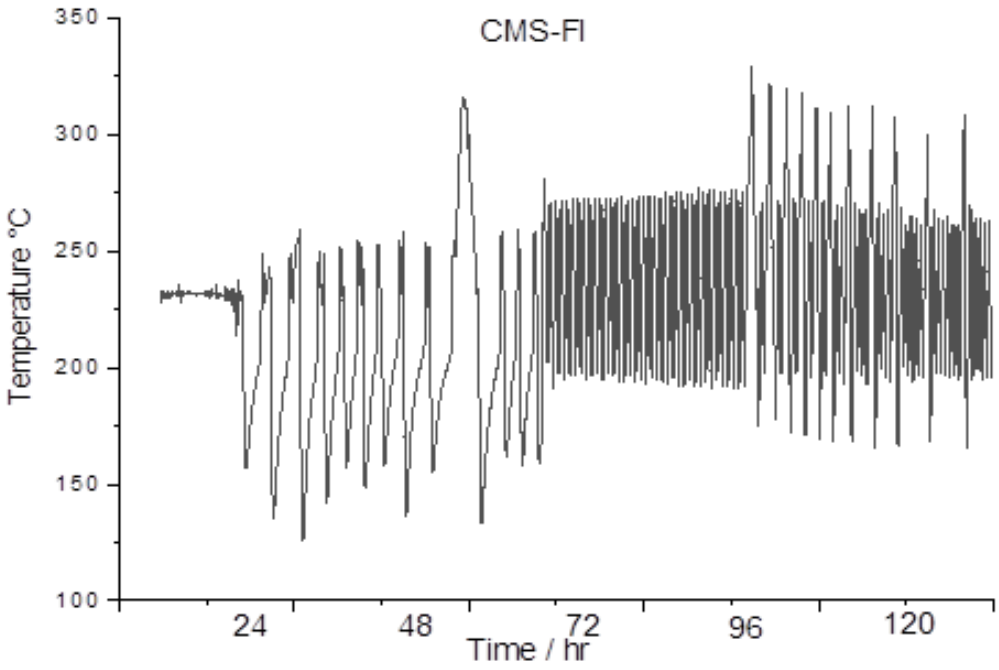

Figure 45. Temperature profile; fully impregnated conventional silica support CMS-FI.

6.3. FTS by the egg-shell catalysts; CMS-ES and MAM-ES

Improving the mass transfer restriction within the catalyst particles is done by loading the active components of the catalyst (Co and Ru) on thicknesses that do not exceed 500 microns.[95] Furthermore, for maintaining a smooth extra particle mass flow, the catalyst particles' size is reported to be optimized in a range between 1-4 mm.[70] Therefore, deposition of the Cobalt on the outer surface of the support particle will be a decent solution for maintaining the mentioned requirements.

The egg-shell catalyst were prepared using both silica and alumina supports by the impregnation technique mentioned in chapter xx. For better perspective, in the first attempt, the FTS reaction with CMS-ES and MAM-ES were performed at the sampe reaction conditions (245 °C, 300 PSI, and 380 h-1) as carried out with fully impregnated catalyst (CMS-FI and MAM-FI). The productivity of the silica supported egg-shell catalyst has increased by marginally close to 2 fold in both volumetric and per unit mass of used Cobalt calculations while in alumina supported case this index accelerated with incrase rate as high as 3.76 times.

In silica supported catalyst, although percent CO conversion in egg-shell was 38 % lower rather than fully impregnated but the percent C_{5+} yield was 54 % higher. As expected, throughly impregnated catalyst converts carbon to the CH_4 3.9 times more than egg-shell. Intrestingly, using the egg-shell resulted to produce heavier hydrocarbon chains, as the result it was producing dominantly (93% wt.) waxes and by increasing the syngas flow this trend was repeated as the wax to C_{5+} ratio was high as 91.6% wt.

The percent crude C_{5+} yield was measured as percent molar mass of product (oil and wax) per total molar mass of generated aquous phase to compare the yield of the process with the theoritical yield. It was 2.6 time higher in silica based egg-shell and 4.3 times higher in alumina based egg-shell catalyst incomper with fully impregnated ones. The egg-shell form showed the smoother themal behavior as the axial tempreture gradient (ΔT_{Axial}) deceased from 17.7 to 7.2 °C/cm and ΔT_{Radial} decreased from 18.2 to 4.5 °C/mm in silica supported. The thermall management in alumina based egg-shell catalyst also decreased with marginally higher rate as ΔT_{Axial} decreased from 17 to 5.2 °C/cm, and ΔT_{radial} reduced from 17.6 to 2.6 °C/mm. Hence, the egg-shell form of catalyst had more uniform tempreture distribution as well as better mass transfer diffusion due to the shorter depth of acticated layer of catalyst.

The FTS reaction condition and performances for each catalys is given in the table 15. In a comparison between alumina and silica base egg-shell catalyst, the dominant product will be the waxes, by increasing the GHSV and tempreture both productivity indexes increases. Under regardless of syngas flow speed, MAM-ES has 3.9 time higher volumetric productivity in at 245 °C in compare to CMS-ES and it is only 1.6 time higher at 255 °C.

It is a well-stablished fact that the production of the high molecular weight waxes is favored by either increasing the pressure or decreasing of the syngas space velocity. By decreasing the path of the activated reagon the partial pressure of the reaction may affected as a result it favores the production of the longer chain species.

The persent carbon converted in MAM-ES catalyst was two time higher than CMS-ES at 245 °C while it is 73% higher at 255 °C. by increasing the GHSV the % CO conversion mariginally declines however, by increasing the tempreture of the reaction from at 245 °C to at 255 °C the rate of CO convertion will be higher. In addition, the synthesis rate could be increased by increasing the tempreture of the reaction as a result productivity of the egg-shell catalyst increases at 255 °C and syngas velocity. As a result of higher conversion and better bulk temperatur gadien, the average percent crude C_{5+} yeild for MAM-ES was 1.94 times higher than CMS-ES.

Table 14. FTS performance for both alumina and silica based of egg-shell and uniformly impregnated catalyst.

	Mass Flow	GHSV	T	Mass of C5+ g			Productivity		Product Analysis						Temprature gradiant	
Catalyst	SCCM	h-1	°C	Oil	Wax	Mass of Aq. Phase g	Per unit mass of Co mg C5+/g Co . h	Per unit vol. of reactor mg C5+/mL Cat . h	% CO Conv.	% SC5+	% SCH4	%S C5+ to Aq.	%S Oil to C5+	% Crude C5+ Yield	ΔT Axial °C/cm	ΔT Radial °C/mm
CMS-FI	100	380	245	3.3	0.5	88	9.9	1.3	55	55	31.4	4.3	86.8	5.5	17.7	18.2
CMS-ES	100	380	245	0.5	6.9	65.5	19.3	2.5	34	85	8	11.3	6.8	14.5	7.2	4.5
CMS-ES	200	765	245	1	11	109	31.3	4.0	31	87	6	11.0	8.3	14.1	7.2	4.5
CMS-ES	100	380	255	2	13.3	99	39.8	5.1	49	80	15	15.5	13.1	19.8	7.2	4.5
CMS-ES	200	765	255	1	30	173	80.7	10.3	47	83	13.6	17.9	3.2	23.0	7.2	4.5
MAM-FI	100	380	245	4.1	1	85	13.3	1.7	57	60	22.8	6.0	80.4	7.7	17	17.6
MAM-ES	100	380	245	9	10.3	75	50.3	6.4	70	88	8.7	25.7	46.6	33.0	5.2	2.6
MAM-ES	200	765	245	12	34	168	119.8	15.3	68	87	6	27.4	26.1	35.1	5.2	2.6
MAM-ES	100	380	255	12	13.5	105	66.4	8.5	85	71	20	24.3	47.1	31.1	5.2	2.6
MAM-ES	200	765	255	23	27	198	130.2	16.6	82	75	18	25.3	46.0	32.4	5.2	2.6

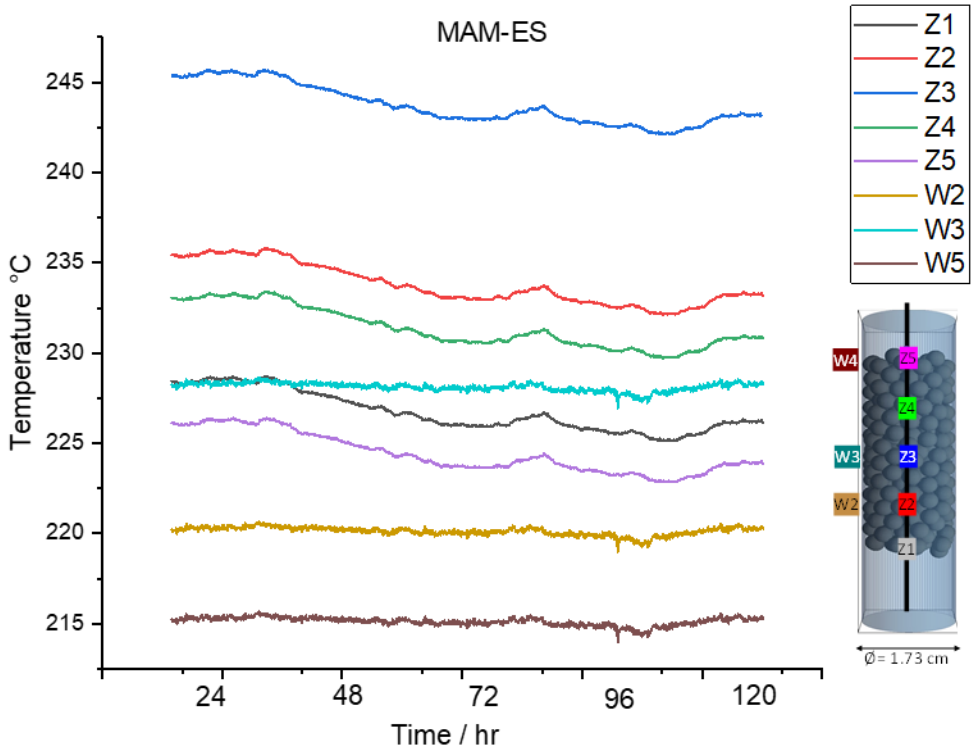

Figure 46. Temperature profile; egg-shell mesoporous alumina support MAM-ES at 245 °C with position of each thermometer in the reactor.

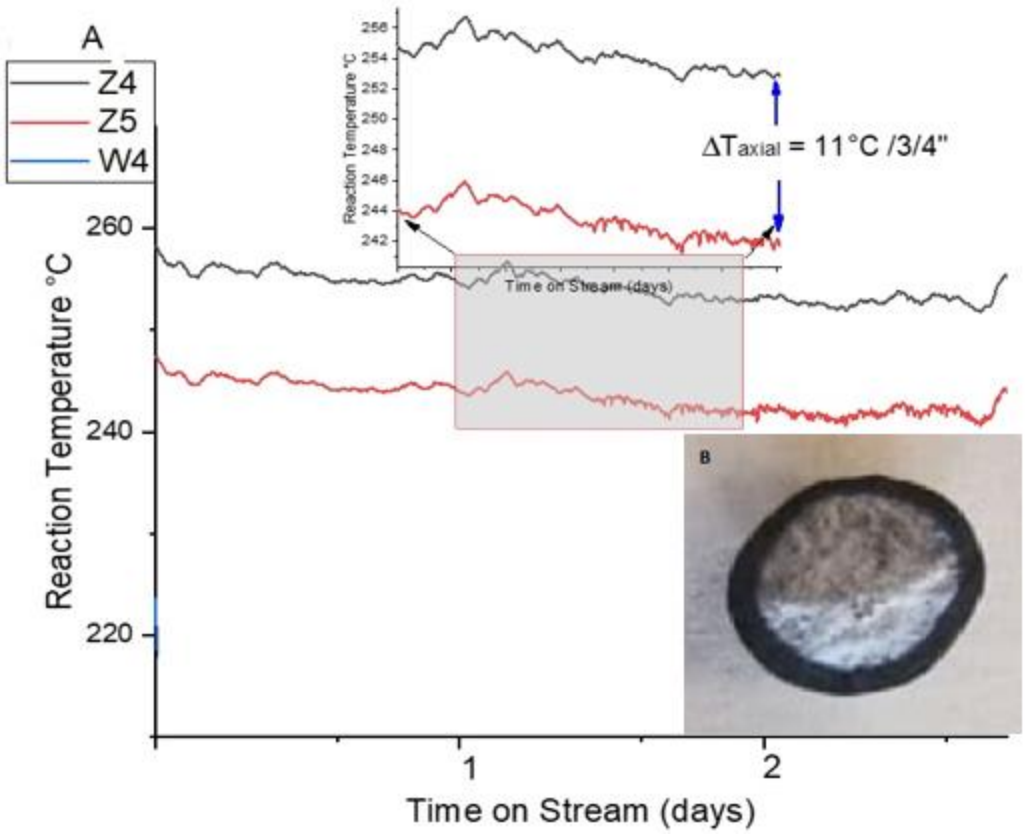

Figure 47. A) Temperature profile; egg-shell mesoporous alumina support MAM-ES at 255 °C. B) 3mm diameter MAM-ES after reaction.

6.4. FTS by the core-shell catalysts; MAM-CS

In the previous section, the improved mass transfer of the FT catalysis is discussed, which is in agreement with the experimental observations for the egg-shell design. The advantages of the egg-shell catalyst due to the better intraparticle mass transfer in comparison with a typical fully impregnated catalyst were examined. Hence, the unused central region of the egg-shell catalyst was replaced with a supper conductive copper sphere. In a typical embodiment, the copper core was coated with the same MAM material and impregnated with same protocol as an egg-shell catalyst, but the thermal property was upgraded by replacement of the ceramic core with the copper. The FT performance was compared with egg-shell design. Please, see the figure 48. B picture of the used core-shell catalyst with 2 mm supper conductive core and 0.5 mm impregnated MAM coating. The textural properties of the shell is same as the MAM used in the egg-shell and fully impregnated catalyst supports with 230 m^2/g surface area, 0.72 cm^3/g pore volume, and 120 Å pore diameter before loading the active catalyst that was measured by N_2 adsorption. The crushing strength of the catalyst was 4 N/mm with an average 3.1 mm diameter.

The MAM-CS catalyst impregnated with 20 % wt. Cobalt and1.5 % wt. Ruthenium and The FTS carried out to investigate the effect of the supper conductive cooper core on the FT performance of the core-shell structure. The mass of cobalt could be estimated based on substraction of mass of used copper spheres from total mass of loaded MAM-CS into the system. The packed catalyst bed kept constant as the previous runs with 15.7 cm^3 and 7.6 cm length and in the same

position. Therefore in core shell catalyst 1.25 g cobalt was used to maintain the 15.7 cm^3 of the catalyst bed. Table xx shows the summary of the results obtained from the FT reaction over 380 h^{-1} and 765 h^{-1} syngas hourly space velocity and at 245 °C and 255 °C and 300 PSI pressure. Table reports the productivity of the process both on per unit mass of used cobalt and unit volume of the reactor per hour. The figure 48. Is shown the schematic diagram of the FT reactor with the position of each thermocouple also the tempreture profile of the MAM-CS catalyst under 380 h^{-1} GHSV and at 245 °C is showing very stable thermal behavior during the reaction. Comparing with egg-shell, the core shell catalyst was showing the lower ΔT_{Axial} of 2.1 °C/cm, which is showing the more overal tempreture uniform through the bed and ΔT_{radial} was measure as 4.1 °C/mm.

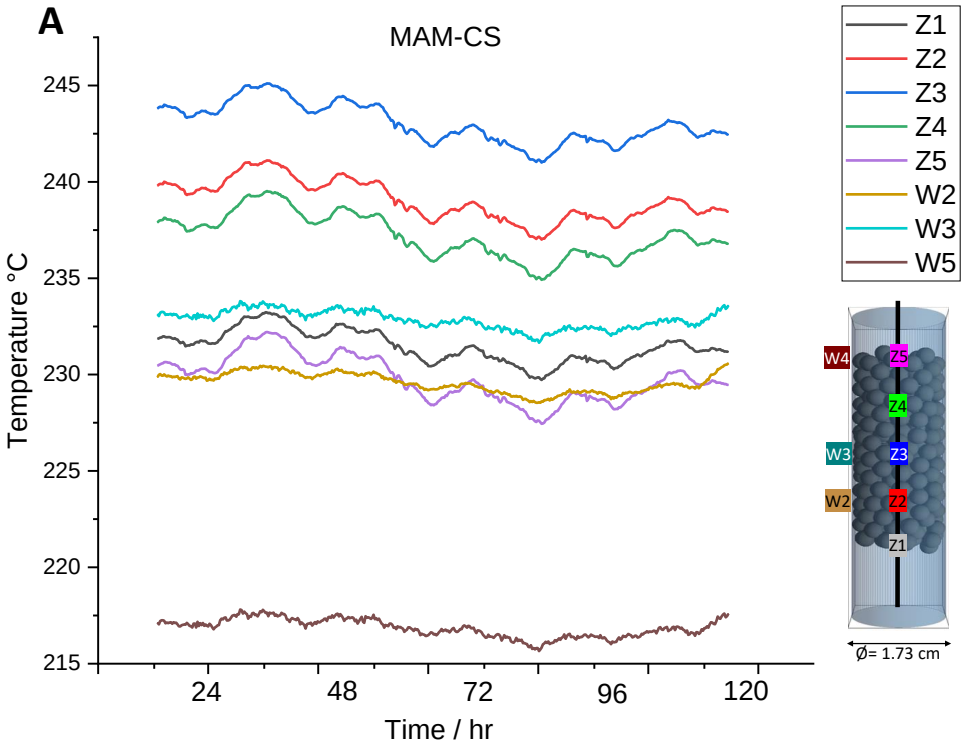

Figure 48. Temperature profile; core-shell mesoporous alumina support MAM-CS at 245 °C.

Figure 49. Core-Shell catalyst support with 2 mm copper core coated with impregnated MAM shell.

By comparing the FT performance of core-shell and egg-shell catalyst under the same reaction conditions it is showing that due to the lower cobalt used in core shell structure and also fast dissipation of the heat generated from the FT reaction the productivity per unit mass of cobalt is almost two times higher than egg shell catalyst while the volumetric productivity shows 26 % increase at 245 °C ans 380 h^{-1}. At the same temperature an only by increasing the GHSV from 380 to 765 h^{-1}, productivity of the process increases increases by 122 % for both volumetric and per mass of Co calculations while in compare with the egg-shell these two indexs showing 18% and 107 % better performance, respectively. At 255 °C, both productivities showing 88% boosts with two fold increase in GHSV. Comparing with egg-shell, at 255 °C nd by increasing the GHSV, productivity per mass of Co is showing 111% and 120% increase and volumetric productivity shows 36% and 32% more product. Depending on both temperature and GHSV, the CO conversions were between 60 % to 70 % in MAM-CS and 68 % to 85 % in MAM-ES case which

is probably caused by presence of 37.5 % wt. more Cobalt in egg-shell catalyst bed in compare to core-sheel. At 255 °C , the MAM-CS is produces a 50% lower methane than the MAM-ES catalyst and average percent crude C_{5+} product yield is marginally better than egg-shell catalyst. Aside all of the mentioned factors, the most intresting fact in comparing the products of the egg-shell and core-shell is that, using later favors liquid range products while the former was making dominantly waxes. It could be casued by more local temperature homogenuity in case using a copper core that maintain a suficiant tempreture to the cold sputs to produce the liquid form products. At 245 °C, 100% of the product were in liquid range and by incresing the tempreture to 255 °C 94.7 % of produced C_{5+} hydrocarbons were liquid. So, using a copper core coated MAM catalyst leads to production of maximum liquid range products.

Catalyst	Mass Flow	GHSV	Temp.	Mass of C5+ g		Mass of Aquous Phase g	Productivity		Product Analysis						Tempratu gradian	
	SCCM	h-1	°C	Oil	Wax		Per unit mass of Co mg C5+ /g Co . h	Per unit volume of the reactor mg C5+/mLCat . h	% CO Conv.	% SC5+	% SCH4	%S C5+ to Aq.	%S Oil to C5+	% Crude C5+ Yield	ΔTAxial °C/cm	ΔT °(
MAM-CS	100	380	245	24.5	0	102	102.1	8.1	61	88	10.2	24.0	100.0	30.8	2.1	
MAM-CS	200	765	245	54.4	0	207	226.7	18.0	60	89	9.0	26.3	100.0	33.7	3.7	
MAM-CS	100	380	255	33	2	132	145.8	11.6	70	85	13.0	26.5	94.3	34.0	5	
MAM-CS	200	765	255	62.5	3.5	245	275.0	21.9	67	85	10.0	26.9	94.7	34.5	5	

Table 15. FTS performance for alumina based of core-shell catalyst.

Catalyst	Mass Flow	GHSV	Temp.	Mass of C5+ g		Mass of Aqueous Phase g	Productivity		Product Analysis						Temprature gradiant	
	SCCM	h-1	°C	Oil	Wax		Per unit mass of Co mg C5+/g Co h	Per unit volume of reactor mg C5+/mL Cat .h	% CO Conv.	% SC5+	% SCH4	%S C5+ to Aq.	%S Oil to C5+	% Crude C5+ Yield	Axial °C/cm	Radial °C/mm
MAM-CS	100	380	245	24.5	0	102	102.1	8.1	61	88	10.2	24.0	100.0	30.8	2.1	4.1
MAM-CS	200	765	245	54.4	0	207	226.7	18.0	60	89	9	26.3	100.0	33.7	2.1	4.1
MAM-CS	100	380	255	33	2	132	145.8	11.6	70	85	13	26.5	94.3	34.0	2.1	4.1
MAM-CS	200	765	255	62.5	3.5	245	275.0	21.9	67	85	10	26.9	94.7	34.5	2.1	4.1

6.5. FTS by the Thermally modified egg-shell catalysts

(Al-MAM-ES, Gr-MAM-ES, RC-MAM-ES, SC-MAM-ES, Cu-MAM-ES)

Gr-MAM-ES

Drawn from the current and previouly reported studies, both mass and heat transfer of catalyst effects are discussed in aformentioned sections. In the other approach for modifying the thermal property of the MAM supports, we tried to add the conductive powders to the formulation of the supports realising a better sidpersion of the thermally conductive spots within the catalyst particle and therefore through the bed. Therefore, the aluminum (Al), graphite (Gr), rainey cobalt (RC), Silica carbide (SC), and copper (Cu) were initially assumed to act as thermal modiefier addetives. The amount of added conductive powders were 16-17% in all supports except in graphite promoted which was 22%. The table xx. shows the physical properties of each composite support were measured by N_2 adsorption and crushing strength test.

Combination of different thermally conductive powders into Ru promoted Co catalyst influenced the catalytic behavior of the FT reaction such as Co conversion, property of the product, selectivity of each component, and profitability of the process so the FTS performance of each thermally modified catalyst support is shown in table 16.

Table 16. FT performans of the thermally modified catalyst supports.

Catalyst	Mass Flow	GHSV	Temp.	Mass of C5+ g		Mass of Aquous Phase g	Productivity		Product Analysis						Temprature gradiant	
	SCCM	h-1	°C	Oil	Wax		Per unit mass of Co mg C5+/g Co.h	Per unit volume of the reactor mg C5+/mLCat .h	% CO Conv.	% SC5+	% SCH4	%S C5+ to Aq.	%S Oil to C5+	% Crude C5+ Yield	Axial °C/cm	Radial °C/mm
Al-MAM-ES	100	380	245	12	13.7	99	78.7	8.5	74	81	16	26.0	46.7	33.3	1.1	3.6
Al-MAM-ES	200	765	245	18.8	25.5	165	135.7	14.7	70	83	13.5	26.8	42.4	34.4	1.1	3.6
Al-MAM-ES	100	380	255	28	11	139	119.5	12.9	76	85	18	28.1	71.8	36.0	1.1	5.2
Al-MAM-ES	200	765	255	45.6	21	233	204.0	22.1	70	86	15	28.6	68.5	36.6	1.1	5.2
Gr-MAM-ES	100	380	259	20	9	148	88.8	9.6	75	79	17	19.6	69.0	25.1	3.1	5.5
Gr-MAM-ES	200	765	259	40.5	18.5	285	180.8	19.6	70	80	16	20.7	68.6	26.5	3.1	5.5
RC-MAM-ES	100	380	245	13	17	133	91.9	10.0	72	77	19	22.6	43.3	28.9	1	2.2
RC-MAM-ES	200	765	245	20.5	30.5	243	156.3	16.9	70	79	16.5	21.0	40.2	26.9	1	2.2
SC-MAM-ES	100	380	245	13	12.5	141	78.1	8.5	76	82	16	18.1	51.0	23.2	2.2	1.7
SC-MAM-ES	200	765	245	19.5	26	233	139.4	15.1	72	83	14	19.5	42.9	25.0	2.2	1.7
Cu-MAM-ES	100	380	261	12	5	128	52.1	5.6	82	50	23	13.3	70.6	17.0	3	6.2
Cu-MAM-ES	200	765	261	19.5	9.5	200	88.8	9.6	80	54	19.5	14.5	67.2	18.6	3	6.2

For taking the advantageous of the higher productivity of the egg-shell impregnated catalyst which is discussed in the previous sections all prepared thermally modified supports were impregnated with the egg-shell form with an average impregnating depth of 0.5 mm. The mass of cobalt on all impregnations were kept constant and were calculated based on mass of the porous alumina in the composite. In all of these FT runs the catalysts contains an estimated amount of 1.7 g Cobalt presented in the reactor. The tempreture pfofile of each catalyst under FT conditions were showing different heat disipation through the catalyst bed. The following graphs are showing the tempreture profiles during the FTS for each thermally modified catalyst support.

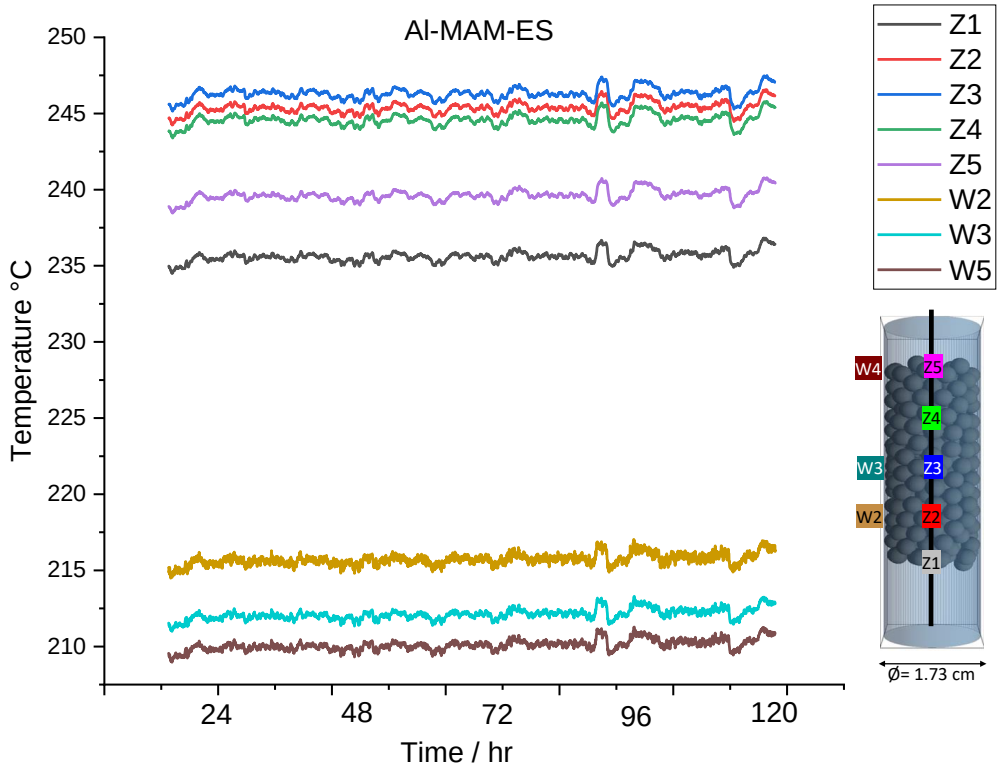

Figure 50. Temperature profile of Al-MAM-ES catalyst under 380 h-1 GHSV and at 245 °C.

The FTS performance of the Al-MAM-ES catalysts were investigated at the same two different temperature and GHSV to compare apply by apple with MAM-CS under the same reactor conditions. At 245 °C the productivity per mass of catalyst was lower than MAM-CS but at 255 °C the same parameter was higher with using the Al-MAM-ES which is showing the better performance at higher temperatures.

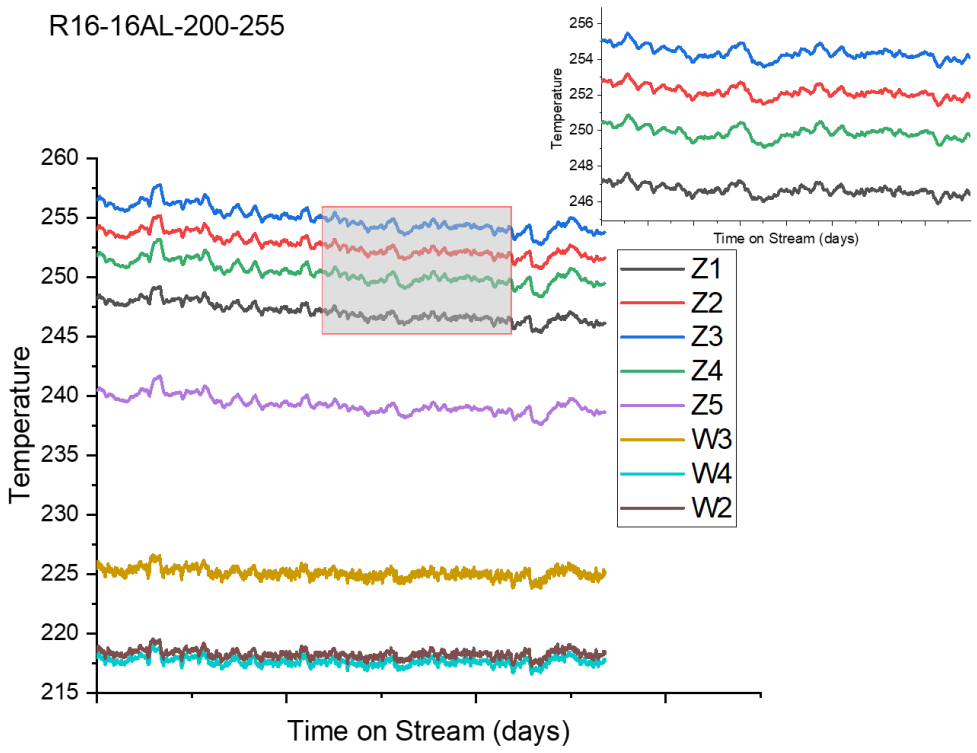

Figure 51. Temperature profile of Al-MAM-ES catalyst under 765 h-1 GHSV and at 255 °C

The volumetric productivity though was almost same by using both catalyst. The average CO conversion was 72.5 % with Al-MAM-ES and 8 % higher than MAM-CS. The average crude C_{5+} productivity Al-MAM-ES was 5.3 % higher than Al-MAM-ES. Depending on reaction temperature Al-MAM-ES catalyst makes 42.4 to 71.8 % liquid oil over total C_{5+} products wich is more than two fold higher than MAM-ES and 3.5 to 6 times better than CMS-ES catalysts. The axial tempreture gradient with using Al-MAM-ES was as low as 1.1 °C/cm and the average radial gradient of the tempreture was lower than in the same range as core-shell catalysts.

Figure 52. Egg-shell impregnated thermally modified Al-MAM support prior to calcination.

By comparing the thermally improved catalysts together, the table xx is showing presence of silica carbide and aluminum powder in MAM could helps the productivity of the FT process. The temperature gradients measuring in both Al-MAM-ES and SC-MAM-ES demonstrates an improvement . As a results using SC-MAM-ES is produces preety much same C5+ with respect to unit volume of the reactor in compare to Al-MAM-ES.

Applying the graphite, rainey cobalt is defenately helps the process in compare to typical egg-shell and fully impregnated catalysts. For activating the Gr-MAM-ES and Cu-MAM-ES catalyst we had to increase the tempreture of the reaction as high as 259 °C for former and 261 °C on later. As it was expected both axial and radial temperature gradients wer improved through addition of themally conductive powders in MAM frame.

By adding the Cupper to the support structure (Cu-MAM-ES) the productivity of the FTS reduces even lower than MAM-ES, the GC-MS results from aquous phase shows that the presence of the Copper in the catalyst matrix

fovors the production of the oxygenates such as alcohols and acetic acid rather than linear alkanes. Among them, the average percent crude oil yield is 33.8 % by using Al-MAM-ES and 27.9 by RC-MAM-ES and 24 % with SC-MAM-ES 25 % when the Gr-MAM-ES is used. However the same parameter was as low as an average of 17.3 when the FT was conducted on Cu-MAM-ES catalyst.

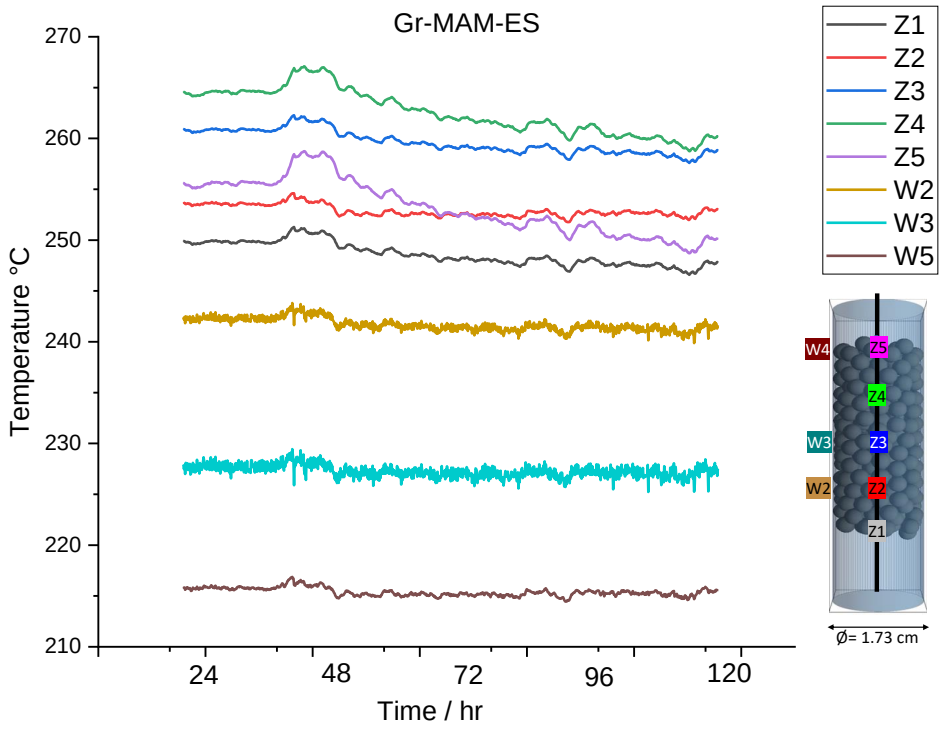

Figure 53. Temperature profile of Gr-MAM-ES catalyst under 380 h-1 GHSV and at 259 °C.

Figure 54. Gr-MAM with catalyst support prior to impregnation.

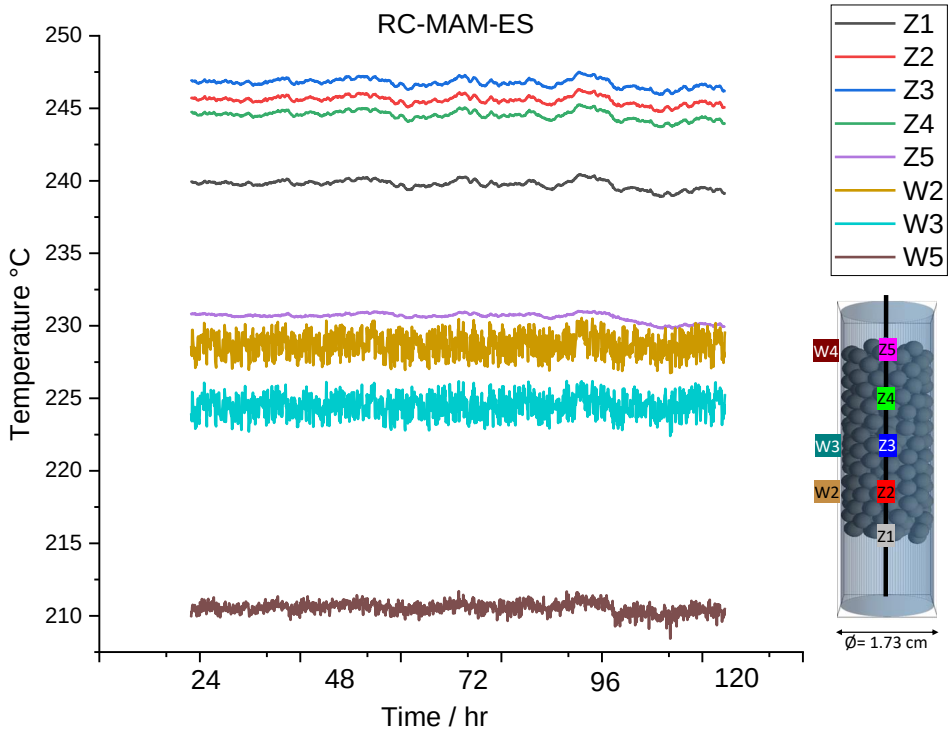

Figure 55. Temperature profile of RC-MAM-ES catalyst under 380 h-1 GHSV and at 245 °C.

Figure 56. Thermally modified RC-MAM catalyst support prior to impregnation.

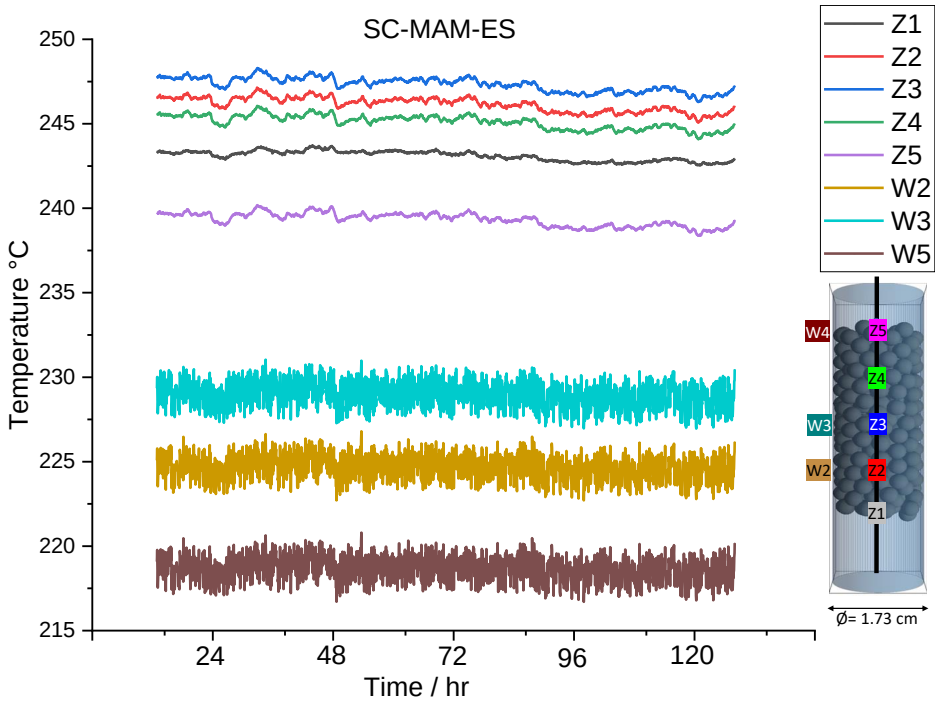

Figure 57. Temperature profile of SC-MAM-ES catalyst under 380 h-1 GHSV and at 245 °C.

Figure 58. Thermally modified SC-MAM catalyst support prior to impregnation.

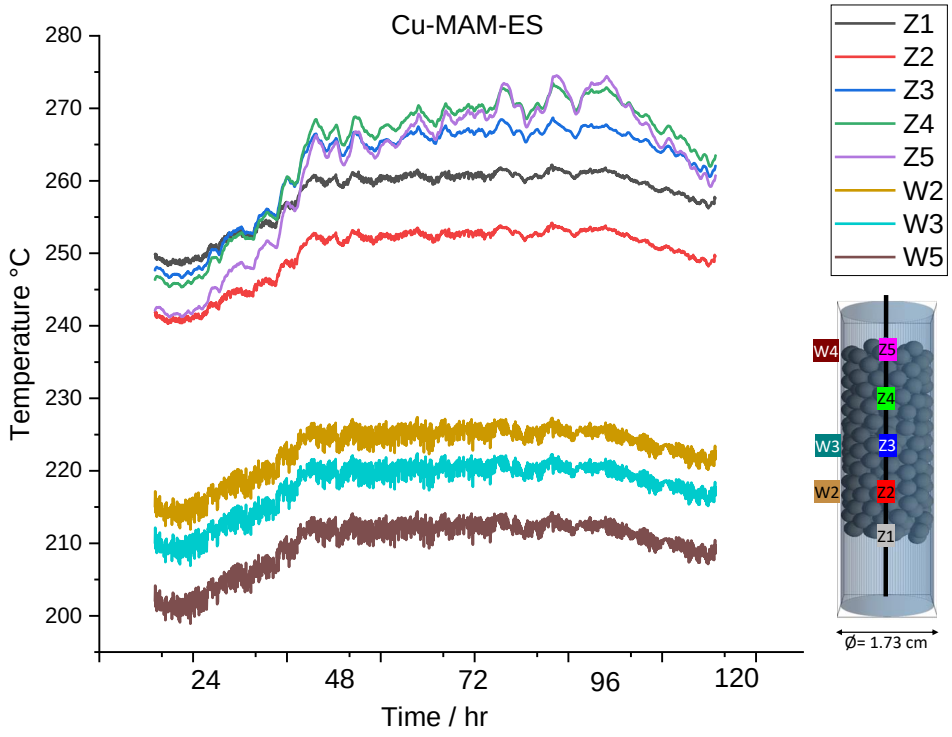

Figure 59. Temperature profile of SC-MAM-ES catalyst under 380 h-1 GHSV and at 261 °C.

Figure 60. Thermally modified catalyst support prior to impregnation.

6.6. FTS by the Thermally modified core-shell catalysts; Al-MAM-CS

In the bolder approach for increasing the thermall conductivity of the catalyst supports for better thermal management of the FT reactor we tried to combine the core-shell format with the thermally improved format. Therefore, in an ambodiment a paste contains 16% aluminum powder was presented in the MAM and coated with a 0.5 mm thickness around the supper conductive copper core. The obtained support were impregnated with cobalt and promoted with rutheneum in the same protocol as used for all previous catalysts. Table 17. is showing the FT performance of the Al-MAM-CS catalyst.

Table 17. FT resuls of ther thermally modified core-shell catalyst Al-MAM-CS.

Catalyst	Mass Flow	GHSV	Temp.	Mass of C5+ g		Mass of Aquous Phase g	Productivity		Product Analysis						Temperature gradient	
	SCCM	h-1	°C	Oil	Wax		Per unit mass of Co mg C5+/g Co . h	Per unit volume of the reactor mg C5+/mL Cat .h	% CO Conv.	% SC5+	% SCH4	%S C5+ to Aq.	%S Oil to C5+	% Crude C5+ Yield	Axial °C/cm	Radial °C/mm
Al-MAM-CS	100	380	245	29	10	147	119.5	12.9	78	82	16	26.5	74.4	34.0	2	2
Al-MAM-CS	200	765	245	55	23	280	239.0	25.9	76	87	11.5	27.9	70.5	35.7	2	2

The axial tempreture gradient ΔT_{Axial} of the catalyst was measured as of 2 °C/cm with the radial ΔT_{Radial} measure of the equal to 2 which is showing the highlly uniform tempreture distribution through the catalyst bed. The FT carried out at 245 °C under 380 h^{-1} and 765 h^{-1} syngas hourly space velocity. Both productivity indexes are show the an two fold increased by doubling down the GHSV parameter of the reaction. Depending on GHSV The productivity per mass of cobalt were 17 % and 5.5 % higher than the core-shel and much higher than all other catalyst designs. Moreover, volumetric productivity boosts 59 % and 44 % with using Al-MAM-CS rather than Al-MAM-ES, respectively. The Al-MAM-CS catalyst has an 70 to 74.4 % oil to C_{5+} ratio which was an average of 9 % more

thatn all thermally improved candidates and in compare to Al-MAM-ES with 94.3 % to 100 % and MAM-ES with 26 % to 47 % ratios which shows an increase in liquid production in compare to egg-shell and thermally improved catalysts. The carbon conversion of the Al-MAM-CS was between 76 to 78 % with respect to different GHSV at measured temperature of 245 °C incompare to 60 to 61 % by MAM-CS and 70 to 74 % via Al-MAM-ES.

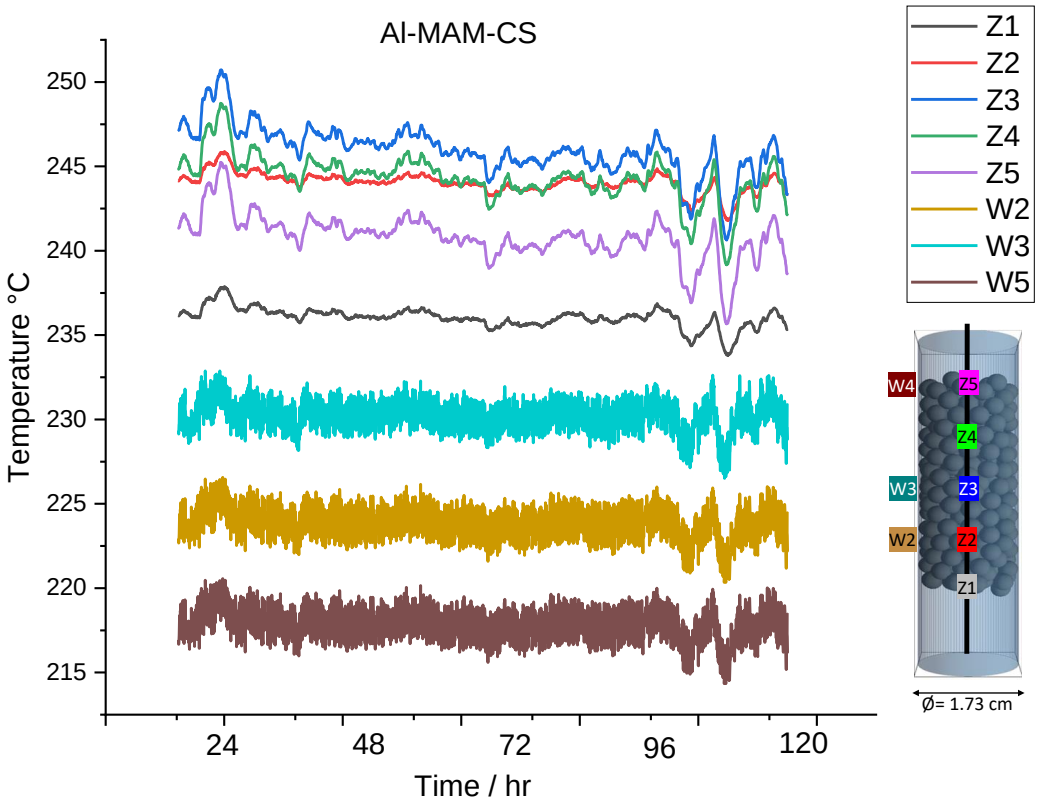

Figure 61. Temperature profile of the Al-MAM-CS catalyst durin the FTS under 380 h-1 GHSV and at 245 °C..

6.7. FT products

The product distribution of the present work is classified in tail gas, light oil, heavy oil, and aqueous phase. The following chromatograms is obtained by GC-MS of the different C_{5+} products collected from the cold and hot traps.

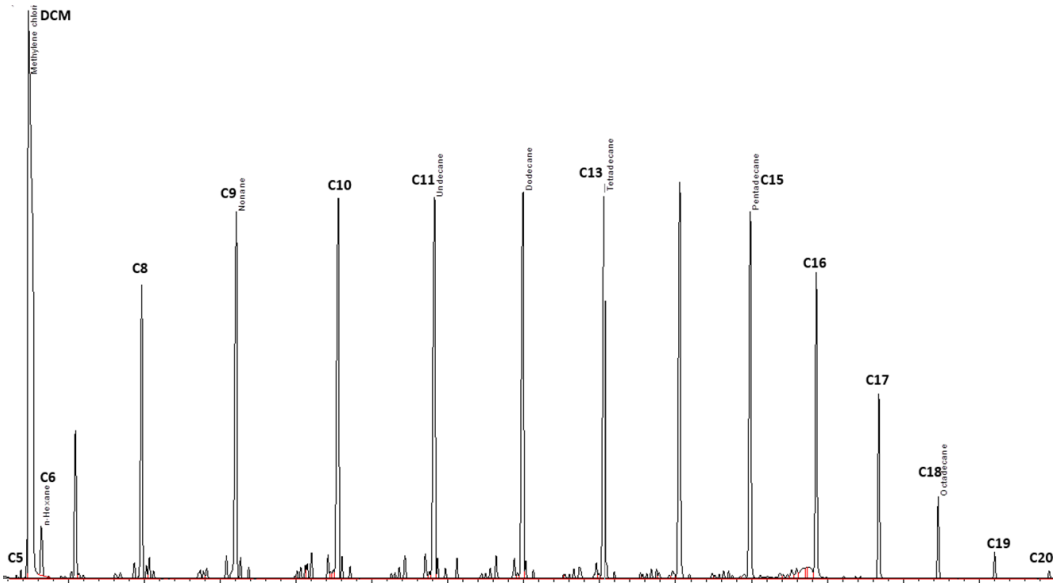

Figure 62. The product distribution of the light oil collected from the cold trap.

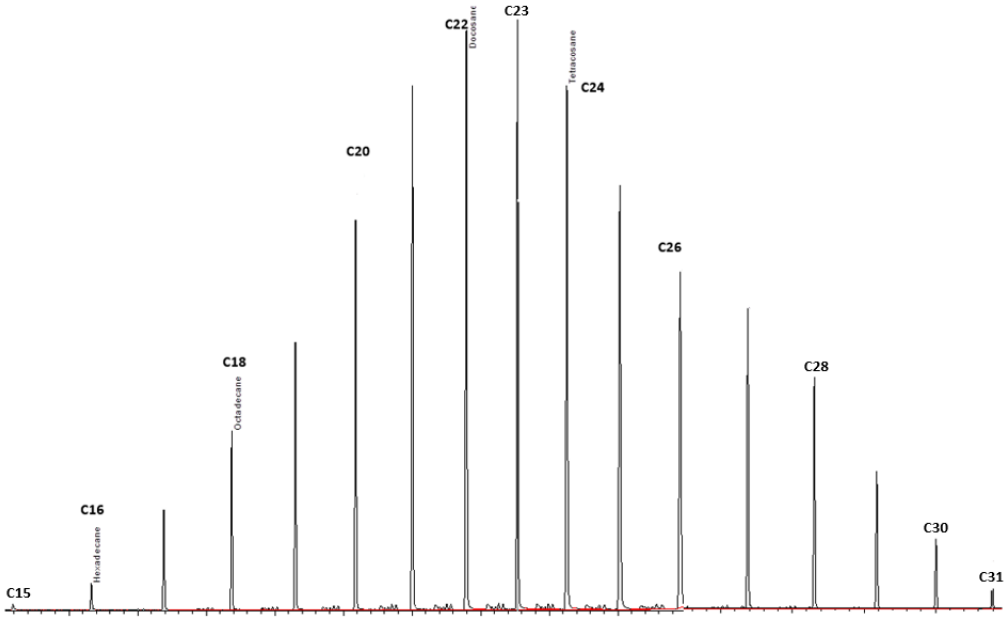

Figure 63. GC-MS; The FT product distribution of The FT wax collected from the hot trap.

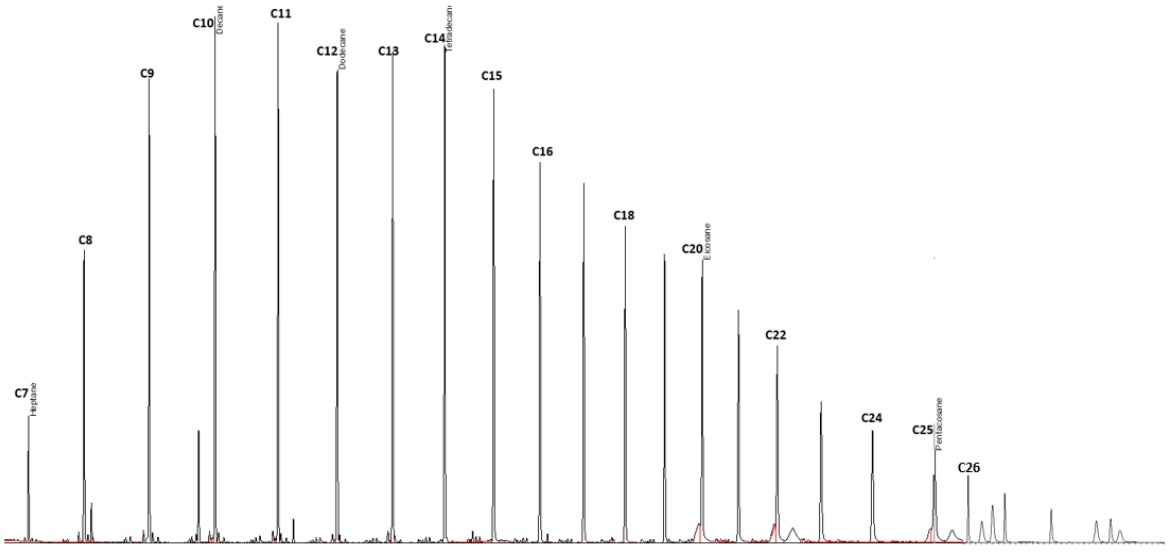

Figure 64. GC-MS; The FT product distribution of a mixture of light and heavy oil.

Reference

(1) Elvidge, C. D.; Zhizhin, M.; Baugh, K.; Hsu, F. C.; Ghosh, T. Methods for Global Survey of Natural Gas Flaring from Visible Infrared Imaging Radiometer Suite Data. *Energies* **2016**, *9* (1). https://doi.org/10.3390/en9010014.

(2) Kanellopoulos, N. *Small-Scale Gas to Liquid Fuel Synthesis*; 2015. https://doi.org/10.1201/b18075.

(3) Klerk, A. de. Fischer–Tropsch Process. *Kirk-Othmer Encycl. Chem. Technol.* **2013**.

(4) Klerk, A. de. *Catalysis in the Refining of Fischer–Tropsch Syncrude Upgrading of Fischer – Tropsch Oxygenates*; 2010.

(5) Dry, M. E. Practical and Theoretical Aspects of the Catalytic Fischer-Tropsch Process. *Appl. Catal. A Gen.* **1996**, *138* (2), 319–344. https://doi.org/10.1016/0926-860X(95)00306-1.

(6) R. Guettel, U. Kunz, T. T. Reactors for Fischer-Tropsch Synthesis. *Chem. Eng. Technol. 31* (5), 746–754.

(7) Guettel, R.; Turek, T. Comparison of Different Reactor Types for Low Temperature Fischer-Tropsch Synthesis: A Simulation Study. *Chem. Eng. Sci.* **2009**, *64* (5), 955–964. https://doi.org/10.1016/j.ces.2008.10.059.

(8) B. H. Davis, M. L. O. Advances in Fischer-Tropsch Synthesis, Catalysts, and Catalysis. *Focus Catal.* **2010**, *2010* (3), 8. https://doi.org/10.1016/s1351-4180(10)70087-8.

(9) Zhan, X.; Davis, B. H. Assessment of Internal Diffusion Limitation on Fischer-Tropsch

Product Distribution. *Appl. Catal. A Gen.* **2002**, *236* (1–2), 149–161. https://doi.org/10.1016/S0926-860X(02)00301-0.

(10) Fischer, F. Über Die Synthese Der Petroleum Kohlenwasserstoffe. *Brennstoff-Chemie* **1927**, *8*, 1–5.

(11) Fisher and Tropsch. Über Die Herstellung Synthetischer Ölgemische (Synthol) Durch Aufbau Aus Kohlenoxyd Und Wasserstoff. *Brennstoff-Chemie* **1923**, *4*, 276–285.

(12) Stranges, A. Germany's Synthetic Fuel Industry, 1927–1945. In *The German Chemical Industry in the Twentieth Century*,; Lesch, J. E., Ed.; 2000; pp 147–216.

(13) Storch, H. H. The Fischer-Tropsch and Related Processes for Synthesis of Hydrocarbons by Hydrogenation of Carbon Monoxide. *Adv. Catal.* **1948**, *1* (C), 115–156. https://doi.org/10.1016/S0360-0564(08)60674-4.

(14) Pichler, H. Twenty-Five Years of Synthesis of Gasoline by Catalytic Conversion of Carbon Monoxide and Hydrogen. *Adv. Catal.* **1952**, *4* (C), 271–341. https://doi.org/10.1016/S0360-0564(08)60617-3.

(15) R.J.Madon. On the Growth of Hydrocarbon Chains in the Fischer-Tropsch Synthesis. *J. Catal.* **1979**, *57* (1), 183–186.

(16) Chabot, G.; Guilet, R.; Cognet, P.; Gourdon, C. A Mathematical Modeling of Catalytic Milli-Fixed Bed Reactor for Fischer-Tropsch Synthesis: Influence of Tube Diameter on Fischer Tropsch Selectivity and Thermal Behavior. *Chem. Eng. Sci.* **2015**, *127*, 72–83. https://doi.org/10.1016/j.ces.2015.01.015.

(17) Iglesia, E.; Reyes, S. C.; Madon, R. J.; Soled, S. L. Selectivity Control and Catalyst

Design in the Fischer-Tropsch Synthesis: Sites, Pellets, and Reactors. *Adv. Catal.* **1993**, *39* (C), 221–302. https://doi.org/10.1016/S0360-0564(08)60579-9.

(18) Iglesia, E.; Soled, S. L.; Baumgartner, J. E.; Reyes, S. C. Synthesis and Catalytic Properties of Eggshell Cobalt Catalysts for the Fischer-Tropsch Synthesis. *Top. Catal.* **1995**, *2* (1–4), 17–27. https://doi.org/10.1007/BF01491952.

(19) Yang, J. Il; Yang, J. H.; Kim, H. J.; Jung, H.; Chun, D. H.; Lee, H. T. Highly Effective Cobalt Catalyst for Wax Production in Fischer-Tropsch Synthesis. *Fuel* **2010**, *89* (1), 237–243. https://doi.org/10.1016/j.fuel.2009.07.008.

(20) Dr. Yuefeng Liu, Prof. Ovidiu Ersen, Dr. Christian Meny, Dr. Francis Luck, D. C. P.-H. *Fischer–Tropsch Reaction on a Thermally Conductive and Reusable Silicon Carbide Support*; 2014; Vol. 7.

(21) Adrien Deneuvea,∗, Ileana Floreab, Ovidiu Ersenb, Patrick Nguyenc, Charlotte Phamc, Dominique Bégina, David Edouarda, Marc-Jacques Ledouxa, C. P.-H. Catalytic Growth of Silicon Carbide Composite with Nanoscopic Properties and Enhanced Oxidative Resistance as Catalyst Support. *Appl. Catal. A, Gen. 385* (1), 52–61.

(22) Lacroix, M.; Dreibine, L.; De Tymowski, B.; Vigneron, F.; Edouard, D.; Bégin, D.; Nguyen, P.; Pham, C.; Savin-Poncet, S.; Luck, F.; et al. Silicon Carbide Foam Composite Containing Cobalt as a Highly Selective and Re-Usable Fischer-Tropsch Synthesis Catalyst. *Appl. Catal. A Gen.* **2011**, *397* (1–2), 62–72. https://doi.org/10.1016/j.apcata.2011.02.012.

(23) Zohdi-Fasaei, H.; Atashi, H.; Farshchi Tabrizi, F.; Mirzaei, A. A. Effects of Mass Transfer on Fischer-Tropsch Kinetics over Mesoporous Silica-Supported Co-Mn-Ce Nano

Catalysts in a Fixed-Bed Reactor. *J. Nat. Gas Sci. Eng.* **2016**, *32*, 262–272. https://doi.org/10.1016/j.jngse.2016.03.090.

(24) Khodakov, A. Y.; Griboval-Constant, A.; Bechara, R.; Zholobenko, V. L. Pore Size Effects in Fischer Tropsch Synthesis over Cobalt-Supported Mesoporous Silicas. *J. Catal.* **2002**, *206* (2), 230–241. https://doi.org/10.1006/jcat.2001.3496.

(25) Borg, Ø.; Eri, S.; Blekkan, E. A.; Storsæter, S.; Wigum, H.; Rytter, E.; Holmen, A. Fischer-Tropsch Synthesis over γ-Alumina-Supported Cobalt Catalysts: Effect of Support Variables. *J. Catal.* **2007**, *248* (1), 89–100. https://doi.org/10.1016/j.jcat.2007.03.008.

(26) Xiong, H.; Zhang, Y.; Wang, S.; Li, J. Fischer-Tropsch Synthesis: The Effect of Al2O3 Porosity on the Performance of Co/Al2O3 Catalyst. *Catal. Commun.* **2005**, *6* (8), 512–516. https://doi.org/10.1016/j.catcom.2005.04.018.

(27) Saib, A. M.; Claeys, M.; Van Steen, E. Silica Supported Cobalt Fischer-Tropsch Catalysts: Effect of Pore Diameter of Support. *Catal. Today* **2002**, *71* (3–4), 395–402. https://doi.org/10.1016/S0920-5861(01)00466-7.

(28) Jung, J. S.; Kim, S. W.; Moon, D. J. Fischer-Tropsch Synthesis over Cobalt Based Catalyst Supported on Different Mesoporous Silica. *Catal. Today* **2012**, *185* (1), 168–174. https://doi.org/10.1016/j.cattod.2012.02.002.

(29) Ghampson, I. T.; Newman, C.; Kong, L.; Pier, E.; Hurley, K. D.; Pollock, R. A.; Walsh, B. R.; Goundie, B.; Wright, J.; Wheeler, M. C.; et al. Effects of Pore Diameter on Particle Size, Phase, and Turnover Frequency in Mesoporous Silica Supported Cobalt Fischer-Tropsch Catalysts. *Appl. Catal. A Gen.* **2010**, *388* (1–2), 57–67. https://doi.org/10.1016/j.apcata.2010.08.028.

(30) Martin Wassermann, A. M. United States Patent (19). 4,048,295, 1977.

(31) Patrick Euzen, Pascal Raybaud, X. K.; Hervi Toulhoat, Jean-Luc Le Loarer, Jean-Pierre Jolivet, A.; Froidefond, C. *Alumina*; WILEY-VCH Verlag GmbH, 2002. https://doi.org/10.1002/9783527618286.

(32) Helmuth Schmidt. Sol-Gel Production. *Trans Tech Publ.* **1998**, *150* (March), 21–32. https://doi.org/10.4028/www.scientific.net/kem.150.21.

(33) M. Absl-Halabi, A. S. and H. A.-Z. STUDIES ON PORE SIZE CONTROL OF ALWINA: PREPARATBN OF ALWINA CATALYST EXTRUDATES WITH LARGE UNMODAL PORE STRUCTURE BY LOW TEMPERATURE HYDROTHEWW TREATMENT. **1991**, 155–163.

(34) F. Morel, S. Kressmann, V. Harle, S. K. Processes and Catalysts for Hydrocracking of Heavy Oil and Residues. In *studies in Surface Science and Catalysis - 106 - HYDROTREATMENTHYDROTREATMENT AND HYDROCRACKING OF OIL FRACTIONS*; G.F. Froment, B. Delmon, P. G., Ed.; Elsevier, 1997; pp 1–16.

(35) Dasgupta, P. K.; Maleki, F. Ion Exchange Membranes in Ion Chromatography and Related Applications. *Talanta* **2019**, *204*, 89–137. https://doi.org/10.1016/j.talanta.2019.05.077.

(36) Maleki, F.; Dasgupta, P. K. Moldable Strong Cation Exchange Polymer and Microchannel Fabrication. *Anal. Chem.* **2020**, *92* (19), 13378–13386. https://doi.org/10.1021/acs.analchem.0c02754.

(37) Stanislaus, D. L. T. and A. THE CONTROL OF PORE SIZE IN ALUMINA CATALYST

SUPPORTS: REVIEW, A. **1986**, *21*, 614.

(38) Shan, Z.; Jansen, J. C.; Zhou, W.; Maschmeyer, T. Al-TUD-1, Stable Mesoporous Aluminas with High Surface Areas. *Appl. Catal. A. Gen.* **2003**, *254*, 339–343. https://doi.org/10.1016/S0926-860X(03)00480-0.

(39) Xu, N.; Liu, Z.; Bian, S.; Dong, Y.; Li, W. Template-Free Synthesis of Mesoporous γ-Alumina with Tunable Structural Properties. *Ceram. Int.* **2016**, *42* (3), 4072–4079. https://doi.org/10.1016/j.ceramint.2015.11.079.

(40) Kim, P.; Kim, Y.; Kim, C.; Kim, H.; Park, Y.; Lee, J. H.; Song, I. K.; Yi, J. Synthesis and Characterization of Mesoporous Alumina as a Catalyst Support for Hydrodechlorination of 1,2-Dichloropropane: Effect of Catalyst Preparation Method. *Catal. Letters* **2003**, *89* (3–4), 185–192. https://doi.org/10.1023/A:1025794127243.

(41) Kim, S. M.; Lee, Y. J.; Jun, K. W.; Park, J. Y.; Potdar, H. S. Synthesis of Thermo-Stable High Surface Area Alumina Powder from Sol-Gel Derived Boehmite. *Mater. Chem. Phys.* **2007**, *104* (1), 56–61. https://doi.org/10.1016/j.matchemphys.2007.02.044.

(42) Yuan, Q.; Yin, A. X.; Luo, C.; Sun, L. D.; Zhang, Y. W.; Duan, W. T.; Liu, H. C.; Yan, C. H. Facile Synthesis for Ordered Mesoporous γ-Aluminas with High Thermal Stability. *J. Am. Chem. Soc.* **2008**, *130* (11), 3465–3472. https://doi.org/10.1021/ja0764308.

(43) Lesaint, C.; Glomm, W. R.; Borg, Ø.; Eri, S.; Rytter, E.; Øye, G. Synthesis and Characterization of Mesoporous Alumina with Large Pore Size and Their Performance in Fischer-Tropsch Synthesis. *Appl. Catal. A Gen.* **2008**, *351* (1), 131–135. https://doi.org/10.1016/j.apcata.2008.09.008.

(44) Cai, W.; Yu, J.; Anand, C.; Vinu, A.; Jaroniec, M. Facile Synthesis of Ordered Mesoporous Alumina and Alumina-Supported Metal Oxides with Tailored Adsorption and Framework Properties. *Chem. Mater.* **2011**, *23* (5), 1147–1157. https://doi.org/10.1021/cm102512v.

(45) White, A.; Walpole, A.; Huang, Y.; Trimm, D. L. Control of Porosity and Surface Area in Alumina. *Appl. Catal.* **1989**, *56* (1), 187–196. https://doi.org/10.1016/s0166-9834(00)80168-2.

(46) Huang, B.; Bartholomew, C. H.; Smith, S. J.; Woodfield, B. F. Facile Solvent-Deficient Synthesis of Mesoporous γ-Alumina with Controlled Pore Structures. *Microporous Mesoporous Mater.* **2013**, *165*, 70–78. https://doi.org/10.1016/j.micromeso.2012.07.052.

(47) Wu, W.; Wan, Z.; Chen, W.; Zhu, M.; Zhang, D. Synthesis of Mesoporous Alumina with Tunable Structural Properties. *Microporous Mesoporous Mater.* **2015**, *217*, 12–20. https://doi.org/10.1016/j.micromeso.2015.06.002.

(48) Cahen, R. M.; Andre, J. M.; Debus, H. R. Process for the Production of Spherical Catalyst Supports. *Stud. Surf. Sci. Catal.* **1979**, *3* (C), 585–594. https://doi.org/10.1016/S0167-2991(09)60236-6.

(49) Deng, S. G.; Lin, Y. S. Granulation of Sol-Gel-Derived Nanostructured Alumina. *AIChE J.* **1997**, *43* (2), 505–514. https://doi.org/10.1002/aic.690430223.

(50) Hou, Z.; Zhang, B.; Zhang, R.; Liu, L. Fabrication of Highly Porous Mullite Microspheres via Oil-Drop Molding Accompanied by Freeze Casting. *Ceram. Int.* **2017**, *43* (12), 8809–8812. https://doi.org/10.1016/j.ceramint.2017.04.012.

(51) Islam, A.; Taufiq-Yap, Y. H.; Chu, C. M.; Chan, E. S.; Ravindra, P. Synthesis and Characterization of Millimetric Gamma Alumina Spherical Particles by Oil Drop Granulation Method. *J. Porous Mater.* **2012**, *19* (5), 807–817. https://doi.org/10.1007/s10934-011-9535-0.

(52) Munnik, P.; De Jongh, P. E.; De Jong, K. P. Recent Developments in the Synthesis of Supported Catalysts. *Chem. Rev.* **2015**, *115* (14), 6687–6718. https://doi.org/10.1021/cr500486u.

(53) Chuansheng Bai, J. W. . L. . B. (12) United States Patent, 2018.

(54) Subero-Couroyer, C.; Ghadiri, M.; Brunard, N.; Kolenda, F. Weibull Analysis of Quasi-Static Crushing Strength of Catalyst Particles. *Chem. Eng. Res. Des.* **2003**, *81* (8), 953–962. https://doi.org/10.1205/026387603322482194.

(55) Knozinger, H.; Weitkamp, J. *Preparation of the Solid Catalysts*; WILEY-VCH Gerhard, 1999.

(56) Avila, P.; Montes, M.; Miró, E. E. Monolithic Reactors for Environmental Applications: A Review on Preparation Technologies. *Chem. Eng. J.* **2005**, *109* (1), 11–36. https://doi.org/10.1016/j.cej.2005.02.025.

(57) US20180264439A1-ALUMINA AND ALUMINA EXTRUDATES AND PROCESS FOR PREPARATION THEREOF.Pdf.

(58) Gregg, S. J.; Sing, K. S. W.; Salzberg, H. W. Adsorption Surface Area and Porosity. *J. Electrochem. Soc.* **1967**, *114* (11), 279C. https://doi.org/10.1149/1.2426447.

(59) Takeshi Kotanigawa, Mitsuyoshi Yamamoto, Masahiro Utiyama, Hideshi Hattori, K. T.

The Influence of Preparation Methods on the Pore Structure of Alumina. *Appl. Catal.* **1981**, *3* (September), 185–200. https://doi.org/10.1016/0166-9834(81)80006-1.

(60) Marvin F.L. Johnson, J. M. The Origin and Types of Pores in Some Alumina Catalysts. *J. Catal.* **1968**, *10* (4), 342–354.

(61) Ono, T.; Ohguchi, Y.; Togari, O. *Control of the Pore Structure of Porous Alumina*; 1983; Vol. 16. https://doi.org/10.1016/S0167-2991(09)60054-9.

(62) PAPPE, R. TERTIAN, R. B. Boehmite and Pseud-Boehmite. 1958, pp 1301–1310.

(63) Bauer, R. US4797139, 1989.

(64) Claude, V.; Garcia, H. S.; Wolfs, C.; Lambert, S. D. Elaboration of an Easy Aqueous Sol-Gel Method for the Synthesis of Micro- and Mesoporous γ-Al_2O_3 Supports. *Adv. Mater. Phys. Chem.* **2017**, *07* (07), 294–310. https://doi.org/10.4236/ampc.2017.77023.

(65) Huang, B.; Bartholomew, C. H.; Woodfield, B. F. Facile Synthesis of Mesoporous γ-Alumina with Tunable Pore Size: The Effects of Water to Aluminum Molar Ratio in Hydrolysis of Aluminum Alkoxides. *Microporous Mesoporous Mater.* **2014**, *183*, 37–47. https://doi.org/10.1016/j.micromeso.2013.09.007.

(66) J. M. Thomas andW. J. Thomas. *Principles and Practice of Heterogeneous Catalysis*; 2018.

(67) Sheldon, R. A.; Arends, I. W. C. E.; Hanefeld, U. *Green Chemistry and Catalysis*; 2007. https://doi.org/10.1002/9783527611003.

(68) Song, D.; Li, J. Effect of Catalyst Pore Size on the Catalytic Performance of Silica Supported Cobalt Fischer-Tropsch Catalysts. *J. Mol. Catal. A Chem.* **2006**, *247* (1–2),

206–212. https://doi.org/10.1016/j.molcata.2005.11.021.

(69) Bukur, D. B.; Mandić, M.; Todić, B.; Nikačević, N. Pore Diffusion Effects on Catalyst Effectiveness and Selectivity of Cobalt Based Fischer-Tropsch Catalyst. *Catal. Today* **2020**, *343*, 146–155. https://doi.org/10.1016/j.cattod.2018.10.069.

(70) Iglesia, E.; Soled, S. L.; Baumgartner, J. E.; Reyes, S. C. Synthesis and Catalytic Properties of Eggshell Cobalt Catalysts for the Fischer-Tropsch Synthesis. *Journal of Catalysis*. 1995, pp 108–122. https://doi.org/10.1006/jcat.1995.1113.

(71) Iglesia, E. Design, Synthesis, and Use of Cobalt-Based Fischer-Tropsch Synthesis Catalysts. *Appl. Catal. A Gen.* **1997**, *161* (1–2), 59–78. https://doi.org/10.1016/S0926-860X(97)00186-5.

(72) Mandić, M.; Todić, B.; Živanić, L.; Nikačević, N.; Bukur, D. B. Effects of Catalyst Activity, Particle Size and Shape, and Process Conditions on Catalyst Effectiveness and Methane Selectivity for Fischer-Tropsch Reaction: A Modeling Study. *Ind. Eng. Chem. Res.* **2017**, *56* (10), 2733–2745. https://doi.org/10.1021/acs.iecr.7b00053.

(73) Jess, A.; Kern, C. Influence of Particle Size and Single-Tube Diameter on Thermal Behavior of Fischer-Tropsch Reactors: Part I: Particle Size Variation for Constant Tube Size and Vice Versa. *Chem. Eng. Technol.* **2012**, *35* (2), 369–378. https://doi.org/10.1002/ceat.201100615.

(74) Sie, S. T.; Krishna, R. Fundamentals and Selection of Advanced Fischer-Tropsch Reactors. *Appl. Catal. A Gen.* **1999**, *186* (1–2), 55–70. https://doi.org/10.1016/S0926-860X(99)00164-7.

(75) Visconti, C. G.; Tronconi, E.; Groppi, G.; Lietti, L.; Iovane, M.; Rossini, S.; Zennaro, R. Monolithic Catalysts with High Thermal Conductivity for the Fischer-Tropsch Synthesis in Tubular Reactors. *Chem. Eng. J.* **2011**, *171* (3), 1294–1307. https://doi.org/10.1016/j.cej.2011.05.014.

(76) Fratalocchi, L.; Visconti, C. G.; Groppi, G.; Lietti, L.; Tronconi, E. Intensifying Heat Transfer in Fischer-Tropsch Tubular Reactors through the Adoption of Conductive Packed Foams. *Chem. Eng. J.* **2018**. https://doi.org/10.1016/j.cej.2018.05.108.

(77) Fratalocchi, L.; Visconti, C. G.; Lietti, L.; Tronconi, E.; Cornaro, U.; Rossini, S. A Novel Preparation Method for "Small" Eggshell Co/γ-Al2O3 Catalysts: A Promising Catalytic System for Compact Fischer-Tropsch Reactors. *Catal. Today* **2015**, *246*, 125–132. https://doi.org/10.1016/j.cattod.2014.09.020.

(78) Regalbuto, J. *Catalyst Preparation: Science and Engineering*; 2007; Vol. 2007. https://doi.org/10.1016/s1351-4180(07)70051-x.

(79) DillenaJ.W.Geusa, J. va. de L. va. der H. M. va. der K. J. va. Preparation and Properties of Supported Cobalt Catalysts for Fischer-Tropsch Synthesis. *Appl. Catal. A Gen.* **1997**, *150* (2), 365–376.

(80) Morbidelli, M.; Gavriilidis, A.; Varma, A. *Catalyst Design*; 2001. https://doi.org/10.1017/cbo9780511721762.

(81) Mark Facchini. A Study of Cobalt Catalysts for Fischer-Tröpsch Synthesis. *Thèse* **2010**, No. 2010.

(82) Fratalocchi, L.; Visconti, C. G.; Lietti, L.; Tronconi, E.; Rossini, S. Exploiting the Effects

of Mass Transfer to Boost the Performances of Co/γ-Al2O3 Eggshell Catalysts for the Fischer-Tropsch Synthesis. *Appl. Catal. A Gen.* **2016**, *512*, 36–42. https://doi.org/10.1016/j.apcata.2015.12.011.

(83) Fratalocchi, L.; Visconti, C. G.; Lietti, L.; Tronconi, E.; Cornaro, U.; Rossini, S. A Novel Preparation Method for "Small" Eggshell Co/γ-Al2O3 Catalysts: A Promising Catalytic System for Compact Fischer-Tropsch Reactors. *Catal. Today* **2015**, *246*, 125–132. https://doi.org/10.1016/j.cattod.2014.09.020.

(84) Zhong, M.; Guo, Y.; Wang, J.; Chen, C.; Ma, Z.; Jia, L.; Hou, B.; Li, D. Facile Preparation of Highly Thermal Conductive ZnAl2O4@Al Composites as Efficient Supports for Cobalt-Based Fischer-Tropsch Synthesis. *Fuel* **2019**, *253* (May), 1499–1511. https://doi.org/10.1016/j.fuel.2019.05.124.

(85) Zhou, Y.; Wang, H. An Al@Al2O3@SiO2/Polyimide Composite with Multilayer Coating Structure Fillers Based on Self-Passivated Aluminum Cores. *Appl. Phys. Lett.* **2013**, *102* (13). https://doi.org/10.1063/1.4798837.

(86) Valero-Romero, M. J.; Rodríguez-Cano, M. Á.; Palomo, J.; Rodríguez-Mirasol, J.; Cordero, T. Carbon-Based Materials as Catalyst Supports for Fischer–Tropsch Synthesis: A Review. *Front. Mater.* **2021**, *7* (February), 1–27. https://doi.org/10.3389/fmats.2020.617432.

(87) Přech, J.; Strossi Pedrolo, D. R.; Marcilio, N. R.; Gu, B.; Peregudova, A. S.; Mazur, M.; Ordomsky, V. V.; Valtchev, V.; Khodakov, A. Y. Core-Shell Metal Zeolite Composite Catalysts for in Situ Processing of Fischer-Tropsch Hydrocarbons to Gasoline Type Fuels. *ACS Catal.* **2020**, *10* (4), 2544–2555. https://doi.org/10.1021/acscatal.9b04421.

(88) Wang, D.; Chen, C.; Wang, J.; Jia, L.; Hou, B.; Li, D. High Thermal Conductive Core-Shell Structured Al2O3@Al Composite Supported Cobalt Catalyst for Fischer-Tropsch Synthesis. *Appl. Catal. A Gen.* **2016**, *527*, 60–71. https://doi.org/10.1016/j.apcata.2016.08.027.

(89) Davis, B. H.; Occelli, M. L. Fischer-Tropsch Synthesis, Catalysts and Catalysis: Advances and Applications. **2019**, 417.

(90) Sandeep Patil, Siddarth Chintamani, Ratan Kumar, B. H. D. Determination of Orthotropic Thermal Conductivity in Heat Generating Cylinder. *Proc. ASME 2016 Int. Mech. Eng. Congr. Expo. IMECE* **2016**, *11*, V011T15A016.

(91) Sandeep Patil, Siddarth Chintamani, James Grisham, Ratan Kumar, B. H. D. Inverse Determination of Temperature Distribution in Partially Cooled Heat Generating Cylinder. *ASME Int. Mech. Eng. Congr. Expo.* **2015**, *57502*, V08BT10A024.

(92) Oscar Fabela, Sandeep Patil, Siddarth Chintamani, B. H. D. Estimation of Effective Thermal Conductivity of Porous Media Utilizing Inverse Heat Transfer Analysis on Cylindrical Configuration. *ASME Int. Mech. Eng. Congr. Expo.* **2017**, *58431*, V008T10A089.

(93) Rahul Upreti, Siddarth Chintamani, Sandeep Patil, Askan Akbariyeh, B. D. Stochastic Finite Element Analysis of a Ball Grid Array Package. *J. Electron. Packag.* **2021**.

(94) H.DennisRatanKumar, S. Real Time Prediction of Internal Temperature of Heat Generating Bodies Using Neural Network. *Therm. Sci. Eng. Prog.* **2021**, *23*.

(95) Iglesia et Al. - 1995 - Journal of Catalysis - Synthesis and Catalytic Properties of Eggshell

Cobalt Catalysts for the Fischer-Tropsch Synthesis.Pdf.